Study of salinity retrieval errors for the SMOS mission

Carolina Gabarró Prats

Doctoral thesis

Advisors: Dr. Jordi Font Ferré and Dr. Adriano Camps Carmona

Dept. de Geologia Marina i Oceanografia Física.
Institut de Ciències del Mar (CSIC), Barcelona

November 2004

A la meva família i especialment a la meva
tieta àvia, que des del primer moment
em va animar a realitzar aquesta tesi.

Agraïments

Ja de petita deia que volia investigar, sense saber massa què significava, però la idea d'explorar allò desconegut em fascinava (de fet, encara em passa ara). També volia ser astronauta, volia veure l'immens espai des de més a prop, i la Terra des de lluny. Bé, no sóc ni una cosa ni l'altra però em sento propera a les dues.

Vull agrair a totes les persones que m'han ajudat en aquest llarg camí que representa fer una tesi.

En primer lloc dono les gràcies als meus directors, el Jordi i l'Adriano, pel seu inestimable ajut i per animar-me a acabar aquesta tesi, en moments que tenia dubtes de si continuar-la o deixar-la. D'ells he après moltíssim.

També agraeixo als meus pares i al meu germà el suport incondicional i la confiança que m'han mostrat durant tot aquest temps i sempre. I vull fer especial menció de la tieta Mari, la meva tieta àvia, que té 93 anys i que des del primer moment em va encoratjar a fer la tesi: em deia que era una molt bona cosa, que m'obriria camins en el futur i que o bé la feia ara, o ja no la faria mai. Tant de bo jo pugui tenir la ment tan clara com ella a la seva edat. Gràcies tieta.

Evidentment, també vull agrair al Marc tot el que ha fet per ajudar-me en els moment de nervis, d'estrès i d'esgotament que m'han acompanyat aquests últims mesos. Gràcies per la comprensió i per fer-me riure quan més ho necessitava.

També, dono les gràcies a l'Agustí per tot el que m'ha ensenyat, a tots els companys del grup d'oceanografia física, amb qui he après, rigut i compartit tantes coses, així com a la Mercè i altra gent del TSC amb qui he pogut comptar sempre que he tingut dubtes.

Vull agrair als meus companys de despatx, el Jordi S., el Jordi I. i l'Antonio el seu incansable ajut, sobretot per resoldre problemes del Latex. També a la Maribel, a la Teresa i a la Sílvia pel seu suport moral i a la resta dels comensals de la taula rodona pels dinars compartits. També a altres persones de l'Institut que m'han ajudat al llarg d'aquest temps.

Vull fer aparèixer en aquests agraïments els amics amb qui he compartit diferents etapes de la meva vida i que m'han fet costat també en aquesta. A tots ells els estimo i necessito: l'Olga, el Marc, el Lluís, l'Anna, la Sònia, la Bea, la Tat, el Miquel, l'Àdam, la Nata, el Ferri, la Cristina, el Miquel, la Glòria, la Marissa, el Pere, la Sílvia, la Marta, la Circe, l' Alicia, el Fer, el Dani, la Mònica, el Lluís, el Martin, l'Oriol, la Mireia, el Joan Carles, la Marta, l'Íngrid, i encara més gent però la llista comença ja a ser massa llarga.

Bé, en definitiva, a totes aquelles persones que m'han envoltat, ajudat, estimat i cuidat en tot aquest temps. Gràcies a tots.

Resum

El treball realitzat en aquesta tesi està emmarcat en la missió SMOS (Soil Moisture and Ocean Salinity) de l'Agència Espacial Europea. El satèl·lit es llançarà el febrer del 2007, i mesurarà la salinitat superficial del mar i la humitat del sòl. L'instrument (MIRAS) consisteix en un radiòmetre interferomètric en banda L (1,400-1,430 GHz). Serà la primera vegada que es posarà en òrbita un instrument d'aquestes característiques i que es mesuraran aquests paràmetres des de l'espai. No obstant, encara son molts els aspectes científics que queden per resoldre. Aquesta tesi, doncs, ha intentat abordar alguns del temes oberts en la recuperació de la salinitat a partir de les mesures de SMOS.

La sensibilitat de la temperatura de brillantor (el què el radiòmetre mesura) a la salinitat és màxima, tot i que no és gaire gran, a la freqüència de 1,4 GHz. Per altra banda la sensibilitat a la temperatura superficial del mar i a la rugositat és del mateix ordre de magnitud. Això implica que per recuperar la salinitat amb una certa precisió, cal també conèixer aquests altres paràmetres anomenats auxiliars.

La recerca feta en aquesta tesi està gairebé tota basada en dades experimentals de diferents campanyes que s'han realitzat utilitzant diferents radiòmetres en banda L, més boies i altres instruments per mesurar les variables in situ.

S'ha fet un estudi sobre diferents models d'emissivitat en banda L de la superfície del mar, que existeixen en l'actualitat. Aquests models, tant teòrics com semi-empírics, s'han utilitzat per recuperar, de la temperatura de brillantor mesurada, la salinitat. Aquesta salinitat recuperada s'ha comparat amb les dades de salinitat adquirides in situ. Els resultats han demostrat que els models semi-empírics recuperen millor la salinitat que no pas els teòrics que s'han analitzat en aquest treball.

Els models actuals descriuen la rugositat del mar en funció únicament del vent present. En alguns casos això no és correcte (mar de fons, mars no totalment desenvolupats). Així, analitzant aquestes limitacions, l'autora proposa un nou model semi-empíric, derivat de dades de la campanya WISE. Aquest model descriu la temperatura de brillantor deguda a la rugositat del mar amb dos paràmetres: la velocitat del vent i l'alçada significativa de l'ona. Aquest nou model resulta ser el que recupera salinitat amb més qualitat a partir de dades radiomètriques de tres campanyes diferents, que s'han realitzat amb diferents instruments i en diverses condicions del mar.

Errors en els paràmetres auxiliars, especialment en la velocitat del vent, degraden la qualitat de la salinitat recuperada. En aquesta tesi, diferents fonts d'informació vent i onatge s'han utilitzat per recuperar la salinitat: models meteorològics i oceanogràfics i dades de satèl·lit. Utilitzant com a paràmetres auxiliars dades obtingudes de models, la salinitat es recupera amb millor qualitat (probablement perquè aquests tenen més resolució espacial i temporal que no pas les mesures des de satèl·lit). De totes maneres aquesta conclusió no es pot extrapolar, ja que això només s'ha provat en una zona geogràfica (la Mediterrània occidental).

En aquesta tesi es proposa obtenir aquests paràmetres auxiliars de les mateixes mesures radiomètriques, així com es fa amb la salinitat. Degut a la configuració de SMOS, cada pícsel serà vist des de diferents angles d'incidència. Això ens permetrà poder recuperar més d'una variable, ja que estem tractant un sistema sobredeterminat. El mètode d'inversió és, aleshores, capaç de recuperar salinitat, velocitat del vent, onatge i la temperatura superficial del mar. Ara bé, quan utilitzem mètodes d'inversió amb restriccions s'obtenen millors resultats. Això consisteix en donar al sistema un valor de referència i el seu error per cada paràmetre. Amb aquest mètode l'error en la salinitat recuperada és de l'ordre de 0.2 psu, mentre que el vent recuperat té un error aproximat de 1 m/s, precisió que no és possible obtenir amb cap model ni satèl·lit simultani al pas de SMOS.

Per acabar, s'ha recuperat la salinitat d'imatges de temperatura de brillantor generades amb el simulador de SMOS. Aquestes imatges tenen la configuració de SMOS i estan afectades d'errors instrumentals, sorolls i biaixos, tal com passarà en el sensor real. Els resultats ens demostren que calen encara molts esforços per buscar una manera de reduir tots aquests errors i així augmentar la qualitat de la salinitat recuperada.

Abstract

This PhD thesis has been done in the framework of the SMOS (Soil Moisture and Ocean Salinity) mission, from the European Space Agency. This satellite will be launched in February 2007 and will provide global sea surface salinity and soil moisture maps, variables that never have been measured before from space. The payload instrument (MIRAS) is an L-band interferometric radiometer. This will be the first time an instrument with this characteristics is put in orbit. However, there are still a lot of issues that need to be solved. This thesis is focused on some open questions of the salinity retrieval process from SMOS measurements.

The sensitivity of the brightness temperature to salinity is maximum at the frequency of 1.4 GHz, even though this sensitivity is not high. The brightness temperature at this frequency is also sensitive to sea surface temperature and to sea surface roughness. Therefore to retrieve salinity with good quality it is necessary to know those parameters, as well.

An important part of the thesis work is based on experimental data obtained from different campaigns, which have been performed mainly in preparation of SMOS. During the campaigns different L-band radiometers have been used as well as buoys and other instruments to measure the in situ parameters.

A study of different sea surface emissivity models has been performed. Several theoretical and semi-empirical models have been used to retrieve salinity from measured brightness temperatures. The retrieved salinity has been compared with the measured, one and results have shown that the semi-empirical models retrieve better salinity than the analysed theoretical models.

Most of the emissivity models consider the roughness as function of the local wind speed, only. In the cases where swell or not fully developed seas are present this is not a good assumption. Therefore, the author proposes a new semi-empirical model derived from the WISE campaign. This new model describes the brightness temperature due to the roughness with two parameters: wind speed and significant wave height. When this model is used, the salinity is retrieved from radiometric data with better quality for three different campaigns data sets performed with different radiometers and in different sea conditions.

Errors on the auxiliary parameters produce additional not negligible errors on the retrieved salinity. Different sources of wind speed and wave height have been used to retrieve salinity: meteorological and oceanographic models and satellite measurements. Better results on the retrieved salinity are obtained, when model

output data are used. This is probably due to their higher spatial and temporal resolution. However, this conclusion can not be extrapolated, since it has been analysed only in one geographical area (Western Mediterranean).

The author proposes then to obtain the auxiliary parameters from the radiometric measurements themselves, as well as salinity. Due to the SMOS configuration, each pixel is seen from different incidence angles. This configures then an overdetermined system, and more than one variable can be retrieved. Therefore the inversion method is capable to retrieve salinity, wind speed, wave height and sea surface temperature. However, better results are obtained when some restrictions are used in the inversion; it is to give reference values and its errors for the different variables to the system. Using this method, salinity can be retrieved with an accuracy of 0.2 psu, and wind speed with an accuracy of 1 m/s, a value that is impossible to obtain from models or satellite measurements simultaneous to SMOS.

Finally, salinity has been retrieved from images crated by the SMOS simulator. These images have the real SMOS configuration and suffer from noise, bias and instrumental errors, as will happen to the real sensor. Results show that important efforts should be done to decrease these errors to improve the quality of the retrieved salinity.

Contents

Chapter 1

General Introduction

This chapter presents a short description of the physical principles of salinity measurements. It reviews the basics of microwave radiometry, and presents, shortly, the types of radiometers existing nowadays. It summarises previous campaigns that intended to measure salinity by radiometry since 1971. And finally two space missions currently under development to measure salinity are presented.

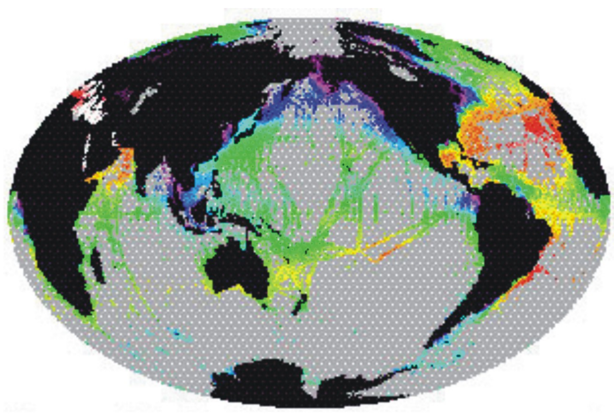

Figure 1.1: 100 years of Sea Surface Salinity measurements. Colours are salinity values. From Aquarius web page (http://aquarius.gsfc.nasa.gov/overview.html).

1.1 Why do we measure salinity ?

Human activities seem to have a significant influence on the climate of our planet and public awareness of possible climate changes has increased in the past few years. The scientific community thus faces a challenging task to answer the most pressing questions:

Is the climate actually changing and, if yes, at which rate, and more importantly, what will be the consequences, in particular with respect to the frequency of occurrence of extreme events?

Significant progress has been made in terms of weather forecasting, climate monitoring, and extreme events forecasting during recent years, using sophisticated models fed, among other things, by data acquired with operational satellites and analysed using super-computers. However, as recently pointed out by several working groups further improvement now depends on the availability of global observations of two crucial variables: Soil Moisture (SM) and Sea Surface Salinity (SSS). To date this information is lacking because *in situ* measurements are far from global, and so far no dedicated, long term, SM and SSS space mission has been attempted.

Knowledge of the global distribution of salt in the ocean and of its annual and inter-annual variability, is crucial in helping to understand the role of the ocean in the climate system. Ocean circulation is manly driven by the momentum and heat fluxes through the atmosphere-ocean interface, which can be partly traced by observation of SSS. In addition, salinity also determines ocean density and hence thermohaline circulation. In some regions (e.g. the Arctic), salinity is the most important variable as it controls processes such as deep water formation by determining, jointly with the temperature the water density. This process is a key component in the ocean thermohaline circulation conveyor belt. Ocean salinity is also linked to the oceanic carbon cycle, as it plays a part in establishing the chemical equilibrium which in turn regulates the CO_2 uptake and release. Therefore, the assimilation of SSS into global ocean biogeochemical models could improve estimates of absorption of CO_2 by the oceans.

Monitoring SSS could also be used to improve ENSO (El Niño Southern Oscillation) prediction by numerical models. Present models assimilate temperature and/or altimeter- derived sea level data only. The lack of salinity measurements results in major discrepancies between modelled near-surface and observed currents.

SSS is also correlated with estimates of the net evaporation minus precipitation (E-P) balance. E-P is difficult to measure accurately over the ocean, so global maps of SSS would provide a constraint on estimates of E-P at a global scale.

In situ salinity measurements are only sparsely distributed over the oceans. Examining available data in 1^o x 1^o boxes over the global oceans shows that salinity measurements exist for only about 70% of them. An even smaller fraction of the boxes contains more than one measurement. As for other oceanographic variables, global monitoring by *in situ* measurements are extremely expensive and a logistically complicated issue. Fig 1.1 shows the measurements of SSS done in 100 years all over the word.

Thereafter, satellite remote sensing, as presently achieved for sea surface temperature (SST) and sea surface height, appears to be an efficient solution to solve the lack of salinity information.

1.2 How to measure salinity?

Salinity is the measure of all the salts dissolved in water and it has traditionally been expressed in parts per thousand (ppt). The average ocean salinity is 35 ppt and the average river water salinity is 0.5 ppt or less. It is that in every kilogram of seawater, 35 grams are salt. Deep water almost always contains more salt than surface waters, since the density of the salty waters is higher.

The salt in the ocean is mostly made up of the elements sodium (Na) and chlorine (Cl). Together they account for 85.7% of the dissolved salt. The other major components of seawater are magnesium (Mg), calcium (Ca), potassium (K) and sulfate (SO_4). Together with chlorine and sodium they make up 99.4% of the salt in the ocean.

Originally, salinity was measured by evaporating the water, and the remaining salts weighted. However such method gave unreliable results. Later, it was done by chemical determinations.

Salinity is now determined by measuring how well electricity travels through water, this is also called conductivity. Water that has dissolved salt in it will conduct electricity better than water with no dissolved salt. The more salt dissolved in the water, the better water conducts electricity.

UNESCO (1978) and other international organisations recommended to define salinity using only conductivity, and they defined the *The Practical Salinity Scale* which is now the official definition.

The salinity of a sample of seawater is measured in terms of a ratio, R_T, which is defined as:

$$R_T = C(S, 15, 1)/C(KCl, 15, 1), \tag{1.1}$$

where C (S, 15, 1) is the conductivity of the sea-water sample at temperature 15°C and standard atmospheric pressure (1 atm), and C (KCl, 15, 1) is the conductivity of the standard potassium chloride (KCl) solution, with a concentration of $32.4356 g\, kg^{-1}$, at temperature 15°C and standard atmospheric pressure. Then the salinity is related to the conductivity ratio by the following equation:

$$S_{psu} = 0.0080 - 0.1692 R_{15}^{1/2} + 25.3851 R_{15} + 14.0941 R_{15}^{3/2} - 7.0261 R_{15}^{2} + 2.7081 R_{15}^{5/2}. \tag{1.2}$$

Salinity is then a unit-less quantity written as psu for *practical salinity unit.*

Conductivity, that depends on salinity and temperature, is measured by placing platinum electrodes in seawater and measuring the current that flows when there is a known voltage between the electrodes. The current depends on the conductivity, voltage, and volume of sea water in the path between electrodes. If the electrodes are in a tube of non-conducting glass, the volume of water is accurately known, and the current is independent of other objects near the conductivity cell. The best measurements of salinity from conductivity give salinity with an accuracy of ± 0.002psu.

Nowadays, the most reliable instruments to measure salinity, are the laboratory salinometers which measure conductivity by relative measurements standardised by comparison with 'standard seawater', or also called 'Copenhagen Water'. This standard seawater is produced by diluting a large sample of seawater until it has a precise salinity of 35 psu. A widely-used instrument of this class is the Guildline 8410 Portable Salinometer.

Microwave radiometry allows us to measure the emissivity of a medium (in this case of sea surface), and Fresnel's equation relates it with the dielectric constant (or permitivity) of sea water. This parameter is dependent on the temperature and also on the type of salt, and its concentration. So, in principle, it is possible to obtain the salinity concentration through that measurement.

After several studies, it has been shown that the sensitivity of brightness temperature to salinity is maximum at low microwave, as shown in figure 1.2, even though it is not very high. The L-band (1.4 GHz-1.43 GHz) is the optimum band for sensing salinity, since it is the first protected one.

At present, two satellite missions are in preparation to measure salinity using L-band radiometry. The present work is mainly a contribution to SMOS (Soil Moisture Ocean Salinity), a European Space Agency mission, planned for launched in 2007. One of its goals is the measurement of sea surface salinity over the oceans with an expected accuracy of 0.1 psu.

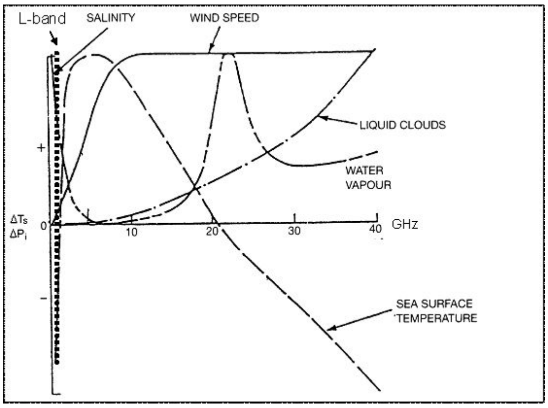

Figure 1.2: Sensitivity of several parameters to frenquency.

1.3 Microwave radiometry: Fundamental concepts

The bulk of energy received by the planet Earth is in the form of solar electromagnetic radiation. Part of the incident solar energy is scattered and absorbed by Earth's atmosphere, and the remainder is transmitted to Earth 's surface. A part of the latter is scattered outwards and the remainder is absorbed. According to thermodynamic principles, absorption of electromagnetic energy by a material medium leads to a transformation into thermal energy, which is accompanied by a rise in the thermometric temperature of the material. The reverse process, that of 'thermal' emission, serves to create the balance between the absorbed solar radiation and the radiation emitted by the Earth's surface and its atmosphere. These transformation processes are treated by the radiative transfer theory.

Radiometry is the field of science and engineering related to the measurement of radiant electromagnetic energy. All material media (gases, liquids, solids and plasma) radiate (emit) electromagnetic energy, which extends over the entire electromagnetic spectrum. A radiometer is a high sensitive and precise receiver capable of measuring low levels of radiation.

1.3.1 Physical principles

Thermal emission in the microwave region

A blackbody is an idealised body, perfectly opaque material that absorbs all the incident radiation at all frequencies, reflecting none. It is, also, a perfect emitter, since otherwise the energy absorbed by a material would increase its temperature indefinitely. The unpolarised blackbody radiation is emitted according to Planck's radiation law uniformly with a spectral brightness shown in equation 1.3.

$$B_f = \frac{2hf^3}{c^2}(\frac{1}{e^{hf/kT}-1}), \tag{1.3}$$

where
B_f = Blackbody spectral brightness, $Wm^{-2}sr^{-1}Hz^{-1}$
h = Planck's constant=$6.63 \times 10^{-34}\ J\ s$
f = frequency, Hz
k = Boltzmann's constant=$1.38 \times 10^{-23} JK^{-1}$
T = absolute temperature, K
c = velocity of light=$3 \times 10^8 ms^{-1}$

In the microwave region, generally $hf << kT$ and then the Rayleigh-Jeans approximation can be applied to equation 1.3 as follows.

$$e^x - 1 = (1 + x + \frac{x^2}{2} + \cdots) - 1 \simeq x, \qquad \text{for } x \ll 1 \tag{1.4}$$

then,

$$B_f = \frac{2f^2kT}{c^2} = \frac{2kT}{\lambda^2}. \tag{1.5}$$

And then, the brightness of a blackbody B_{bb} at a temperature T, and for a bandwidth of Δf, is:

$$B_{bb} = B_f \Delta f = \frac{2kT}{\lambda^2} \Delta f. \tag{1.6}$$

Real materials, usually referred as *grey bodies*, do not necessarily absorb all the energy incident upon them, and so emit less than a blackbody does. Then, considering a semi-infinite material, if its brightness, which may be direction-dependent, is $B(\theta, \phi)$ and its physical temperature is T, a blackbody equivalent radiometric temperature may be defined so that $B(\theta, \phi)$ can assume a form similar to 1.6. Such a temperature usually is called the *brightness temperature*, $T_B(\theta, \phi)$, and accordingly,

$$B(\theta, \phi) = \frac{2k}{\lambda^2} T_B(\theta, \phi) \Delta f \tag{1.7}$$

The brightness of a material relative to that of a blackbody at the same temperature is defined as the *emissivity* $e(\theta, \phi)$:

$$e(\theta, \phi) = \frac{B(\theta, \phi)}{B_{bb}} = \frac{T_B(\theta, \phi)}{T} \tag{1.8}$$

Since $B(\theta, \phi) \leqslant B_{bb}$, $0 \leqslant e((\theta, \phi) \leqslant 1$. Thus, the emissivity is a dimensionless quantity ranging from unity (for perfect blackbody) to zero (for perfect reflectors), and it is polarisation dependent. Then, the brightness temperature of a material is always smaller than or equal to its physical temperature. For a flat surface, the emissivity can be written, also, as follows:

$$e(\theta) = 1 - R(\theta), \tag{1.9}$$

where R is the Fresnel power reflection coefficient dependent on the polarisation (horizontal and vertical).

Sea-surface emissivity

It is the surface emissivity at L-Band which carries information regarding SSS. The emissivity and the power reflection coefficient R are related as expressed in 1.9. For a plane surface, R is the Fresnel reflection coefficient, and is dependent on the incident radiation zenith angle θ, and on the complex dielectric constant of sea water, ε:

$$\begin{aligned} R_H &= \left|\frac{\cos\theta - \sqrt{\varepsilon - \sin^2\theta}}{\cos\theta + \sqrt{\varepsilon - \sin^2\theta}}\right|^2, \\ R_V &= \left|\frac{\varepsilon\cos\theta - \sqrt{\varepsilon - \sin^2\theta}}{\varepsilon\cos\theta + \sqrt{\varepsilon - \sin^2\theta}}\right|^2. \end{aligned} \tag{1.10}$$

Figure 1.3 illustrates the general shape of the variation of emissivity as function on the incidence angle.

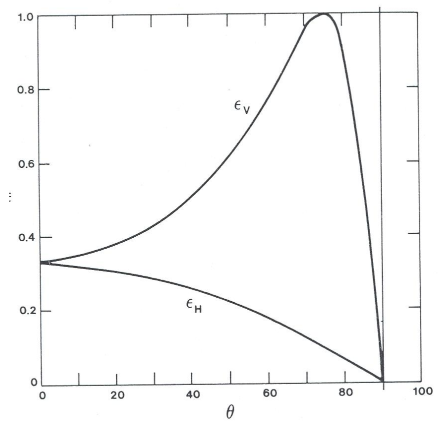

Figure 1.3: Typical shape of the horizontal and vertical emissivity with the incidence angle (from Swift (1980)).

The complex dielectric constant (or permittivity) of the sea water is dependent on temperature and on the concentration of salt. It can be calculated at any frequency, within the microwave band, from Debye (1929) expression:

$$\varepsilon = \varepsilon_\infty + \frac{(\varepsilon_s - \varepsilon_\infty)}{1 + i\omega\tau} - i\frac{\sigma}{\omega\varepsilon_0}, \tag{1.11}$$

in which i is the imaginary number, ε_∞ is the electrical permittivity at very high frequencies, ε_s is the static dielectric constant, τ is the relaxation time, σ is the ionic conductivity, and $\varepsilon_0 = 8.854 * 10^{-12} F/m$ is the permittivity of free space. ϵ_s, τ and σ are functions of the temperature and salinity of sea-water, and have been evaluated by Klein and Swift (1977), Ellison et al. (1998) and Blanch and Aguasca (2004) (these models will be explained later in this document).

Skin depth of sea surface emission

In a conducting medium, a high frequency signal will only penetrate a limited depth into the material. The penetration depth will depend on the frequency of the radiation and on the conductivity of the medium. Thus on the sea, the penetration depth depends on the salinity as well as the frequency. The skin depth δ_s is defined as the distance into the medium at which the power of the electromagnetic radiation is reduced by a factor e^{-2}.

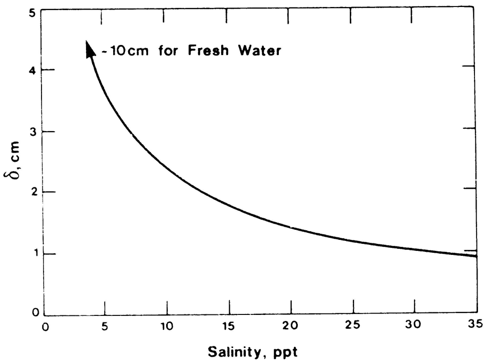

Figure 1.4: Variation of electromagnetic penetration depth with sea-water salinity, at 1.43 GHz and 20°C (from Swift (1980)).

Figure 1.4 shows that as the salinity is reduced the skin depth increases, up to about 10 cm for fresh water. So, for open oceans (approx. 35 psu), the penetration depth at L-band is less than 1 cm, at 20° C.

Radiation received by the antenna

The microwave radiometric measurement is the brightness temperature, which is defined in equation 1.8, as $T_B(\theta,\phi) = e(\theta,\phi)T$ and its sensitivity is proportional to $(B\tau)^{-1/2}$, where B is the bandwidth and τ is the integration time. Hence, for precision radiometry it is desirable to use a bandwidth as large as possible, because for a radiometer on a moving platform the upper limit on τ usually is constrained by the platform parameters (height and speed) as well as antenna beamwidth and scanning configuration.

The *apparent temperature* $T_{AP}(\theta,\phi)$ is the energy incident to the antenna in the direction of the main lobe. The most influent term to T_{AP} is the brightness temperature of the pixel, T_B, at which the antenna is pointing. However other sources are also measured by the antenna; one is the atmospheric self-emission, denoted by T_{UP}. Another source sensed by the antenna is the radiometric temperature scattered by the terrain (T_{SC}) in the direction (θ,ϕ), formed by the addition of two terms: the reflected downward emitted atmospheric radiation (T_{DN}) and the reflected extraterrestrial radiation. The terms emitted by the sea ($T_B + T_{SC}$) are attenuated by the atmospheric loss factor L_a as the energy travels from the terrain to the antenna (see figure 1.5). So,

$$T_{AP} = T_{UP} + (T_B + T_{SC})\frac{1}{L_a}, \tag{1.12}$$

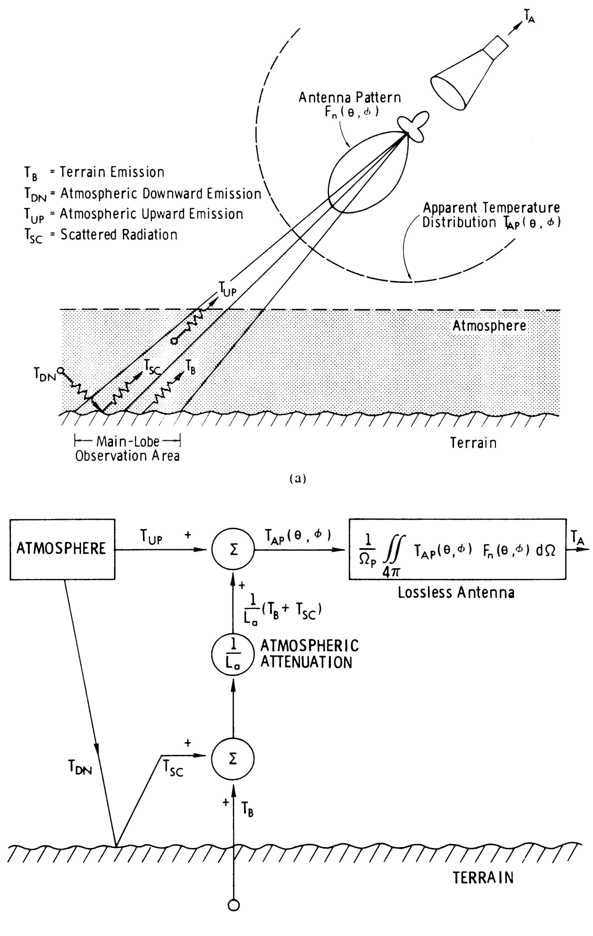

Figure 1.5: a) Schematic representation of the relationship between T_B, T_A and T_{AP}, b) block-diagram representation (from Ulaby et al. (1981)).

and

$$T_A = \frac{A_r}{\lambda} \iint_{4\pi} T_{AP}(\theta, \phi) F_n(\theta, \phi) d\Omega. \tag{1.13}$$

The antenna temperature, T_A, is the integral of the apparent temperature multiplied by the antenna pattern (see equation 1.13), therefore side and back lobes of the antenna pick up energy from other areas that are not the target. The aim of antenna design is to achieve a power pattern having a strong narrow main beam and low side lobes, so that T_A is a good approximation of the average value of T_B.

The power measured by an antenna observing a thermally radiating background can be related to an *antenna temperature*, by using the Rayleigh-Jeans approximation as follows:

$$P = kBGT_A \tag{1.14}$$

where B is the bandwidth of the system and G the gain of the radiometer.

One characteristic of radiometric measurements is that at microwave frequencies the emission is very weak, and the signal received at the sensor is therefore weak, even in some cases, smaller than the receiver's noise power. Also, for this reason, it is necessary to work under frequency bands protected, at least theoretically, against human emissions of any kind, otherwise they would mask the signal to be measured.

Frequently passive microwave systems share frequency allocations with radio astronomy, this is the case of the range of 1.400-1.427 GHz at L-band. Additional frequencies have been allocated for radiometry on a shared bias, but some points of the globe will be inaccessible for their sensing due to radio frequency interference (RFI).

1.3.2 Brightness temperature sensitivity to geophysical parameters

Figure 1.6 shows that sensitivity of the dielectric constant to the salinity is maximum at low microwave frequencies, so the best conditions for sensing salinity from space are found at low microwave frequencies and at protected bands. So, the range from 1.4-1.427 GHz, which holds at L-band, is established for sensing salinity.

However it must be stressed that, even being the best situation, sensitivity of the brightness temperature to the SSS at this frequency, is low: 0.5 K/psu for a sea surface temperature of 20°C, decreasing to 0.25 K/psu for a SST of 0° C,

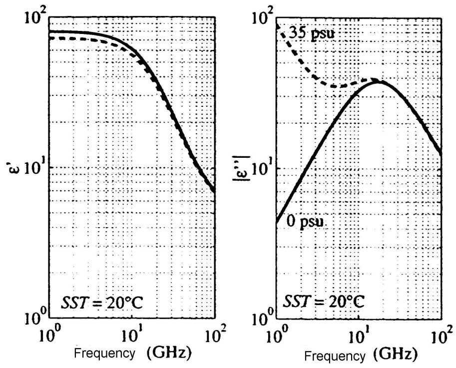

Figure 1.6: Sea water dielectric constant for 35 psu and for pure water, as function of frequency, computed with Klein and Swift (1977) model. On the left, real part of ε, on the right the imaginary part of ε (from Dinnat (2003)).

both at nadir (Skou, 1995, Lagerloef et al., 1995, Lagerloef, 1998). Figure 1.7 shows the sensitivity of T_B to salinity as a function of the incidence angle, and it indicates that the vertical polarisation is about 30% more sensitive to the SSS than the horizontal polarisation.

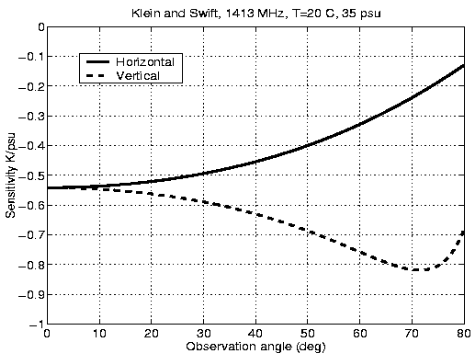

Figure 1.7: Sensitivity to sea surface salinity at L-band.

Figure 1.8 illustrates the resulting variation of brightness temperature for different SST and salinity conditions at L-Band. It shows that the brightness temperature is more sensitive to SSS for warm and more saline waters and that at high salinities the brightness temperature actually decreases as SST increases.

Since other variables than SSS influence the T_B signal (sea surface temper-

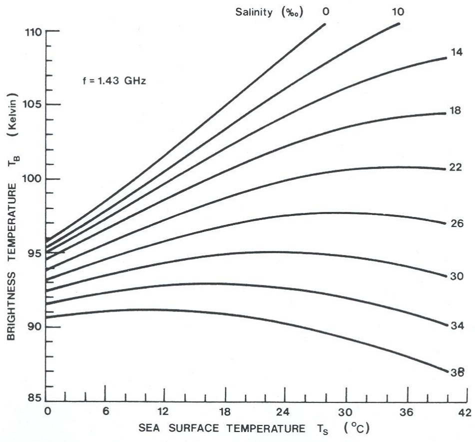

Figure 1.8: Variation of brightness temperature at normal incidence with SST, for different water salinities, at 1.43 GHz (from Swift (1980)).

ature, surface roughness and foam), the accuracy of the SSS measurement will degrade unless these other influencing effects are properly accounted for.

The sensitivity of T_B to sea surface temperature is not slight, and it depends on the salinity concentration and on the incidence angle, the maximum is 0.6 $K/°C$. However, near 35 psu and 25$°C$ it is near to zero.

Experimental data-sets reveal a sensitivity to wind speed extrapolated at nadir of $\backsim 0.23K/(m/s)$, or somewhat higher $\backsim 0.25K/(m/s)$ when the atmospheric instability or only the measurements corresponding to $U_{10} > 2$ m/s are accounted for (Camps et al., 2004a). This sensitivity increases at H-polarisation up to $\backsim 0.5K/(m/s)$ at 65°, and decreases at V-polarisation down to $\backsim -0.2K/(m/s)$ at 65°, with a zero-crossing around 55°-60°. From this information one realises that the effect on T_B of an increment of wind speed of 1m/s, is approximately similar to a change of 1 psu of sea surface salinity.

A modulation of the instantaneous brightness temperatures due to wave slopes (and also foam) has been observed, and makes the standard deviation of this modulation increase with wind speed at a rate of $\backsim 0.1 - 0.15K/(m/s)$, depending on polarisation, and very weakly on incidence angle. Sensitivity of T_B with respect to significant wave height is about $\backsim 1K/m$, extrapolated at nadir, increasing at H-polarisation up to $\backsim 1.5K/m$ at 65°, and decreasing at V-polarisation down to $\backsim -0.5K/m$ at 65°.

In addition, a small azimuthal modulation $\backsim 0.2 - 0.3K$ peak to peak has been observed for low-to-moderate wind speeds. However, very large peak-to-peak modulations of 4-5 K have been also observed during a strong storm, which cannot be predicted with current numerical methods and sea surface spectra. A full analysis of these results is presented in Camps et al. (2004a).

Campaigns data confirm a small, but non-negligible impact of the presence of sea foam on the L-band brightness temperature at wind speeds above 10 m/s. The foam effect could represent an increment on the T_B of about $\backsim 0.2 - 0.3$ K for typical values of 1-2% of foam coverage at $U_{10} \approx 15$m/s (Villarino et al., 2003).

1.3.3 The Stokes parameters

Any plane wave can be decomposed in two orthogonally polarised components, horizontal and vertical polarisations, as follows:

$$E(z,t) = E_h(z,t)\vec{h} + E_v(z,t)\vec{v}, \tag{1.15}$$

and each projection is defined as:

$$\begin{aligned} E_h(t) &= Re\{E_{0h}(t)e^{-j\omega t}\} = E_{0h}(t)\cos(\omega t + \delta_h), \\ E_v(t) &= Re\{E_{0v}(t)e^{-j\omega t}\} = E_{0v}(t)\cos(\omega t + \delta_v), \end{aligned} \tag{1.16}$$

where E_{0h} and E_{0v} are the amplitudes of the $\vec{E}$ field, at H-polarisation and V-polarisation respectively, ω is the instantaneous wave frequency and δ_h and δ_v are the phase factors ($\delta = \delta_v - \delta_h$).

The four Stokes parameters are a very useful way to describe the polarisation state of an electromagnetic wave, even if it is a full polarised, partial or non-polarised wave. The Stokes parameters describe the total energy transported by the wave and the kind of polarisation. Then the Stokes parameters can be defined as:

$$\begin{bmatrix} I \\ Q \\ U \\ V \end{bmatrix} = \begin{bmatrix} T_H + T_V \\ T_V - T_H \\ T_{45^\circ} - T_{-45^\circ} \\ T_{l\,cir} - T_{r\,cir} \end{bmatrix} = \frac{\lambda^2}{kB\eta} \begin{bmatrix} \langle |E_h|^2 \rangle + \langle |E_v|^2 \rangle \\ \langle |E_h|^2 \rangle - \langle |E_v|^2 \rangle \\ 2Re\langle E_v E_h^* \rangle \\ 2Im\langle E_v E_h^* \rangle \end{bmatrix} \tag{1.17}$$

where λ is the radiometer's wavelength, k is Boltzmann constant, B the bandwidth and η is the medium impedance (air).

I represents the total power transported by the wave, Q is the difference between the power brought by the H-pol and the V-pol, and represent the linear polarisation oriented in the reference direction. U represents the linear polarisation component oriented in $+45^\circ$ and -45°. V is interpreted as the difference between left-hand and right-hand circularly polarised brightness temperature.

Both U and V can be measured by two total power radiometers or by a complex correlation radiometer.

If the wave is completely coherent then, $I = Q^2 + U^2 + V^2$, if not, this results in an inequality, $I^2 > Q^2 + U^2 + V^2$. If the wave is completely unpolarised then Q=U=V=0.

Polarimetric radiometers measure the energy coming at H-pol and V-pol separately and they usually use what is called the modified Stokes vector. Expressing energies in terms of brightness temperatures, it results:

$$\vec{T}_B = \begin{bmatrix} T_H \\ T_V \\ T_3 \\ T_4 \end{bmatrix} = \frac{\lambda^2}{kB\eta} \begin{bmatrix} \langle |E_h|^2 \rangle \\ \langle |E_v|^2 \rangle \\ 2Re\langle E_v E_h^* \rangle \\ 2Im\langle E_v E_h^* \rangle \end{bmatrix}. \tag{1.18}$$

Then, it can be defined $T_1 = T_h + T_v$ and $T_2 = T_v - T_h$, that are the equivalent of the first and second Stokes parameters.

1.3.4 Influencing effects on antenna temperature

Several effects external from the instrument can induce errors on the brightness temperature measurements. Yueh et al. (2001) made an exhaustive study of the possible error sources which could effect the accuracy of the salinity retrieved from microwave radiometric measurements. Some of the most important problems are reviewed hereafter.

Faraday rotation

The plane of polarisation of microwave radiation that travels from Earth's surface trough the ionosphere to the satellite is rotated by an angle φ (Faraday rotation). The amount of rotation depends on the position of the ray path with respect to the Earth's geomagnetic field and on the ionospheric electron content.

This rotation is higher for low microwave frequencies, and as SMOS measurements require a great accuracy, this factor should be taken in consideration. An average daytime rotation angle can be calculated as:

$$\varphi = 17^\circ / f^2, \tag{1.19}$$

where f is in GHz, so at L-band the mean rotation angle is 8.7° during daytime, but depending on the hours and the incidence angle, this value can reach 28° (Skou (2003)).

As SMOS will have a 6 a.m. orbit, the Faraday rotation will be between 5 and 10°. Then it will mix the polarisations as follows:

$$T_{Bh}^{F} = T_{Bh}\cos^2(\varphi) + T_{Bv}\sin^2(\varphi),$$
$$T_{Bv}^{F} = T_{Bh}\sin^2(\varphi) + T_{Bv}\cos^2(\varphi). \quad (1.20)$$

This could produce errors on the brightness temperature of the order of 2 K, which results in errors on the retrieved salinity between 2 and 4 psu.

If the first Stokes parameter is used, as shown in equation 1.17, I is the sum of vertical and horizontal polarisations, such as: $I = T_{Bh}^{F} + T_{Bv}^{F} = T_{Bh}(\cos^2(\varphi) + \sin^2(\varphi)) + T_{Bv}(\sin^2(\varphi) + \cos^2(\varphi)) = T_{Bh} + T_{Bv}$, thereby measurements are independent of Faraday rotation.

However, the problem when using this method is that less independent measurements are obtained, half of them, which can lead to less accuracy in the retrieved SSS. This aspect is nowadays under study.

Atmospheric and extraterrestrial sources

As explained briefly in section 1.3.1, atmospheric attenuation and emission affect over-ocean brightness temperature measured at 1.4 GHz.

Equation 1.12 express the apparent temperature observed by the satellite radiometer viewing the earth and considering the atmospheric consequences. Atmospheric effects at 1.4 GH are determined primarily by rain, clouds, water vapour and atmospheric oxygen content (Goodberlet and Miller, 1997).

$T_{UP}(h)$ is the brightness temperature of upwelling atmosphere emission as seen by a downward looking radiometer at altitude (h in km), and it can be approximated by (Ulaby et al., 1981):

$$T_{UP}(h) \approx (0.412h - 0.030h^2)/cos(\theta). \quad (1.21)$$

$T_{SC}(\theta, p)$, which is polarisation dependent, is the brightness temperature scattered by sea surface. It is due to two factors:

$$\begin{aligned} T_{SC}(f,\theta,p) &= R(f,\theta,p)(T_{DN}(f,\theta,p) + T_{EXT}(\theta)) \\ &= [1 - e(f,\theta,p)](T_{DN}(f,\theta,p) + T_{EXT}(\theta)), \end{aligned} \quad (1.22)$$

where T_{DN}, is the downwelling atmospheric emission as seen by an upward looking radiometer at the ocean surface. The calculation of this parameter is described in Ulaby et al. (1981) and at 1.4 GHz it can be approximated to $2.1/\cos(\theta)$ in K.

T_{EXT} is the brightness temperature of extraterrestrial sources, which consists of two terms : $T_{EXT} = T_{COS} + T_{GAL}$.

T_{COS} is referred to as the cosmic background temperature, and it is a remnant of the origin of the universe in a 'Big Bang'. At 1.4 GHz it is essentially constant in both space and time with a value of 2.7 K.

T_{GAL} represents the average emission of our galaxy, the Milky Way. At frequencies above 5 GHz it can be neglected, but at 1.4 GHz until now it was approximated to 1.3 K. However, a recent study by Le Vine and Abraham (2004), shows that at L-band the galactic brightness temperature can be important and that unlike the cosmic background, this radiation is spatially and temporal variable and it is polarised. These authors present a radiometric map of the sky at L-band, and T_{GAL} can vary (over a perfectly reflecting surface) between 1 - 6 K depending on the orientation of the sensor and orbit, and the season. The highest values are observed near the galactic plane. This is an important issue that needs to be deeper analysed for SMOS.

1.4 Microwave radiometer design

The type of instrument that is used to measure the radiation from real materials is normally refereed to as a radiometer, or in this case a microwave radiometer. In this part of the spectrum, the Rayleigh-Jeans approximation is valid, thus the power received by the radiometer is $P = kBGT_A$, where G is the gain of the radiometer and B is the bandwidth of the system.

1.4.1 Real aperture radiometers

The received power is extremely small, so the receiver must be very sensitive. Furthermore, in real life, the noise produced by the radiometer itself (T_N) is added to the input signal. Because the brightness temperature signal is also a noise signal (since it is incoherent radiation) and both signals are independent, they will add and cannot be separated later.

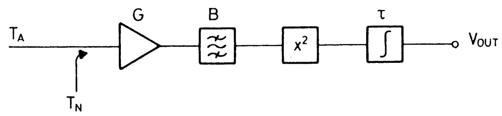

Figure 1.9: Total power radiometer diagram representation (from Skou (1989)).

For the case of a *total power radiometer* (see figure 1.9), $V_{out} = c(T_A + T_N)G$

is totally dependent on T_N and G, and in general, this is not stable enough to satisfy reasonable requirements of absolute accuracy.

The basic radiometer design in remote sensing applications is the *Dicke radiometer*. The principle of this radiometer is not to measure directly the antenna temperature, but rather the difference between this and a known reference value, called T_R (see figure 1.10). Then the sensitivity of the measurement to gain and noise temperature instabilities is greatly reduced. The input of the radiometer rapidly ($F_s = 1000Hz$) switches between antenna temperature and a reference load which is known.

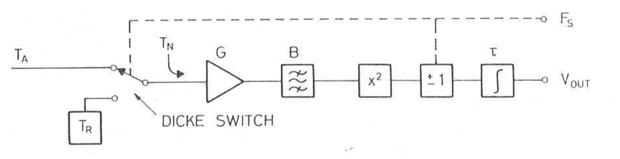

Figure 1.10: Dicke radiometer diagram representation (from Skou (1989)).

Then the output of the radiometer is given by the following expression:

$$V_{out} = c(T_A - T_R)G \tag{1.23}$$

Here T_N is eliminated, but G is still present, while with less weight, since T_R is in the same range as T_A. This configuration gives less sensitivity to instabilities, but poorer sensitivity is achieved, since half of the measurement time is spent on the antenna signal. The sensitivity is degraded by a factor of 2 as compared with the total power radiometer.

The *noise-injection radiometer* (NIR) represents another step forward for better accuracy, since the output is independent of gain and noise temperature. This radiometer is a specialisation of a Dicke radiometer in which the output is always zero, controlled by a servo loop.

Figure 1.11 shows that this configuration uses a Dicke radiometer, with the difference that the input signal to the Dicke radiometer is $T'_A = T_A + T_I$, where T_I is the output of a variable noise generator, and that T'_A (the input to the Dicke radiometer) has the same value as the reference temperature T_R, and a zero output results. A servo-loop adjusts T_I to maintain the zero output condition. So the output value is independent to the gain, as follows:

$$V_{out} = c(T'_A - T_R)G = 0 \tag{1.24}$$

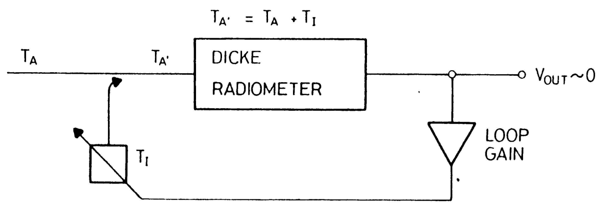

Figure 1.11: Noise-Injection radiometer diagram representation (from Skou (1989)).

$$T_A = T_R - T_I \tag{1.25}$$

The sensitivity of the noise-injection radiometer is found using:

$$\Delta T = 2\frac{T_R + T_N}{\sqrt{B\tau}} \tag{1.26}$$

More information can be found in Ulaby et al. (1981).

1.4.2 Synthetic aperture radiometers

When dealing with real aperture radiometers, the angular resolution can be described in a rough approximation (since it depends on antenna design and on gain) as $\beta = \lambda/D$ radians, where D is the diameter of the antenna. Thus the required antenna size for a given footprint d is $D = \lambda h/d$. Therefore, at L-band ($\lambda = 21$ cm), a radiometer flying at 700 km would need an antenna of 5 m in diameter to have a 30 km footprint, thus an antenna of such dimensions is complicated to put in orbit.

By using interferometric radiometers, this problem is solved. This technique uses many small receivers, that measure the phase difference of the incident radiation. By cross-correlating the radiofrequency (RF) signals received by each pair of antennas that have an overlapping FOV, a two-dimensional image is created. In this way a big antenna is "synthesised"simulated, and a high angular resolution is achieved.

Real aperture radiometers image the brightness temperature by scanning their antenna across the field of view (FOV). The resolution of the image is consequently determined by the beamwidth of the antenna. Interferometric imaging radiometers, on the other hand, generate an image indirectly by measuring the Fourier transform of the brightness temperature distributed over the FOV.

This measurement is refereed as the visibility function and is, afterwards, inverse Fourier transformed to form the image.

SMOS will be the first satellite that will carry a 2-D synthetic aperture radiometer at L-band. Only the synthetic aperture technique allows a reasonable spatial resolution measurement.

For more information about 2-D synthetic aperture technique refer to Camps (1996) and Ruf (1988).

1.5 Previous salinity missions and campaigns

During nearly 40 years, several campaigns and studies have been carried out to investigate the possibility of measuring sea surface salinity from radiometric acquisitions. Here we make a short presentation of some of these scientific studies, split into three different kinds of platforms used.

1.5.1 Fixed-based platforms

A fixed ocean platform provides the advantages of high spatial resolution on sea surface, excellent ground truth, and a relative ease of radiometer calibration and determination of antenna characteristics as compared to an aircraft platform. In addition, there is not a need for correcting atmospheric losses between the antenna and the sea.

Argus Island Tower measurements - Hollinger

The measurements described by Hollinger (1971) were made from Argus Island tower at 1.41, 8.36 and 19.34 GHz, in March 1970. Argus Island is located approximately 45 km south-west of Bermuda at 60 m of water depth. The microwave radiometers consisted of a parabolic antenna and linearly polarised feed system followed by a conventional Dicke receiver. Since the antennas were able to rotate around their electrical axes, any plane of linear polarisation could be measured, so the vertical and horizontal components were acquired. Measurements were made at a series of incremented incidence angles (5-10 degrees). The absolute error in antenna temperature and the relative errors in the brightness temperature were about $\pm 2K$. The absolute errors on the brightness temperature were about 5 to 10 percent.

The conclusions from Hollinger's paper are that observations of microwave brightness temperature of the sea showed a definite dependence on wind speed.

The work affirms that this dependence is due to roughness effects of the surface associated with wind-driven waves, and that it is frequency dependent.

Cape Cod Canal measurements - Swift

C. T. Swift and his team carried out several measurements during a nine-month period, in 1972, at the Cape Cod Canal in Massachusetts (Swift, 1974). A four-frequency microwave radiometer system was installed on a railroad bridge over the Canal, and several ground truth sensors were installed to correlate radiometric data with environmental changes. The antennas operated at frequencies of 7.5, 4.0, 1.4 and 0.75 GHz, performed elevation scans from -23° to 162° with steps of 3° or 6°, and measured the horizontal and vertical brightness temperatures.

The measurements showed that sea surface roughness causes a general increase in the horizontally polarised component of the brightness temperature of about 3 to 9 K, that is weakly dependent on the viewing angle and frequency. Also they observed that for vertical polarisation at 60° the brightness temperature is independent of roughness.

The author presents, also, measurements of specular reflection and scattering of the sunlight. He also explains that foam streaks which, were swept through the beams of the antennas, caused no measurable increase in the brightness temperature, even though he mentions that it is in contradiction with other authors results.

1.5.2 Airborne

Airborne campaigns provide the advantage of performing long distance measurements, allowing the detection of salinity fronts and other spatial variations.

Chesapeake Bay Measurements - Blume

On 24 August 1976, an L and S-band radiometer system (built by NASA Langley Research Center) was installed on one NASA C-54 aircraft and operated in a flight from NASA Wallops Flight Center over the lower part of Chesapeake Bay and adjacent Atlantic Ocean (Blume et al., 1978). This area was selected because the mixing of fresh and salt water results in strong salinity gradients. Some sea truth data were obtained from several locations in the measurement area. Whereas the S-band radiometer was a superheterodine type, the L-band radiometer was a direct-type receiver.

Sea conditions for the measurements were fairly calm with a 3.5 m/s surface wind. The airplane flown at 1.4 Km height and all measurements were nadir observations. The radiometric data were corrected for cosmic and galactic radiation, atmospheric effects and antenna-beam efficiency, but no correction for surface roughness due to wind speed at L-band was included, since they believed it was negligible at this frequency. Some comparison was made between salinity obtained from radiometric measurements and ground truth for several points, and the mean deviation was 0.5 psu with a standard deviation of 0.91 psu.

SLFMR

The Scanning Low Frequency Microwave Radiometer (SLFMR) - also known as salinity mapper- is a 1.4 GHz radiometer designed and built for the National Oceanic and Atmospheric Administration (NOAA). SLFMR has 6 beams located across the flight track, and are oriented at 39°, 22° and 7° off nadir on each side of the plane. The aircraft also carries an infrared radiometer to measure sea surface temperature with a beamwidth equal to the SLFMR.

The system was completed in June 1993 and in August it was mounted on the VIMS aircraft and flown over areas around the southern part of the Chesapeake Bay. The general performance of the system was good, however the data collected by the SLFMR suffered from contamination from man-made Radio Frequency Interference (RFI). Further flights in the same area encountered the same levels of RFI which made impossible to retrieve salinity from radiometric measurements. Afterwards, SLFMR was flown over Delaware Bay, in an attempt to escape from the high RFI. Here, it was experienced annoying, but tolerable amount of RFI at the flight altitude of 609 m. The average difference between the time series of salinity derived from SLFMR and in situ data was less than 1 psu, after applying a 9 point running average to the SLFMR measurements (Miller et al., 1998).

ESTAR

Electronically Scanned Thinned Array Radiometer (ESTAR) was the first prototype built to test a new technology being developed for passive microwave remote sensing: aperture synthesis. This approach permits substantial reduction in the antenna aperture needed for a given spatial resolution.

The radiometer was developed as part of cooperative research at the NASA Goddard Space Flight Center, the University of Massachusetts, and the USDA Agricultural Research Service in Beltsville.

It is an L-band hybrid real-and-synthetic aperture radiometer that employs real aperture antennas to achieve resolution along track and uses aperture synthesis to achieve resolution in the across track dimension (more information in Le Vine et al. (1994)). ESTAR is a H-polarisation radiometer and was designed for the remote sensing of soil moisture.

A series of measurements called the Gulf Stream Experiment were conducted during summer 1999. The ESTAR radiometer (H-pol) and the SLFMR (V-pol) were placed on NASA P-3 Orion aircraft. Also a C-band radiometer, a scatterometer, and an infrared radiometer were installed in the plane. Surface salinity measurements were provided by thermosalinographs and surface drifters deployed by research vessels. Salinity retrieved with ESTAR was in good agreement with the salinity measurements from the vessels. Similar results were obtained with SLFMR.

PALS

The Jet Propulsion Laboratory (JPL) designed and built a Passive/Active L/S-band (PALS) microwave airborne instrument to measure ocean salinity and soil moisture. The instrument requirements were determined to allow salinity measurements to be made with an accuracy of 0.2 psu over open ocean. This instrument has dual-frequency, dual polarisation radiometers and polarimetric radar sensors, and was installed in a NCAR C-130 aircraft. The antenna is a high beam efficiency conical horn with relatively low sidelobes pointed at 38° incidence angle (Wilson et al. (2001)). The instrument is non-scanning, thus a single-footprint track is sampled along the flight path. An IR temperature sensor was used to measure the changes in sea surface temperature.

The first set of ocean measurements were made in July 1999, southeast of Norfolk VA. over the Gulf Stream, and out into the open ocean. The surface truth measurements of SSS, SST and surface winds were gathered by a ship from Duke University. Measurements demonstrated that PALS is a radiometer with an absolute accuracy <2 K, and a relative stability of $\backsim 0.2$ K over a few hours. A sudden decrease of 0.2 K measured in the brightness temperature corresponded to the salinity increase of 0.4 psu measured by the vessel.

Other experiments were carried out in the summers of 2000 and 2002, and the plane performed seven flights over a buoy off the California coast near Monterey bay. A research ship performed some *in-situ* measurements.

In October and November 2001, PALS radiometer brightness temperature measurements were made from a saltwater pond over a temperature range from 8.5 to 32 °C and salinity from 25 to 40 psu (Wilson et al. (2004)). The study shown that Klein and Swift dielectric model had the best agreement with the saltwater pond data (RMS<0.1 K, which corresponds to a salinity error of <0.2 psu); however, all the models had RMS differences within 0.3 K.

These campaigns were in support of the development of ocean surface salinity remote sensing techniques for the future Aquarius space mission from NASA.

1.5.3 Spaceborne

Experiment S-194 on Skylab.

An L-band radiometer (Experiment S-194) was mounted on the NASA Skylab spacecraft and was used to remotely determine soil moisture over various types of terrain, and sea surface salinity content of sea water.

The spacecraft was launched in May 1973; the NASA manned mission extended through February 1974. The Skylab orbit included a mean altitude and inclination of 439 Km and 50 degrees, respectively. In addition, a 5-day repeating orbital period of 93 minutes each was achieved at an altitude velocity of 7.65 km/s.

The L-band radiometer was mounted on the spacecraft's exterior surface to provide a nadir ground footprint of 115 Km. Scientific data was digitally recorded on magnetic tape and subsequently returned to Earth by the on board manned crew.

A self-calibration, Dicke-switched radiometer was developed for reliable unattended operation in deep space, and a fixed planar array antenna oriented towards nadir was used to provide a low-loss and high efficiency transducer with controlled beamwidth characteristics.

The radiometer exhibited temperature sensitivities of less than 0.5 K, and accuracy better than 0.7 K at a source temperature of 296 K for an RF bandwidth of 27 MHz and an integrating time of 1s. In addition, long-term drift was measured to be less than 0.2 K (Flattau et al., 1976).

Table 1.1 summarises the measurements performed until now with L-band radiometers. Some of the campaigns will be largely explained in next chapter.

1.6 Current satellite salinity missions

Currently two space missions are in progress to measure sea surface salinity (SSS) from space. The first one is a mission from the European Space Agency, SMOS, which was approved in 1999 and the launch is planned for 2007. The second mission is AQUARIUS, from NASA, which is planned to be launched in 2008. The nominal life time for both is 3 years, so more than one year of tandem mission will be possible.

1.6.1 SMOS

In 1999, the European Space Agency (ESA) selected the Soil Moisture and Ocean Salinity (SMOS) mission as an Earth Explorer Opportunity mission (Sivestrin

Campaign/author	year	Meas. Conditions	Incidence angles	polarisation
Hollinger	1971	platform	20°-65°	H & V
SKYLAB	1974	Spaceborne	0°	H & V
Swift	1976	bridge on canal	25°-55°	H
Blume	1976	airborne	0°	H & V
Webster et al.	1976	airborne	0°	linear
SLFMR-NOAA	1993	airborne	7°-39°	V
ESTAR/SLFMR	1999	airborne	0°-60°/7°-39°	H &V
JPL-PALS	1999	airborne	40°	H&V
WISE	2000/2001	platform	25°-65°	H&V
EuroSTARRS	2001	airborne	0°-75°	V
LOSAC	2001/2003	airborne	22°-52°	4 stokes
PLATA	2003/2004	airborne	7°-39°	V

Table 1.1: Available L-band radiometric data.

et al., 2001, Font et al., 2000). This intended to be a very cost-effective space mission, implemented on short time-scales. SMOS will be launched on February 2007, if no delays occur, and it will have a nominal duration of 3 years (5 expected).

The goal of the SMOS mission is to observe two key parameters, which have never been measured by satellite before: Soil moisture (SM) over land, and sea surface salinity (SSS) over the sea by means of an L-band (1.400-1.427 GHz) microwave imaging radiometer. SMOS will contribute also to the research of the cryosphere, through the assessment of the snow mantle and of the multi-layered ice structure.

SMOS aims at providing, over the open ocean, global salinity maps with an accuracy better than 0.1 psu, every 30 days and 200 x 200 km spatial resolution; over land surfaces, global maps of soil moisture, with an accuracy better than 4% every 3 days with a space resolution better than 60 Km, as well as vegetation water content with an accuracy of 0.2 kg/m^2 Font et al. (2003b).

SMOS will fly in a sun-synchronous (6 a.m. ascending), near-circular, 755 km altitude orbit, with a revisiting time between 1 and 3 days. The satellite will be put in orbit with a Russian Rockot launcher, and will be carried on a standard 'spacecraft bus' called PROTEUS developed by the French Space Agency, CNES. The total mass of SMOS is 683 Kg.

SMOS is a demonstrator mission, with ambitious scientific objectives, based in an innovative approach and concept: the use of an L-band 2-D interferometric polarimetric radiometer, called MIRAS (Microwave Imaging Radiometer by Aperture Synthesis).

This novel measuring technique permits to SMOS to be the first ever spaceborne mission that will provide global maps of soil moisture and ocean salinity.

Instrument characteristics

MIRAS (Microwave Imaging Radiometer with Aperture Synthesis) is a synthetic aperture radiometer that allows measuring T_B over a large range of incidence angles, for two polarisations (Martín-Neira and Goutoule, 1997). It consists of a central structure with three deployable arms in a Y-shape (see figure 1.12a). Each arm has a longitude of 3.36 m, and carries 21 receivers, within a spacing of 0.88λ. MIRAS has 69 L-band receivers in total (see figure 1.12b).

The antenna will view an area of almost 3000 km in diameter. However, due to the interferometric measurement principle, the Y-shape antenna and the spacing between antenna elements, the field of view is limited to an hexagonal shape area of about 1000 km across (see figure 1.12c). This shape is due to the aliasing effect, which is presented when ambiguities are detected in the measurement of the phase differences.

The nominal spatial resolution is 50 km (35 km at the FOV centre) for a circular orbit of 755 km and 32° tilt angle. At boresight the radiometric resolution for each polarisation will be about 2.4 K (for 1.2 sec integration time), degrading out-of-boresight.

EADS-CASA Espacio, Spain, is the prime contractor for MIRAS. The antenna-receivers, also called LICEF, are developed at MIER S.A., Catalonia, Spain. They use multi-layer 'microstrip' technology to achieve best performance in terms of gain, bandwidth and differentiation of horizontal and vertical polarisation components. Each LICEF antenna weights 190 g, is 165 mm in diameter and is 19 mm high.

MIRAS can operate in two measurement modes - dual-polarisation or full-polarimetric mode. The baseline is the dual-polarisation mode, where all the LICEF antennae will be switched between horizontal and vertical measurements, thus permitting the measurement of the horizontal and vertical components of the received microwaves. In addition, the full-polarimetric mode has been implemented to acquire both polarisations simultaneously. The advantage of this enhanced mode is that it provides additional scientific revenue, however, the amount of data that has to be transmitted to the ground is doubled. Only in-flight experiences will show whether the dual-polarisation mode satisfies the scientific mission objectives, or whether MIRAS will be continuously operated in the more demanding full-polarimetric mode.

Receiver parameters are sensitive to temperature and ageing. Therefore, they need to be regularly calibrated in flight to ensure that the mission required accuracy is met. Several times per orbit an internal calibration system injects a signal of known characteristics into all the LICEF receivers (they are total power radiometers). In addition, every 14 days an absolute calibration with deep space or celestial target of known signal strength will be performed, requiring the satellite to perform specific attitude manouvers.

The radiation emitted by the Earth is measured by each antenna-receiver and transmitted later to a central correlator unit, which performs all the cross-correlations of the signals between all possible combination of receiver pairs. By performing the pre-processing on-board, the amount of data that has to be transmitted to the ground is greatly reduced.

The satellite position and its orientation need to be known at each moment, to properly geo-locate ground targets. These data will be provided by a GPS receiver and by star trackers.

The information will be stored in memories, and transmitted to the ground by a X-band downlink every time the ground station is seen by the satellite.

Multi-angular capability

Thanks to the large field of view of SMOS, as the satellite moves along its orbital path each pixel is observed under several incidence angles, which range from $0°$ to $55°$ approximately (see figure 1.12d). This feature is very important, since each snap shot (every 0.3 s) will be independent from the others, so the observations of a pixel from different incidence angles will be independent. This is crucial for the development of new and more efficient retrieval methods (Camps et al., 2002b). Latter, several spatial and temporal averaging can reduce the noise of the measurements.

For each satellite overpass, the spatial resolution of SMOS varies between 30-60 km, and the expected accuracy of SSS is about 1 psu.

The Global Ocean Data Assimilation Experiment (GODAE), a pilot experiment set-up by the Ocean Observations Panel for Climate, aims to demonstrate the feasibility and practicality of real-time global ocean data modelling and assimilation systems, both in terms of their implementation and their utility (Smith and Lefebvre, 1997). Following the recommendations of the Ocean Observing System Development Panel, the proposed GODAE accuracy requirement for salinity retrieved from satellite data is specified as 0.1 psu for a 10 day and $2^\circ \times 2^\circ$ resolution requirement for global ocean circulation studies. Considering the exploratory nature of SMOS, the GODAE requirement represents a technically challenging objective. It will be possible to average data over 30 days or longer periods for many climate studies and thereby further reduce of the random measurement noise. Monthly averages over 100 km boxes would provide data comparable to the standard climatologies (Levitus et al., 1994). Lower accuracy, higher resolution measurements (typically 0.5 psu, 50 km, 3 days) provide a means to monitor salinity fronts in various regions.

SMOS expects to meet, in some cases, the GODAE requirements, so having SSS measurements with an accuracy of 0.1 psu, for 10 days and over boxes of 200×200 km boxes. For that a large averaging in time and space is needed.

Auxiliary data problem

To retrieve SSS from radiometric measurements other parameters, not measured by SMOS, are needed. The most important are: SST, wind speed, and maybe significant wave height. These parameters, called auxiliary parameters, must be known with good accuracy, since the sensitivities of T_B to them are similar to or larger than the sensitivity to SSS.

In most occasions the SMOS satellite overpasses will not coincide with other satellite sensors sampling the parameters needed. Also numerical and diagnostic models will probably not give a value for the time and position of SMOS acquisition. Under such circumstances, maybe the auxiliary parameters should be estimated somehow in the SSS retrieval algorithms using combined information.

Part of the work presented here is focused on studying how to obtain these auxiliary parameters data, the impact of errors on them to the retrieved salinity, and to analyse which is the best method to be used by the SMOS processing chain.

1.6.2 AQUARIUS

Aquarius is a NASA/Earth System Science Pathfinder (ESSP) mission focused in measuring global Sea Surface Salinity. The mission science goals are to observe and model the processes that relate salinity variations to climatic changes in the global cycling of water, and to understand how these variations influence the general ocean circulation.

The goal of Aquarius is to provide global observations of SSS, covering the Earth's surface once every 8 days, and to deliver monthly 100 km resolution SSS maps with an accuracy of 0.2 psu.

The instrument, built by NASA, consists of three real aperture L-band polarimetric radiometers and a scatterometer at 1.26 GHz, which will measure the sea surface roughness, a crucial variable to retrieve salinity. The size of the deployable antennas is 3 m x 6 m x 4 m. The footprint sizes are: 62-68 km, 68-82 km and 75-100 km. The spacecraft (SAC-D) will be contributed by Argentina's Comisión Nacional de Actividades Espaciales (CONAE).

In September 2008, Aquarius will begin its 3-year mission on a Delta II rocket launched from Vandenberg Air Force Base in California. The science instrument will be carried into a 600 km sun-synchronous orbit, with revisit time at 6 am/6 pm polar orbit. CONAE will conduct operations, provide command capability and receipt of telemetry and scientific data.

Other instruments on board the SAC-D are: the New InfraRed Scanner Technology (NIRST) camera; the K-band radiometers, which will provide complementary surface temperature measurements, surface winds, rainfall and characteristics of sea ice; and a high sensitivity Optical Camera and the Data Collection Transceptor complete the set of Argentine instruments that shall be designed and built by CONAE with the participation of other scientific organisations in the country. Other possible contributions are: the LAGRANGE instrument of the Italian Space Agency (ASI), devoted to observations of GPS satellite occultations in order to supply information about the atmosphere temperature, pressure and water vapour pressure contents and the SODAD instrument of the French Centre National d'Etudes Spatiales (CNES), for the measurement of the properties of micrometeorites and space debris (more information in http://aquarius.gsfc.nasa.gov/).

Many projects have been carried out during the period 2000-2003 to increase our knowledge of the salinity retrieval from L-band measurements, and especially the effects of the different geophysical factors in this retrieval. Several studies and field experiments have been conducted, including those sponsored by ESA during the SMOS extended phase A, by national agencies in Europe, and in the USA in support of the Aquarius/SAC-D mission. Significant progress has been made in many aspects of the problem. Font et al. (2004) makes a review on the clarifies aspects and also the ones which still unclear.

1.7 Objectives and thesis plan

The objective of this thesis is to analyse several aspects of the SSS retrieval process which are still unclear, using several campaign datasets and the SMOS End-to-End Performance simulator. This study is a first step to clear up some of the open questions of the SMOS processing chain.

The thesis treats the emissivity modelling aspect by explaining the different forward models necessary to describe the emissivity of the sea. Latter the state of the art of them is exposed and compared. A new model derived by the author is presented.

The thesis also approaches the problem of the auxiliary parameters. A study of the impact on the retrieved salinity of auxiliary parameters errors has been performed and some possible sources for the roughness parameters has been tested. Finally a new method less sensitive to auxiliary parameters errors, and developed by the author, is exposed.

The thesis organisation is as follows:

- **Chapter 2** presents the field campaigns whose data have been used to perform the study. The first two are largely explained and results exposed, since the author participated very actively in the preparation and results analysis. Other campaigns are shortly described.

- **Chapter 3** describes some of the emissivity models that are best accepted in the literature. A new model derived from campaign measurements that is proposed by the author, is presented in this chapter.

- **Chapter 4** introduces some possible sources of auxiliary parameters that can be used for retrieving SSS from campaign measurements. Their temporal and spatial resolutions are exposed, and a comparison of them in a specific period and area is done.

- In **Chapter 5** the salinity retrieval process from radiometric measurements is performed. First the emissivity models are studied, and results are compared. Secondly different auxiliary sources are tested. A new method for obtaining these auxiliary data is proposed.

- **Chapter 6** uses the SMOS End-to-End Performance simulator to address the same problems that have been addressed in the above chapter by using real data.

- **Conclusions** on the issues investigates are exposed. Some recommendations are done for SMOS Level 2 retrieval process, and future works are suggested.
- **Appendix A** presents a list of articles and communications on congresses that have been derived from this work. Two peer review articles performed by the author are attached.
- **Appendix B** reviews the inversion methods used in this thesis.
- **Appendix C** presents technical documentation of instruments used in the campaigns where the author has participated.

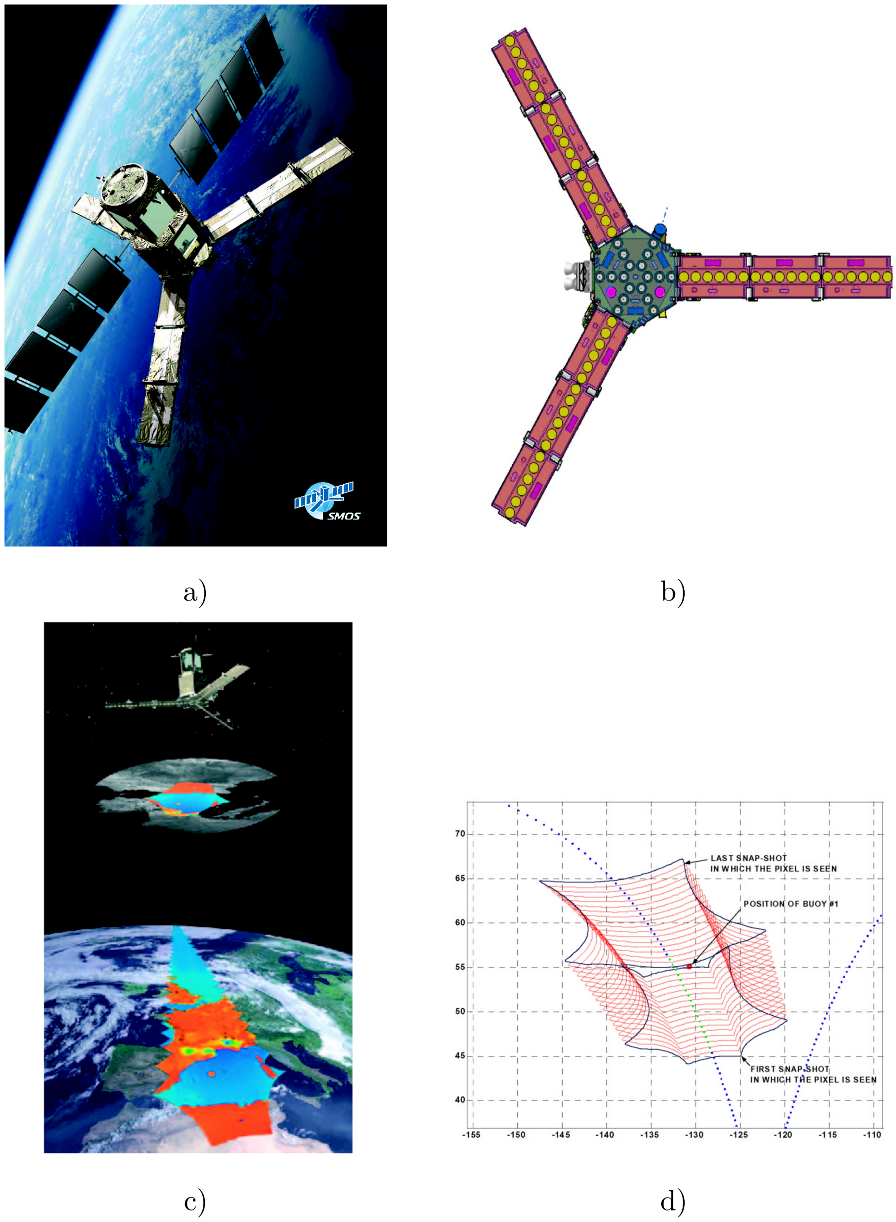

Figure 1.12: a) Artist's view of SMOS (from ESA Medialab). b) Proposed design of the Y-shaped MIRAS radiometer with 18 receivers per arm (from EADS-CASA). c) Field of view of SMOS (from ESA Medialab). d) A single spot (e.g. a buoy) is seen in successive snapshots under different angles and spatial and radiometric resolutions depending on its position within the instrument alias-free field-of-view (from Camps et al. (2002a)).

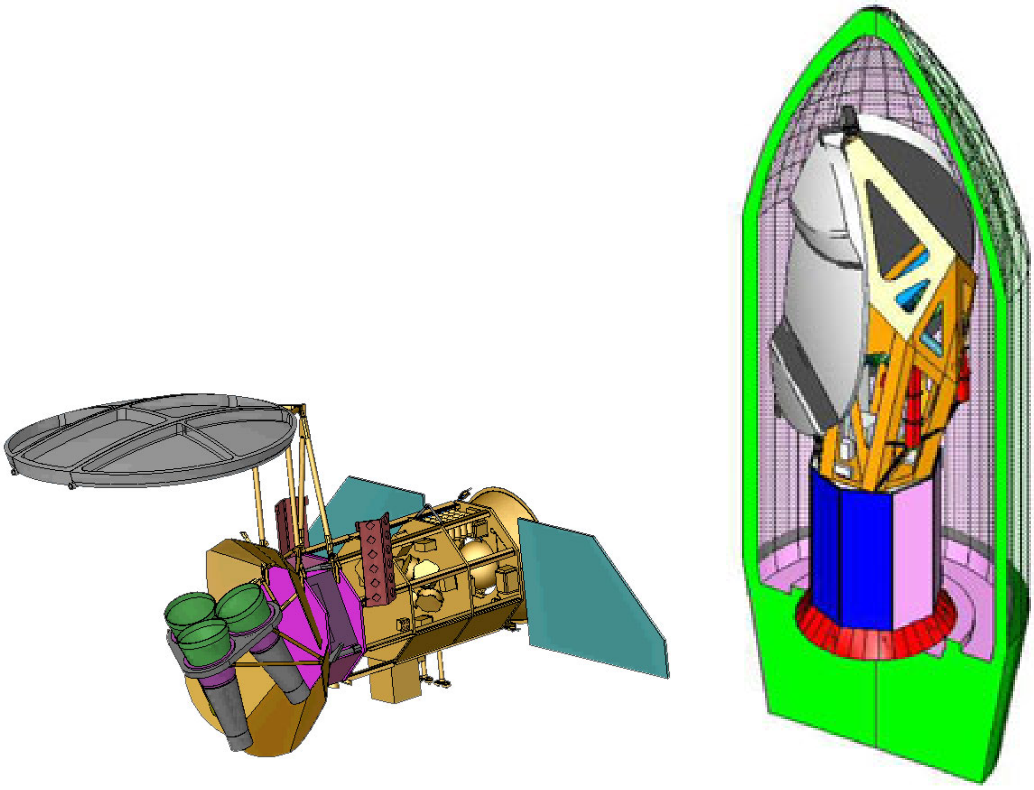

a) b)

Figure 1.13: a) SAC-D/Aquarius aircraft. b) Aquarius folded into the rocket.

Chapter 2

Campaigns

Several dedicated campaign activities were conducted during the feasibility and design phase of the SMOS mission.

WISE 2000 and 2001 were carried out at an oil rig in the North West Mediterranean to examine the relationship between the radiation emitted from the sea surface at L-band under varying sea-state conditions as a result of different wind speeds and direction, different wave types, and varying foam coverage.

EuroSTARRS was an aircraft campaign that carried an L-band radiometer. It was flown over the oil rig area, when WISE 2001 was going on. EuroSTARRS had a similar acquisition as SMOS, and the objective was to measure the influence of some meteorological and oceanographic effects on the measurement of ocean salinity.

FROG 2003 experiment was addressed to understand the effect of foam and rain on the L-band emissivity measurements.

Finally the Plata campaign, consisted in a ship and an airborne survey that was performed at the La Plata river mouth area, were strong gradients on salinity are encountered (South Atlantic).

These campaigns and their results are largely explained in this chapter, since this experimental data is the basis of most of the work done during this thesis. The author has considered that an exhaustive explanation of the experimental campaigns and it results is essential to estimate the quality of the results obtained in this work.

Since 2000, the author of this thesis has been working very actively on the preparation, execution and data processing of the WISE and EuroSTARRS campaigns. Those activities had a very long duration (around 1.5 years), so it has been considered that a detailed explanation of them was required in this document.

On the other hand, the author did not participate in the FROG campaign neither la Plata preparation, but their data have been used.

Therefore this chapter has been divided in two sections. The first one will explain, describe and show the results of the two campaign in which the author participated actively. The second section will present the campaign in which the author has not been working, but data has been used in the thesis. Of course the first part will be exposed in much more detail.

2.1 Campaigns with active participation of the author

2.1.1 WISE

The determination of the L-band brightness temperature sensitivities to wind speed and their azimuthal variation were addressed through two ESA-sponsored joint experimental campaign called WISE (WInd and Salinity Experiment) involving 6 research teams from Spain (Universitat Politècnica de Catalunya, Institut de Ciències del Mar - CSIC, and Universitat de València), France (Laboratoire d'Océanographie Dynamique et Climatologique, and Centre d'Études Terrestres et Planétaires), and the USA (University of Massachusetts, as a guest institution during WISE 2000).

The WISE 2000 and 2001 campaigns took place at the Casablanca oil rig, located at 40°43.02' N 1°21.50' E, 40 km away from the Ebro river mouth at the coast of Tarragona, Spain. The sea bed is at 165 m depth, and the sea conditions are representative of the Mediterranean shelf/slope region with periodic influence of the Ebro river fresh water plume. WISE 2000 data acquisition spanned from November 25th, 2000 to December 18th, 2000 and from January 8th, 2001 to January 15th, 2001, and WISE 2001 from October 23rd, 2001 to November 22nd, 2001.

The following instruments were deployed: a fully polarimetric L-band radiometer (UPC, Fig. 2.1a), a fully polarimetric Ka-band radiometer (UMass, Fig. 2.1b, only in WISE 2000), four oceanographic and meteorological buoys from ICM and LODYC (Figs. 2.1c, 2.1d, 2.1e and 2.1f; buoy 3 get damaged during mooring in WISE 2000), a portable meteorological station (UPC), a stereo-camera from CETP (Fig. 2.1g) mounted on a handrail and pointing to the North during WISE 2000 and to the West during WISE 2001 to provide sea surface topography and foam coverage, a video camera from UPC mounted on the antenna pedestal (Fig. 2.1a), and a CIMEL infrared radiometer from UV to provide SST estimates mounted on the antenna pedestal during WISE 2000, and on a handrail and pointing to the West during WISE 2001. Additionally, satellite imagery and water samples were acquired.

Figures 2.2a and 2.2b show the location of the instrumentation during WISE 2000 and WISE 2001, respectively. In WISE 2000 the radiometers and the stereo-camera were pointed to the North, in the direction of the dominant winds. However, due to the RFI (Radio Frequency Interference) coming from Tarragona city and probably the Barcelona airport, in WISE 2001, the instrumentation was pointed most of the time to the West, except in the afternoon-evening were it was pointed to the North-East to avoid the Sun. The microwave radiometers and the video camera were mounted on a special terrace built to install the radiometers at the 32 m deck that allowed performing an azimuth scan from 80 W to 40 E and an elevation scan from about 25 incidence angle to an elevation of 140°(when pointing to the zenith the radiometer collected radiation from upper floors and the helipad). The IR radiometer was mounted on the radiometer pedestal during WISE 2000, and on a handrail at the 28 m deck during WISE 2001. The stereo-camera was mounted on a handrail at the 28 m deck. The control room was, also, at the 28 m deck. Figure 2.2c shows a picture of the North side of the Casablanca oil rig indicating the position of the L-band radiometer. The instrumentation deployed is described below:

- L-band Automatic Radiometer (LAURA): The UPC L-band AUtomatic RAdiometer is a fully polarimetric radiometer (Fig. 2.1a) designed and implemented in the facilities of the Department of Signal Theory and Communications (TSC) of the Polytechnic University of Catalonia (UPC) (Villarino et al. (2002)). The antenna is a 4 x 4 microstrip patch square array, with a half-power beamwidth of 20°, measured side lobe levels at E- and H-planes of -19 dB and -25 dB, respectively, a cross-polarisation smaller than -35 dB in the whole pattern, and smaller than -40 dB in the main beam, and a main beam efficiency (MBE) of 96.5% defined at the side lobe level. The antenna pedestal was oriented by computer controlled step-motors and gear-reductions, and the antenna elevation was measured by means of a Seika inclinometer mounted on its back with a resolution $<0.01^{o}$ with a $\pm 70^{o}$ angular range. The radiometer architecture is based on 2 homodyne L-band receivers with I/Q down-conversion. Receiver inputs can be switched between three inputs: (i) the H and V antenna ports and (ii) two matched loads, or (iii) a common noise source. The in-phase components of both channels are connected to two power detectors. The Dicke

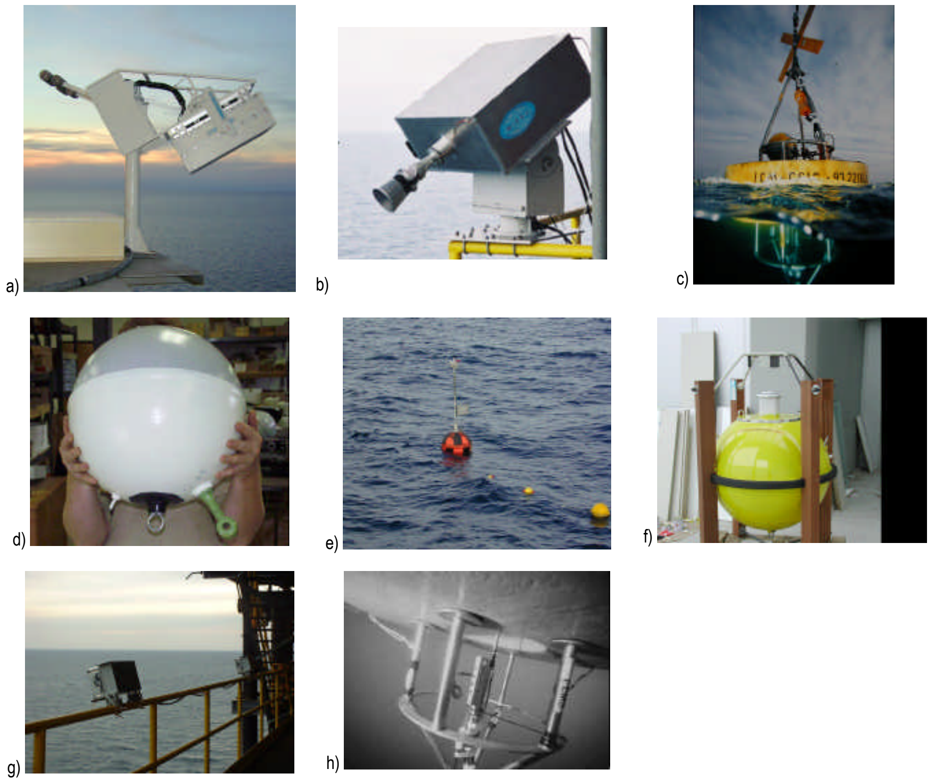

Figure 2.1: Instrumentation deployed during WISE 2000 and 2001: a) L-band polarimetric radiometer (UPC), video camera (UPC) and IR radiometer (UV), b) Ka-band polarimetric radiometer (UMass, only in WISE 2000), c) EMS buoy (buoy 1, ICM), d) Clearwater SVP buoy (buoy 4, LODYC), e) Aanderaa CMB3280 buoy (buoy 2, ICM), f) Datawell wave buoy (buoy 3, LODYC), g) pair of stereo-cameras (CETP), and h) underwater view of the CTD recorder in buoy 1 to sample near-surface salinity.

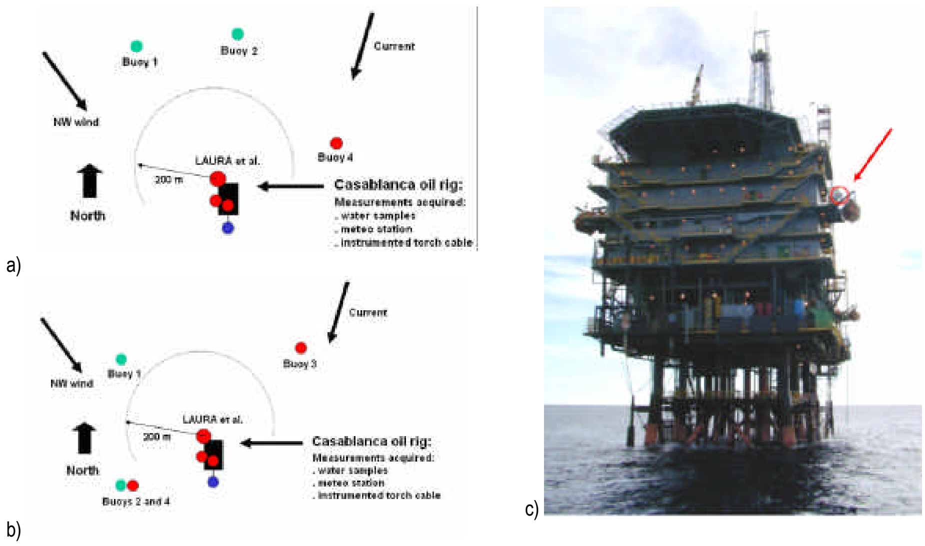

Figure 2.2: Instrumentation and buoy location during (a) WISE 2000 and (b) WISE 2001, and (c) North side of the Casablanca oil rig indicating the position of the UPC radiometer.

radiometers are formed by switching receivers inputs from positions (i) and (ii), and performing a synchronous demodulation. The third and fourth Stokes parameters were measured with a complex digital correlator.

- Meteorological Stations: Rain rate, atmospheric pressure, relative humidity and air temperature at 30 m height were measured by the UPC meteorological station connected to the same radiometer computer. These data were used in the numerical models to estimate the down-welling atmospheric temperature. Additionally, on the Casablanca platform there is an automatic MCV S.A. meteorological station installed on the top of the communications tower, 69 meters above the sea level, including the following sensors: wind speed, wind direction, air temperature, air pressure, and relative humidity. These data were recorded and used only as backup information due to the lower resolution and temporal sampling (15 min). However, they were of crucial importance in the WISE 2001 data processing due to the lost and fatal damage of the buoy sensors during a storm on November 15th, 2001.

- Oceanographic Buoys:

The oceanographic and meteorological characterisation of the sea environment during WISE 2000 and 2001 was mainly provided by sensors located in 4 buoys moored at bottom depths from 145 to 175 m in an area restricted to navigation within 500 m around the oil platform and close to the radiometers field of view (Figs. 2.2a and 2.2b). These buoys were specifically deployed for the campaign. Additionally, some extra data were collected from the platform itself. Within the WISE team the oceanographic data acquisition and analysis were performed by ICM-CSIC (buoy 1, buoy 2, instruments on platform, and sea operations) and LODYC (buoy 3 and buoy 4).

- Buoy 1 (Fig. 2.1c)

  The objective for buoy 1 was to collect conductivity and temperature data near the sea surface close to the radiometers field-of-view, and send them to a data logging station installed on the platform, using a real time link. The buoy was designed and built for WISE 2000 by EMS Environmental Monitoring Systems S.L., and modified for WISE 2001 mainly to host extra power batteries. It was a toroidal body with an inox steel structure to allocate the signalisation elements (flash, radar reflector, and satellite ARGOS beacon) and the measuring and transmitting instruments. The net buoyancy was near to 400 kg.

  The main instrument in buoy 1 was a SeaBird MicroCAT system (model SBE37-SM) (Fig. 2.1h). It allows recording in a RAM water temperature and conductivity for further salinity determination. An RS-232 interface allows real-time data transmission by an external UHF link. An additional submersible pump was added to ensure a constant water flow through the conductivity cell. The water inlet was situated at 20 cm below sea level in the central part of the toroid, to minimise the effect of waves (possibility for air bubbles being introduced into the measuring cell).

  Temperature and conductivity sensor characteristics are summarise in table B.1 from appendix B.

  This allows computing salinity, according to established standards (UNESCO (1978)), with 0.003 psu/month stability, and 0.0002 psu resolution. It has to be noticed that the conductivity cell is equipped with a chemical poison device to avoid biofouling, and the corresponding degradation of the conductivity measurement.

  One of the conclusions from WISE 2000 (see below) was the need to increase the quality of wind speed measurements for use in emissivity models improvement. For WISE 2001 a Doppler ultrasonic anemometer model 5010-0005 from USONIC, UK was added to buoy 1. This instrument provides a better sensitivity to wind speed (especially at low speeds) than the traditional rotor anemometers and avoids their possible mechanical problems.

It measures wind speed every 0.3 second and transmits it in real time by a standard RS-232 interface. Wind direction measurements were not used, since the anemometer was installed on a moving platform (moored buoy) without any extra compass for absolute direction determination. The sensor characteristics are summarised in table B.3 in appendix B.

A microprocessor, programed by the author of this thesis, received data from the anemometer every 10 s, collected this data stream together with the MicroCAT data received every 2 min., and sent the whole data set every 30 min., via a radio modem, to a receiver placed in the platform. Additionally, the microprocessor averaged the anemometer data every 30 s and stored them in a RAM. A diagram of data acquisition and transmission in this buoy, as well as the specifications of the microprocessor are added in appendix B

– Buoy 2 (Fig. 2.1e)

The objective was to characterise the sea surface state in the field-of-view during radiometer measurements. Buoy 2 was a standard Coastal Monitoring Buoy (CMB3280) from Aanderaa Instruments, Norway that includes a meteorological station, a significant wave height and period recorder (accelerometer), and an acoustic surface (1 m) current meter. The main floating body has a "wet" diameter of 90 cm and a total buoyancy of 345 kg. The buoy carries security elements (flash, radar reflector), is powered by solar panels, records data internally, and transmits them by VHF in real time.

A high sampling rate produces rapid power consumption and miss functioning of the whole system after a few days. To avoid this, the current meter and the air pressure sensors (both not crucial and highly power consumers) were disconnected.

The remaining parameters recorded by the buoy were: Wind speed, wind direction, air temperature, solar radiation, relative humidity, wave height and wave period, and the accuracy of those measurements are summarised in table B.4 in appendix B.

– Buoy 3 (Fig. 2.1d)

A Spear-F Datawell waverider buoy was provided by LODYC to record the surface wave spectrum in 14 frequency bands every 3 h and transmit it via satellite (Argos system), following the procedure used by

MétéoFrance. In addition it transmits the significant wave height and the dominant period of waves. In WISE 2000 the buoy was damaged when trying to deploy it under rough seas, and could not further be used. In WISE 2001 it operated successfully during the entire campaign.

– Buoy 4 (Fig. 2.1f)

  A redundant surface temperature and salinity measurement was obtained from a Clearwater SVP small float equipped with FSI temperature and conductivity sensors that were also transmitting data, measured once per hour, via satellite. The expected accuracy at sea is 0.1 psu and 0.1°C for salinity and temperature respectively. In WISE 2000 this float was moored separately, but was lost after one month of operation. In WISE 2001 it was attached to buoy 2 line with a 10 m long iron cable protected with a semi-rigid plastic cover. The buoy 4 satellite Argos beacon was then also used as an extra security element for buoy 2.

The deployment of buoys was difficult in 2000 due to limited availability of adequate ships, and mainly to bad weather conditions. In WISE 2000 only buoy 4 could be moored at the beginning of the experiment (November 15^{th}). The sensors at the platform could be installed on November 29^{th}, and buoys 1 and 2 moored on December 2^{nd}, although part of buoy 2 sensors were not operational until December 13^{th} due to a technical failure. Additionally, the wind speed sensor on buoy 2 did not work for 14 days during the second half of December. As previously said, buoy 3 could not be deployed. The wind sensors on the platform were operational from November 14^{th}. Buoy 4 was lost by mid December, probably after being trawled by a ship. Buoys 1 and 2 were recovered on January 20^{th}, while the instruments on the platform were disassembled on 14 and 15 January, after completion of the experiment.

In WISE 2001 the buoys deployment was made without problems on October 4^{th} from the CSIC research vessel García del Cid, except buoy 1 that was not ready until October 23^{rd}, just at the beginning of the experiment. The instruments on the platform were installed on October 24^{th}. On November 15^{th} a violent storm (easterly wind bursts higher than 120 km/h) occurred on the Casablanca area with maximum waves over 12 m. It was the strongest storm ever recorded in the platform since it was installed in the early 80s, and produced serious damage to its structure. It partially destroyed buoy 2 (that ceased operating and lost stored data) and the anemometer on buoy 1. The link that attached buoy 4 to buoy 2 was broken, and the float drifted away until it could be rescued 230 km south. On November 22^{nd} the buoys were recovered and the instruments on the platform disassembled.

- Measurements from the platform

  To complement the oceanographic measurements made by the moored buoys, an extra instrument was deployed on the platform itself. A winch with a hydrographic cable available in the southern side of the platform, hanging from the structure of a gas torch at some 40 m above sea level allowed deploying instruments at any depth.

  Using this cable a second SeaBird MicroCAT (without additional pump) was located at 5 m below sea level. The purpose was to record temperature and conductivity at a depth that will be the standard for in situ data to be used for SMOS salinity data validation (e.g. Argo profiling floats). The comparison between the time series recorded by the two identical instruments provided valuable information for the future SMOS data validation strategy. During WISE 2000 the winch was operated in several occasions to obtain vertical T, S profiles in the top 0-5 m. In 2001 this option was discarded as it resulted to be of poor use, the operation was not easy, and produced interruptions in the 5 m time series.

  In 2000 an Aanderaa RCM9 Doppler currentmeter was also hung from the cable to record water velocity (plus temperature and conductivity) at 2 m below sea level, as substitution for the sensor that had to be disconnected in buoy 2. This information intended for air-sea flux computations resulted of no further use, and was not implemented in the 2001 campaign.

  To check for possible drifts in the conductivity sensors, water samples were taken when deploying and recovering the buoys for later salinity determination with a Guildline Autosal salinometer (performance characteristic in appendix B). These instruments, when used under strictly controlled room conditions, can provide the best salinity values by comparing the relative conductivity of the sample to a reference standard water of 35.0000 psu. The absolute accuracy is 0.002 psu and the resolution 0.0002 psu.

  The sampling rate for the data acquisition system on buoys 1 and 2, and the MicroCAT hung from the platform, was set at 2 minutes. This was the minimum allowed to keep all the sensors working properly with enough power available for 2 months of operation. After calibration and cross-comparison of all the deployed instruments with water samples analysed on the laboratory, we can conclude that the recorded temperature and salinity values are correct within 0.02 °C and 0.02 psu, a sufficient quality for the

WISE objectives. An exception to this is the conductivity sensor in buoy 4 that produced an underestimation of salinity of around 0.15 psu.

- Stereo Camera: The system consists of two digital video cameras Canon Powershot 600 (832x624 pixels), spaced 4 meters and located at 28 m over the sea surface, just below the radiometers terrace (Fig. 2.1g). During WISE 2000 they were pointed to the North, where the radiometers were supposed to point most of the time (upwind direction of dominant winds). However, during WISE 2001 they were pointed to the West, as it was the radiometer to avoid RFI. Of course, to avoid Sun glitter with this orientation, measurements with the stereo-camera were restricted to the morning. Systematic measurements coincident with the radiometer were performed every day from 9 AM to 10 AM. The stereo-camera provides sea foam coverage estimates and sea surface topography, by observing the sea surface from an incidence angle under two different views.

- Video Camera: A video camera (8.5 mm lens, auto-iris, resolution 512 x 582 pixels, field of view: 35.6° in horizontal and 25.2° in vertical) was mounted in the antenna pedestal (Fig. 2.1a) to provide an instantaneous view of the sea surface being measured by the radiometer. Images were stored every second. The analysis of the images restricted to a 20° field of view (coincident with the antenna beamwidth) have been used to evaluate the sea foam coverage as a function of wind speed (by analysis of the image histograms), to make an estimate of the sea foam emissivity by comparing the instantaneous sea foam coverage and the instantaneous brightness temperatures (T_h and T_v), and disregard erroneous measurements when the security vessel that makes circles around the platform, birds, or even whales pass through the antenna beamwidth.

- Infrared radiometer: The CIMEL CE 312 thermal-infrared radiometer is a four-band radiometer covering 8-13 μm, 11.5-12.5 μm, 10.5-11.5μm ,and 8.2-9.2 μm, with radiometric sensitivities 0.008 K, 0.05 K, 0.05 K, and 0.05 K; and radiometric accuracies 0.10 K, 0.12 K, 0.09 K and 0.14 K, at 20°C, with a field of view of 10°. It was used to provide sea surface temperature estimates, simultaneous with LAURA's measurements. During WISE 2000 the CE 312 was mounted on the LAURA pedestal (Fig. 2.1a) to observe the sea surface with identical conditions (zenith and azimuth angles). However, since the CE 312 read-outs are brightness temperatures, these data have to be corrected for the atmospheric and sea emissivity effects, before being compared with the SST estimates from the AVHRR and the oceanographic buoys. This means that the IR radiometer needed to point to incidence angles larger than 90° more often than the LAURA radiometer in order to measure the down-welling sky radiance. To overcome this conflict, and taking into account that the best SST estimates were found for the lowest observation angles, in WISE 2001 the IR radiometer was mounted alone on a handrail pointing to the sea (West direction) with an observation angle of 25° and the down-welling sky radiance was simulated using the MODTRAN 4 radiative transfer code.

- Satellite imagery and other data:
  - QuikSCAT Wind speed data. Measurements of the NASA satellite-borne QuikSCAT scatterometer (nudge algorithm) at 25 km resolution co-located with the platform using a radius of 0.27° latitude and 0.37° longitude were collected. During WISE 2000 and 2001, 196 and 74 measurements were found, respectively. Since the scatterometer cannot approach closer than 50 km from the coast there were not measurements coincident with the platform: all of them were East and South. These wind speed data were averaged for each satellite pass and the resulting averages were compared with one-hour average of the in-situ measurements. The accuracy at global scale is about 2 m/s.
  - AVHRR SST data. LAC images of the AVHRR instrument at 2 km resolution were recorded and processed by the SATMOS data center (Service d'Archivage et de Traitement Meteorologique des Observations Spatiales, Méteo-France/ CNRS). Many images were cloudy. During WISE 2000 the Ebro plume was observed, but not during WISE 2001.
  - ARPEGE wind speed data. Surface wind speed from the analyzed surface fields of ARPEGE, the meteorological model of MéteoFrance, have been co-located with the Casablanca Platform. The resolution of the model is 25 km, 6 h. The co-location radius is the same as for QuikSCAT, that is 0.27° latitude and 0.37° longitude, resulting in nine grid points co-located for each field. The data are from October 1^{st} to November 30^{th}, 2001 and the format is the same as QuikSCAT.

WISE 2000 buoy data analysis

The resolution, accuracy, and hence consistency, between all sensors were good enough to provide the required temperature and salinity data set and reconstruct time series to complement the radiometer measurements.

The surface temperature temporal evolution was typical of the autumn season. November is usually the month when the erosion of the summer stratification is speed up by the occurrence of strong and cold winds: SST values that can be above 25°C at the end of the warm season (September) will drop to around 13°C after completion of the winter vertical mixing (February). In total SST ranged from 17.5° to 14°C (Fig. 2.3). Sea Surface Salinity remained always near 38 psu (Fig. 2.3), a value typical of the Mediterranean open sea waters that, unlike temperature, do not display a clear seasonal salinity signal. This means that the WISE area was usually out of the direct influence of the Ebro river discharge. The salinity time series shows the occurrence of some low SSS events that typically had a duration of 5-6 days. These events, especially the one around December 12^{th} (strongest SSS drop), are associated to similar SST decreases, a possible indication of the river plume reaching the Casablanca area, as continental waters are not only fresher but also colder than ambient water. This interpretation has been confirmed by the sequence of satellite infrared images that display the evolution of the cold-water tongue from the river mouth to this offshore location.

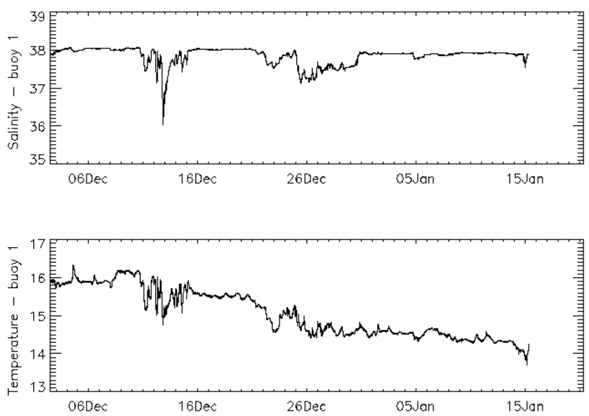

Figure 2.3: Surface salinity and temperature recorded by buoy 1 during WISE 2000.

The two main events detected in WISE 2000 resulted in recorded SSS values 2 psu (December 12^{th}) and almost 1 psu (December 25^{th}) lower than the regular 37.9-38 psu observed all around the experiment.

An important issue related to salinity remote sensing is the possible presence of a vertical salinity gradient. A microwave radiometer will only measure the very surface values, which is not the case of in situ sampling, where sensors have to be completely immersed in seawater. Validation of SMOS salinity determinations will strongly rely on in situ measurements made from standard moored or drifting buoys, or even hydrographic casts or underway measurements from research or opportunity vessels. In all theses cases temperature, and especially conductivity, sensors are not operated close to the surface to avoid interference from air bubbles and even to protect them from possible sources of dirt. A present standard value for near surface salinity measurement is 5 m below sea level. In some cases, especially after strong rainfall when the wind speed is low, salinity at this depth can be significantly different from SSS and then errors can be introduced by comparing both values.

The difference between salinity close to the surface (-20 cm, buoy 1) and at 5 m was monitored during WISE by deploying a second instrument at this depth.

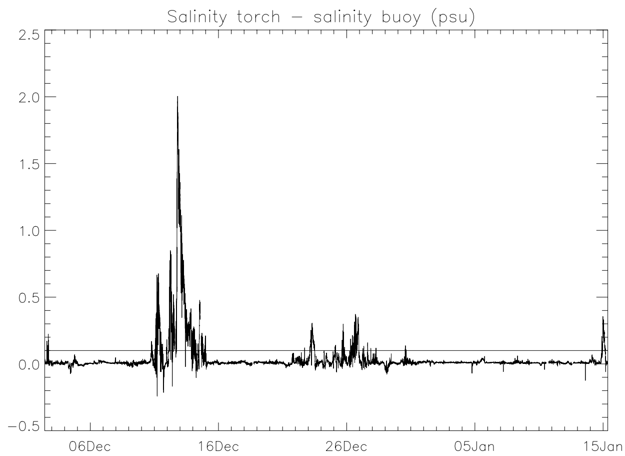

Figure 2.4: Salinity difference between sensors located at -5 m and -0.2 m.

Most of the time the difference between both time series is below 0.1 psu (Fig. 2.4), a value that can be considered a threshold for SSS satellite remote sensing resolution. It is only remarkable during the reported low salinity events, especially that of December 10-15 when the difference reached up to 2.0 psu. The latter is another confirmation that this event was due to an intrusion of the river plume, a near-surface phenomenon, since at 20 cm the salinity drop from ambient water was almost 2.1 psu while at 5 m it was only 0.8 psu maximum.

To increase the knowledge on the vertical resolution of the salinity gradient the sensor at -5 m was manually raised to -2 m, -1 m and to the surface in several occasions. The resulting profiles, with typically a duration of about one hour and a half, display very small salinity variations (usually less than 0.01) except those on December 12^{th} and 14^{th} (low salinity event) and January 10^{th} at surface (probably effect of air bubbles) that can reach up to 0.3 psu. In these specific cases it is remarkable the high temporal variability of the salinity values, which reflects the dynamic behaviour of the event. This was also observed in the SSS time series, where changes of the order of 2 psu can be recorded in very few hours.

This poses an additional problem to the satellite SSS validation that has to be analysed in the framework of the general cal/val strategy and considering the decorrelation scales at open oceans.

Wind data, from both buoy 2 and the Casablanca tower, were mapped to 10 m for standard analysis. The hypotheses of neutral stability was checked for the periods where air temperature was available. In general the atmosphere appeared to be slightly unstable.

The wind speed averaged during the whole period is 6.8 m/s. Wind speeds higher than 15 m/s were observed during few days. Unfortunately the strongest winds were observed during the Christmas period during which the radiometer manned experiments were not operating. Wind direction was mainly from the W and NW, with few events from open sea (SE, E or NE). The strongest speeds correspond always to northwesterlies.

The data gathered by the two instruments, mapped to 10 m height was compared, during the period of common measurements. For the comparison to be meaningful the measurements were averaged during one hour. Figure 2.5 shows data from the meteorological station on the platform against simultaneous data from buoy 2. The measurements in the range 3 - 15 m/s (most commonly observed wind speed range and optimal range for instruments) and in the whole data range were fitted.

In the range 3-15 m/s the equation of the fit is: $U_M = 1.09U_B + 0.07$, where U_M is the meteorological station measurement and U_B is the buoy measurement, with an explained variance of 92%. In the whole range it is $U_M = 1.17U_B + 0.20$ with an explained variance of 96%. The mean difference between the instruments is $U_B - U_M = -0.92$ m/s with a standard deviation of 1.83 m/s (Font et al. (2003a)). In the most commonly observed range the instruments differ by about 10%, the standard deviation of the difference being rather high. It was checked that the measurements were nevertheless usable for emissivity models study. This discrepancy might be due to several factors:

- different instruments
- different height: the mapping to 10 m is not perfect and from 69 m it is a large correction (atmospheric stability corrections did not improve the result), the platform is likely to disturb the air flow less at the top than at low altitude.

To compare with the future SMOS situation, when wind data will be needed from other sources, spaceborne wind information has also been analysed. Measurements of the QuikSCAT satellite scatterometer (nudge algorithm) were colocated with the platform. These data were averaged for each satellite pass and the resulting average was compared with one-hour average of the in-situ measurements. The QuikSCAT data have been compared to the meteorological station measurements at 10 m height. The equation of the fit in the range 3-15 m/s is: $U_Q = 0.97U_M + 0.68$, where U_Q is the QuikSCAT measurement, with an explained variance of 74%; the mean difference between the instruments $< U_M - U_Q >$ is 0.44 m/s with a standard deviation of 2.8 m/s. The points are rather dispersed, probably due to the imperfect co-location, but they compare rather well. The three wind speed data series (buoy 1, tower station and QuikSCAT) are presented in Fig. 2.6.

During the five weeks when significant wave height (average of the highest third of the waves) could be recorded, data ranged from 0.1 to 4.0 m, with an average of 0.9 m. Wave periods ranged from 1.6 to 7.5 s, with an average of 3.2 s. Most of the time wave height is correlated to wind stress, however, some times during WISE 2000 considerable wave heights were recorded without simultaneous high wind. This is an indication that the wave field at the Casablanca site was at that moment not originated by local winds, but arrived there from other areas (swell). This is also an important issue to be solved for SMOS salinity retrieval if wind speed information has to be used in the computation.

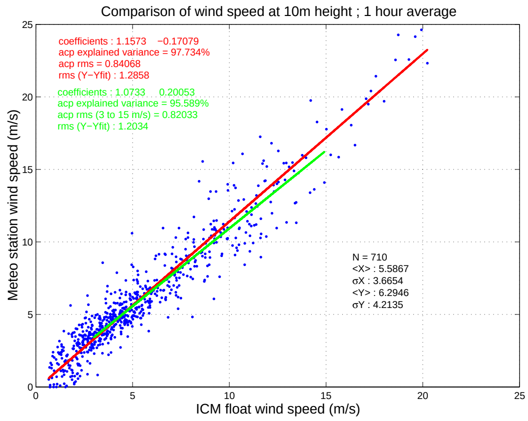

Figure 2.5: Wind speed (at 10 m) comparison for the two in situ data sources during WISE 2000 (from Drange et al. (2001)).

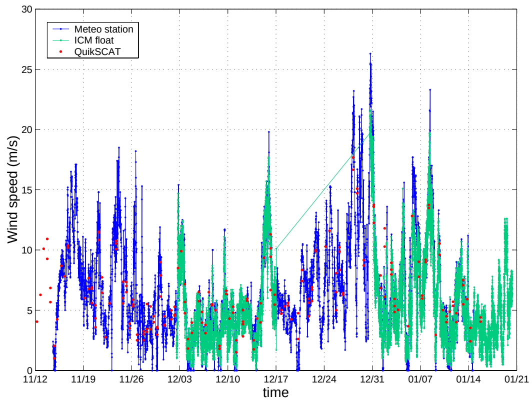

Figure 2.6: Integration of the three wind speed data sets obtained for WISE 2000 (from Drange et al. (2001)).

WISE 2001 buoy data analysis

The 2001 campaign took place also in autumn, but almost one month in advance with respect to the previous year. As previously said, and after the experience gained with WISE 2000, the buoys deployment was made more efficiently using a research vessel, and all the buoys were in place before the beginning of the radiometer measurements. The data intercomparison and analysis was made

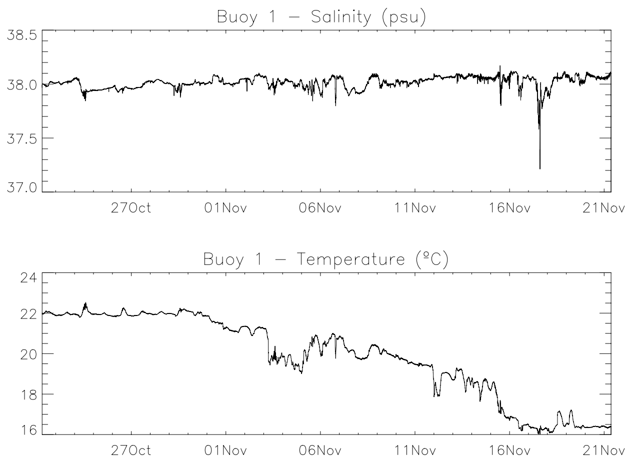

Figure 2.7: Surface salinity and temperature recorded by buoy 1 during WISE 2001.

following the same procedure described for WISE 2000.

At the beginning of the period, the temperature (Fig. 2.7) was still slightly above 22, and did not initiate a clear decrease until early November. A cold event (a drop of almost 2 °C) occurred on 4 November, but after two days the temperature recovered and continued the slow decreasing trend. After the storm of November 15th the decrease was accentuated and by the end of the campaign the temperature was quite stable around 16 °C, practically the same value observed the previous year at that date.

Salinity was very constant around 38.0 psu (Fig. 2.7). Only in 8 short occasions (usually few minutes) during the 30 days period the values differed from this mean by more than 0.1 psu, the expected threshold for salinity detection by SMOS. And just twice the difference was above 0.2 psu, the most remarkable on 18 November (down to 37.2 psu) after an intense rain event.

The vertical structure of salinity near the surface is still more homogeneous than in WISE 2000 (Fig. 2.8). The difference between the values measured by the sensor situated at -5 m and the sensor close to surface overpasses 0.1 psu in few occasions and always during few minutes. Only once, during the rain event mentioned in the previous paragraph, a significant difference persisted for 4 h and reached a maximum of 0.7 psu.

The same wind data analysis as performed in WISE 2000 was applied to the 2001 records. We expected to have better quality data with the ultrasonic Doppler anemometer added to buoy 1, but unfortunately several technical problems reduced the usable information to only two short series. It was due mainly

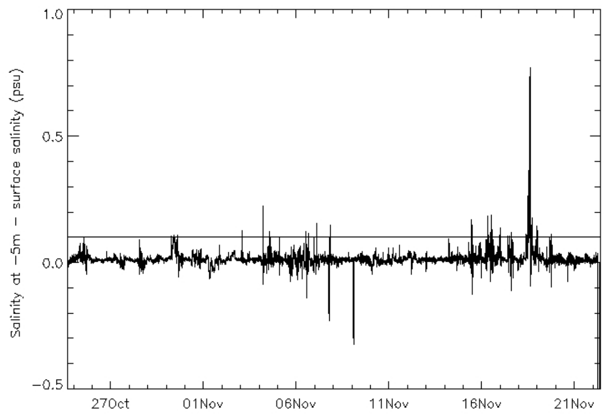

Figure 2.8: Difference in psu between salinity recorded at 5 m below sea level (platform) and at 20 cm (buoy 1) from 23 October until 22 November 2001.

to malfunctioning of the microprocessor that controlled the anemometer data acquisition and transmission just 2 days after deployment. And when this problem could be definitively fixed, the violent storm destroyed the instrument after 6 days of correct operation.

In Fig. 2.9 we present the reconstructed wind speed data series from the different instruments from 4 October (buoys deployment) until 22 November (end of the experiment). The direction was very variable until early November, with two events of strong winds from NE and one from SW. After that, while increasing notably the speed, it was usually from the N and NW with storms (more than 20 m/s) every two days from 9 to 15 November, and all of them from NW except the 'big one' that was from E. After a last minor storm on the 17, the tendency was to lower the speed until the end of the experiment.

Unlike what happened in 2000, during WISE 2001 the radiometer measured under really intense wind and rough sea conditions. Especially remarkable were the two severe storms that occurred on November 11^{th} and 15^{th}. As previously said, the second one produced serious damages to the buoys and to the Casablanca platform structure. Although it was not possible to keep the radiometer working continuously during the storms, data could be recorded under very rough seas.

Fig. 2.10 shows the recorded wave height (four times the variance of the wave slopes), that overpassed 6 m during several hours in both storms, and the peak wave period recorded by the waverider buoy during the whole duration of WISE 2001. It has to be recalled that the spectral wave height (3 h average) recorded by buoy 3 is by definition square root of 2 higher than the significant wave height

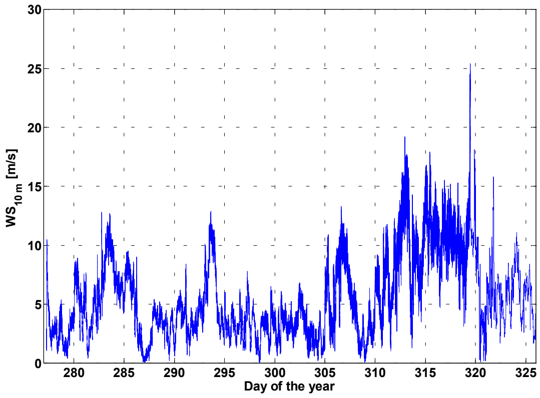

Figure 2.9: Complete wind speed series (mapped to 10 m) measured during WISE 2001.

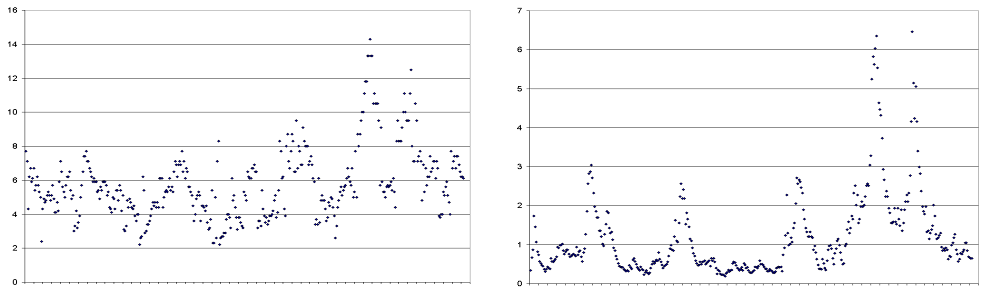

Figure 2.10: Three hours average wave height (left, m) and peak wave period (right, s) recorded by buoy 3 during WISE 2001, from October 4^{th} to November 22^{nd}.

Figure 2.11: STARRS instrument installed on a DLR plane.

recorded (every 2 minutes) by buoy 2.

2.1.2 EuroSTARRS

The EuroSTARRS campaign was also sponsored by the European Space Agency (ESA) and the objective was to provide data for the scientific studies supporting the SMOS mission. In particular it acquired 'SMOS like' (in the sense of simultaneously multi-angular) data to advance the knowledge of the passive microwave multi-incidence observations at L-band for various surface types.

The STARRS L-band radiometer is owned by the *Naval Research Laboratory* (NRL), USA, and was available for use by the EuroSTARRS campaign between November 17^{th} and 23^{rd} 2001. The instrument was installed on board a Dornier 228 aircraft from the *German Aerospace Center* (DLR) (see figure 2.11). STARRS instrument has 6 antennas that measure at V-polarisation, only. The radiometer was tilt 12°, respect to nadir when mounted in the plane, to achieve more varied angle measurements, permitting to acquire data at incidence angles of -26.5°, -9.0°, 5.5°, 19.5°, 34.0° and 50.5°.

Data acquired by EuroSTARRS was intended to help to improve the scientific understanding of emissivity in relation to different surface characteristics for retrieving ocean salinity and soil moisture fields. EuroSTARRS was simultaneous to WISE2001 experiment and to the acquisition of data from a dedicated oceanographic research vessel.

Different land surface sites were selected in Europe, and two salinity sites where chosen. One site was Bay of Biscay, around the French meteorological Gascogne Buoy, to study the effects of strong changes in salinity from the coast to the inner part of the Atlantic Ocean. The other site was around the Casablanca oil rig, near the mouth of the Ebro river (Tarragona), mainly to study the effect of

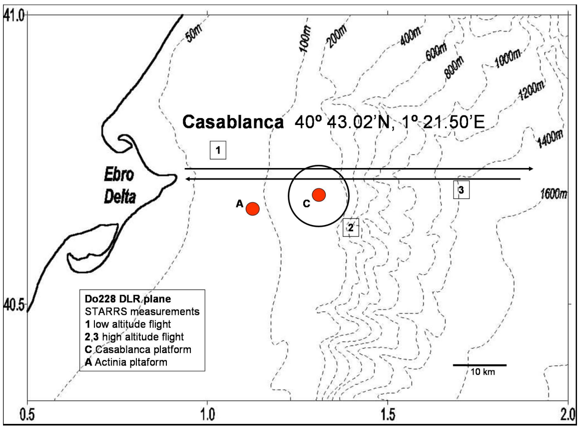

Figure 2.12: EuroSTARRS Casablanca campaign area. Plain and ship path.

wind speed on the salinity measurements and to investigate azimuth dependence.

In the Casablanca area, the flight acquisition plan consisted in three phases. The first one was to draw a transect from the coast near Ebro Delta towards the Casablanca platform (40 km) and until the continental slope (100 km) at 1640 m height (fig. 2.12). This transect was selected to avoid interferences from the platform. The second phase, consisted of performing 10 circles at a constant bank angle of 22° at 278 m height. Given the 12° tilt of the antenna mounting, a range of angles from 4.5°to 72.5° is obtained. The last phase was the reverse course along the first transect and flown at 278 m. The measurements were made after sun shine, in order to avoid the interference from sun glint.

The Institut de Ciencies del Mar (ICM) participated actively during the flight over the Casablanca oil rig, on the November 21^{st}. Simultaneously to the airborne flight two kind of measurements were made at the area. First, the CSIC Research Vessel, 'García del Cid' carried out a survey in a rectangular area extending from 1° to 2° E around the Casablanca platform on November 21^{st}-22^{nd} (fig. 2.12) coincident with the plane overflight on November 21^{st} late afternoon. The oceanographic data collected were:

- Underway near surface temperature and salinity records following the flight line.
- Vertical salinity and temperature profiles spread across the rectangular site measurement area.
- Acoustic Doppler current profiles (ADCP)
- An on-board meteorological station was operating in a continuous mode.

The second data set was obtained from sensors installed in buoys moored close to the platform and in the platform itself from the simultaneous WISE 2001 experiment.

The R/V 'García del Cid' left Barcelona on November 21^{st} at 7:00 h and arrived to the Casablanca measurements area at 12:00 h. The underway near-surface measurements were completed on the November 22^{nd}. The analysis of the sea surface fields and the vertical structure can be found in Emelianov et al. (2003).

During the STARRS flight the wind speed in the area was very low, between 3-5 m/s, and direction veering continuously from 75° to 50°. This low wind speed, did not allow to analyse the azimuthal effect.

A strong source of interference was identified when the antenna was pointing towards the city of Barcelona. These interferences make the data not useful during the periods when the antenna was pointing at that direction.

Vessel measurements brought the following conclusions:

- Both temperature and salinity near surface presented a small spatial variability across the sample area, with means values of 17 °C and 38.05 psu.
- Vessel underway high horizontal resolution sampling allowed observing that the temperature spanned over a range of 1.4 °C and the salinity, much noisier, only over 0.3 psu.
- The main gradients were found in the onshore-offshore direction, the same followed by the flight.

2.2 Other campaigns

2.2.1 FROG 2003

The FROG (Foam, Rain, Oil slicks and GPS reflexions) campaign took place in the IRTA (Institut de Recerca i Tecnologia Agroalimentàries) facilities, located in the Ebro River Delta in the south of Catalonia, from March 13^{th} to May 5^{th}. The main objectives of FROG 2003 campaign were the following:

- Acquisition of radiometric measurements of an artificially generated foam covered water surface.
- Acquisition of foam vertical profile snapshots, and measurement of the main parameters to describe the foam by theoretical models.
- Acquisition of radiometric measurements of an artificially generated-rain.

- Acquisition of radiometric measurements of a water surface covered by an oil slick.

This campaign was organised and lead by the Polytechnic University of Catalonia (UPC) team, with collaboration of the University of Valencia for IR measurements.

To achieve these objectives, a pond of 3 m × 7 m dimensions was utilised. The instruments used were: the LAURA L-band full-polarimetric radiometer (the same radiometer used for WISE), a portable meteorological station to measure the atmospheric pressure, temperature, relative humidity and rain rate. Two video cameras were mounted, also, to measure foam coverage and foam vertical profile. Finally a water roughness meter and a water conductivity meter were also installed. An infrared radiometer was placed to measure the SST of the sea water. Figure 2.13 shows the instrument set-up.

To generate the foam, an array of 104 air diffusers was mounted in the pool floor, allowing to regulate the air flux, with a maximum of 500 m^3 per hour.

To generate a controlled rain fall a matrix of 14 diffusers were distributed along 3 rows (6 m long, 1.5 m wide) and was mounted on a crane at a maximum height of 13m above the water surface, from where the water drops reached the limit velocity before splashing in the water pool. This set-up generated an equivalent rain rate of approximately 4000 mm/h.

To minimise the radiation coming from buildings and atmosphere, the pool was surrounded by a metallic net. Another effect to consider was the galactic noise, and to minimise this contribution, the radiometer was pointed to the north. To avoid the sun glitter effect, all the measurements were acquired during night-time.

The measurements were done in elevation scans from 20° to 55°, with steps of 1° or 5°, depending on the objective of the measurements. All measurements were repeated in a wide range of salinities from $\backsim$ 0 to $\backsim$ 34 psu in steps of 5 psu, obtained by mixing sea water with fresh water.

Calibration was performed at the beginning and at the end of each measurements cycle (less than 100 min). It consisted in measuring a hot load (microwave absorber) and a cold load (sky) during two hours at each position.

For further information on this campaign and the experiment results refer to Ramon Villarino's PhD thesis dissertation and Villarino et al. (2003).

2.2.2 The Plata Campaign

Scientists from Argentina, Brazil, Uruguay and US working within the framework of the South Atlantic Climate Change Consortium (SACC), sponsored by the Inter-American Institute for Global Change Research (IAI), have outlined a

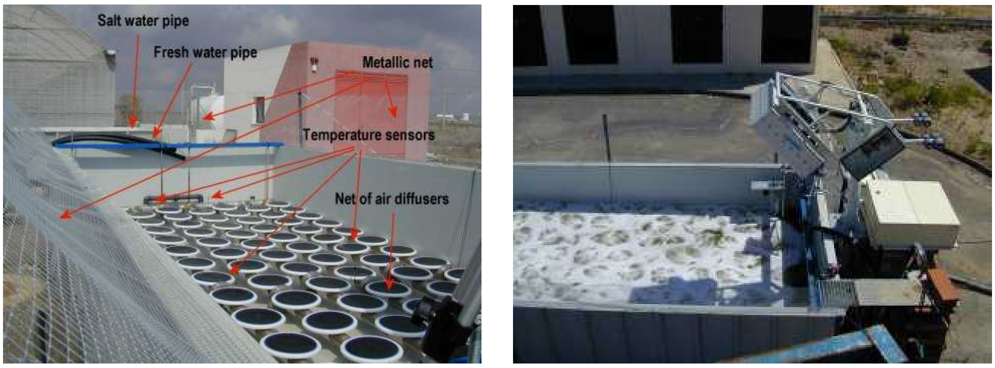

a) b)

Figure 2.13: a) Visual description of the FROG experiment set-up, b) Radiometer pointing to the foaming pool.

research project to study the impact and variability of La Plata river (Argentina) plume on the adjacent ocean. The main goal of this project, co-financed by IAI and the U.S. Office of Naval Research, is to characterise the seasonal variations of the Plata plume and the Subtropical Shelf Front, their impact on the circulation and on the chemical and biological processes of the continental shelf.

With a mean annual discharge of 23590 m^3/s of freshwater La Plata river produces an extraordinary impact over the continental shelf of northern Argentina, Uruguay and southern Brazil. The river waters are a significant source of nutrients, dissolved and suspended matter and, due to their low salinity, induce strong vertical stratification over the adjacent shelf. Studies based on historical hydrographic data (Piola et al., 2000) reveal that La Plata derived low salinity waters present seasonal fluctuations of several hundred kilometres over the shelf. Consequently, large seasonal variations of environmental conditions occur over the continental shelf of eastern South America between 38 and 25° S.

The first field activity carried out within the Plata project was a large-scale winter oceanographic survey and an airborne salinity measuring survey. The Plata winter survey was carried out between Mar del Plata, Argentina and Itajaí, Brazil, from 20 August to 2 September 2003.

The campaign was carried out on board the oceanographic vessel ARA PUERTO DESEADO. The vessel departed Mar del Plata, Argentina, 20 August 2003 at 12.15 local time and docked in Itajaí (Brazil) at 08.45 local time (GMT+3) 2 September 2003. 83 CTD stations were performed in eleven cross-shelf sections spanning from the near coastal region (10 nautical miles from shore) to the western boundary currents offshore, at depths greater than 1000 m (Figure 2.14a).

The sections were designed to cover the area of influence of the Río de la Plata and the Patos/Mirim Lagoons over the shelf and its northward extension, characteristic of Austral winter. During the CTD stations salinity measurements were performed. Moreover the ship carried a thermosalinograph instrument, which measured sea surface salinity during the whole path of the ship.

The airborne survey was one of the components planned for the Plata project, funded by the ONRIFO (U.S. Office of Naval Research International Field Office), through the Naval International Cooperative Opportunities in Science and Technology Program, the IAI (Inter-American Institute for Global Change Research) and Uruguayan local funding. The survey was carried out on a CASA 212 Aviocar of the Fuerza Aérea Uruguaya (C-212 FAU 532). The mission consisted in a series of flights covering the study area, using the STARRS (Salinity, Temperature, and Roughness Remote Scanner) instrument, provided by the US Naval Research Laboratory.

Two kinds of surveys were planned (see figure 2.14a and b):

- Large surveys, intended to cover the positions of the oceanographic stations covered by the ARA PUERTO DESEADO. Flight altitude was normally 900 - 1200 m. The corresponding transects were named LEG1, LEG2 and LEG3.
- Small surveys, two located in the Río de la Plata (Plata Mouth and Plata Front), and a third at the mouth of the Patos Lagoon in Brazil (Patos Outflow). These flights were made at 2440 m. The data obtained allows the construction of a salinity map, with less space between consecutive track lines.

The STARRS instrument has 6 antennas and measures only at V-pol, as explained before. In this case the instrument was not tilt, so the measurements were performed at the incidence angles of -38.5°, -21.0°, -6.5°, 7.5°, 22.0° and 38.5°.

The surveys were made at night, in order to avoid the interference from sun glint. There were in total more than 45 hours of survey, and more than 7200 nautical miles of navigation.

Sea surface salinity is an excellent indicator of the horizontal extent of riverine constituents over the continental shelf. Figure 2.14c presents the first truly synoptic sea surface salinity distribution constructed combining the Plata winter cruise CTD and thermosalinograph data after preliminary calibration. Because there are no waters fresher than 33.5 on the northern Patagonia continental shelf (Guerrero and Piola (1977)), all water fresher than 33.5 must contain La Plata mixtures. Thus, the 33.5 isohaline marks the outer edge of La Plata plume. Surface salinity shows a well developed, continuous near coastal plume extending

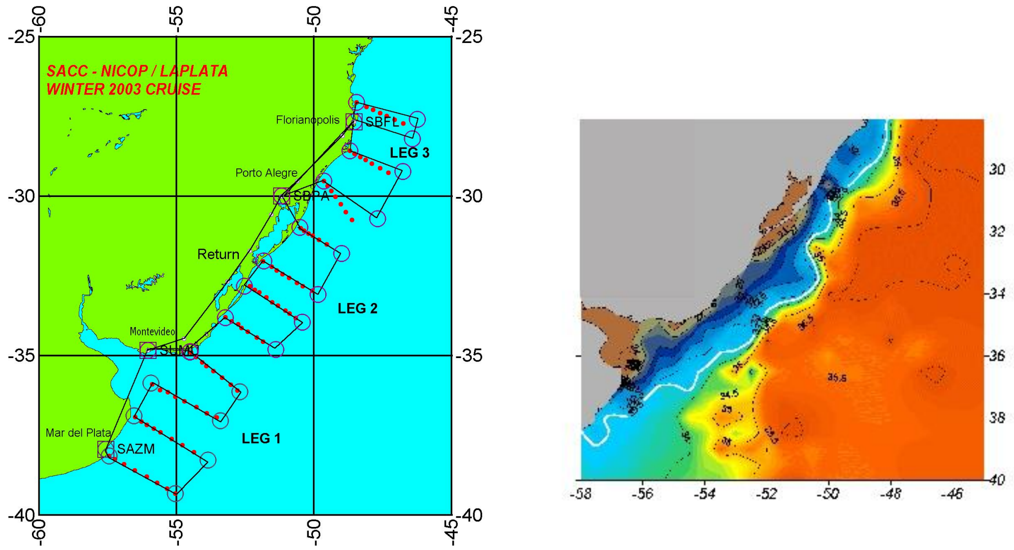

a) b)

Figure 2.14: a) Ship CTD stations and the plane track overplotted in blue line. b) Sea surface salinity distribution as observed during the Plata winter cruise 2003. The white contour is the 33.5 isohaline, which marks the outer edge of La Plata plume. (from survey reports and Piola et al. (2000)).

from La Plata estuary to 26 ° S, beyond the northernmost locations occupied during the cruise.

Another survey was performed in the same area under the same project, in February 2004, but calibrated data was not still available to be included in the analysis performed in this thesis.

More information on this campaign can be found in:
http://glaucus.fcien.edu.uy/pcmya/sacc/LaPlataW2003/index.html.

Acknowledgements: The L-band data from the Salinity, Temperature, and Roughness Remote Scanner (STARRS) was available thanks to the support of Office of Naval Research Global's NICOP program and the Naval Research Laboratory's Salinity Driven Advection in Littoral Deep Areas (SALIDA) project (award number NRL BE-435-017) and its participants. The ship-based in-situ temperature and salinity data were graciously provided by Argentina's Servico Hidrografia Naval as part of the multi-national (Argentina, Brazil, Uruguay, and USA) "La Plata" campaign which was conducted under the auspices of the South Atlantic Climate Change consortium sponsored by the Inter-American Institute for Global Change Research (IAI).

Chapter 3

Modelling the brightness temperature of the sea

This chapter presents a review on the most accepted models existent in the literature that describe the natural emissivity of the sea at L-band. Some of the models presented here are based on theoretical approaches and others are semi-empirical propositions. Also a new semi-empirical model, developed by the author, is presented. This new model, based on WISE dataset, is analysed and compared with other models. In chapter 5 some of these models will be used to retrieve salinity from campaign measurements, and depending on the quality of the retrieved salinity the models will be evaluated.

3.1 Theoretical models

One of the main tasks for the SMOS science development team is to select the forward models that best describe the natural sea surface emissivity process. This is a key issue since the SSS retrieval algorithm for SMOS will be based on these models.

To perform this work in situ measurements are needed, to enable to choose the model that best fits measured data. However, at L-band very few campaigns have been performed, and very few data sets were acquired. For this reason, ESA sponsored the three campaigns, WISE, EuroSTARRS and LOSAC (Wursteisen, P. and Fletcher, P. (2003)), which permitted to acquire a wealth of in situ data, and allow scientists to advance significantly. However, it is not still clear now what will be the best model to use in the retrieval algorithm, and more data is needed. ESA is planning to perform a large airborne campaign in 2005, called CoSMOS to address several of the open issues.

As presented earlier, sea emissivity is governed by some geophysical parameters, as salinity, temperature, sea surface roughness, foam (if present). Emissivity also depends on the sensor parameters: frequency, incidence angle (θ), azimuth look direction (ϕ), and polarisation (p).

To express sea surface emission at L-band, three different kind of models are necessary:

- **Dielectric constant model**, which from surface salinity, sea surface temperature and frequency data, allows to predict the complex dielectric constant value.
- **Sea roughness spectrum**, which describes the spectrum of sea surface when roughness is present (not flat surface). A good knowledge of this model is important since a different modulation of sea roughness spectrum will lead to different values of emission.
- **Electromagnetic scattering model**, which describes the way in which energy is scattered from sea surface when roughness is present.

3.1.1 Dielectric constant models

In section 1.3.1 the dielectric constant, ε, has been presented, and it has been explained that it depends on frequency, temperature and salinity.

Several models of sea water complex permittivity exist in the literature. However, most of them have been obtained for frequencies higher than L-band.

Also several expressions have been obtained from measurements performed with NaCl solutions, but an important difference in the permittivity obtained using purely NaCl waters with respect to sea waters has been reported (Ellison et al., 1998).

At L-band the most accepted models are the ones proposed by Klein and Swift, Ellison et al., and more recently by Blanch and Aguasca.

All the authors base the permittivity model on the Debye expression (equation 1.11), and using different techniques they obtain experimental values for the following variables: ε_s static dielectric constant, τ relaxation time, σ ionic conductivity. These variables are a function of salinity and temperature.

Klein and Swift dielectric constant model

During the 70's Ho and Hall (1973) and Ho et al. (1974) performed measurements of the dielectric permittivity at L- and S-band with NaCl solutions and sea water samples. The precisions on the measurements at L-band were of 0.2% and 0.4% for the real and imaginary part, respectivelly.

Later on, in 1977 Klein and Swift (1977) did a reanalysis of the same measurements, and they found a bias on the ε_i measured by Ho et al. Thereby, they proposed a new ε_i formulation, which appeared to have more precision.

The accuracy of the model they proposed is at least of 0.3 K in the brightness temperature, and it should be valid for salinities in the range from 4 to 35 psu.

However, there were very few measurements done on the salinity range from 30-40 psu, which are the most common values in the world's oceans.

Ellison et al. dielectric constant model

Ellison et al. (1998) measured the complex permittivity at the laboratory for several frequencies between 6-90 GHz. The technique chosen at low frequencies was to measure the transmission coefficient with a coaxial line method.

The water samples were collected at sea, and covered most of the physical conditions found in the world's oceans.

To model the permittivity of sea-water at 1.43 GHz, the authors extrapolated the results from higher frequencies. This could be one of the reasons why this model is a little bit divergent from the other two models.

Blanch and Aguasca dielectric constant model

In Blanch and Aguasca (2004) a new method for computing the permittivity of sea water has been used. They proposed a static structure based on the propagation method, using a standard rectangular waveguide, which has two transitions for the input signal and one for the output signal that will be measured.

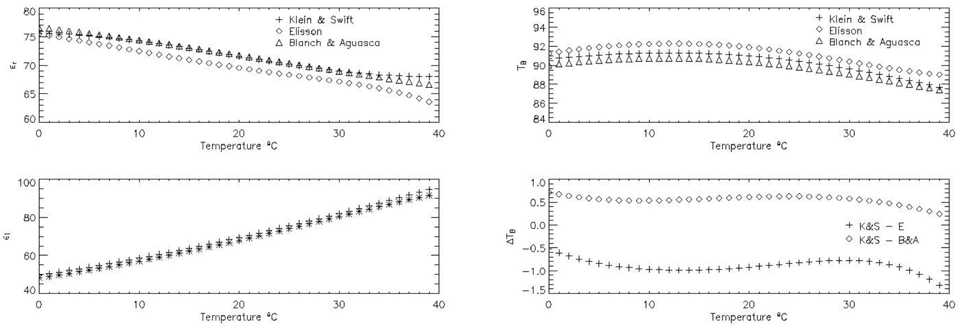

a) b)

Figure 3.1: Comparison of three different permittivity models. a) Real and imaginary parts of permittivity at 1.4 GHz, for salinity of 37.5 psu, b) Brightness temperature for normal incidence, for salinity of 37.5 psu at 1.4 GHz.

The measurements were done at 1.43 GHz, with seawater samples with salinities in the range of 0-40 psu, in steps of 2 psu for low salinities, and steps of 1 psu for high salinities. The temperature changed from 0° to 40°, in steps of 0.7°. The authors curve-fitted the equations with the results, and they finally got their model.

Figure 3.1 shows a comparison of the three models presented above. It shows that Klein & Swift and Blanch & Aguasca, are quite similar for mid temperatures, while Ellison model differs a bit from the others, specially for the real part of the permittivity. Also, the K&S and B&A models give similar results on brightness temperature, while Ellison tends to overestimate it.

Recently, William Wilson from JPL performed L-band radiometric brightness temperature measurements in a saltwater pond as a function of salinity and temperature. They conclude in Wilson et al. (2004) that measurements are in good agreement with the Klein and Swift dielectric model over a temperature range from 8° to 32° C and a salinity range from 25 to 40 psu.

3.1.2 Wave spectrum theoretical models

Sea surface spectrum models are the basic statistical tools used for the rough sea surface description within asymptotic emissivity models and their range of validity are therefore very important for SSS retrieval algorithms accuracy.

Durden & Vesecky

Durden and Vesecky (1985) empirical sea surface spectrum model was one of the first used for describing the electromagnetic scattering. This model is commonly used jointly with two-scale and SPM/SSA models for the emissivity scattering modelling. Surprisingly this wave spectrum model multiplied by two provides improved results when used in asymptotic models for computing sea surface emissivity. This model is only applicable for fully developed seas, i.e. seas that are in equilibrium with the local winds. Thereby this wave spectrum is described uniquely with the wind vector at 1.4 GHz.

Elfouhaily

Elfouhaily et al. (1997) developed the so-called 'unified spectrum', solely from in situ measurements. The main characteristic of this model is that it is dependent on the age of the waves, by the parameter u^*/C_p for which u^* is the surface wind friction velocity and C_p is the phase speed of the waves at the peak of the spectrum. This model reproduces the significant wave-height for developing seas.

Kudryatsev

Kudryatsev et al. (1999) presented a new model where a new physical approach of the short wind wave spectrum is used, which takes into account the statistical properties of breaking waves and the mechanisms of capillaries generation. Here, analytical expressions for the spectral forms are deduced from the theoretical energy sources equations. The age of the waves is taken into account here, also.

A restriction of some of these wave spectrum models is that they consider fully developed seas. The models that takes into account the wave age, theoretically can deal with partial developed seas, but in practise it is very difficult to evaluate this parameter. Miranda et al. (2003) emphasis that the fully developed sea condition are an unusual situation in real case, since usually the sea is growing or decreasing. Also it should be underlined that these models do not consider the occasions where the sea state is not dependent on local wind, but on far and ancient winds, as happens when swell is present.

3.1.3 Surface roughness scattering models

The emissivity of a calm, smooth sea surface may be calculated by using the specular Fresnel reflection expression given in 1.9 and 1.10. However, when the surface is roughened by wind action, its emissivity and scattering behaviour become more complicated.

Two main asymptotic theories have been used as potential forward models for SMOS, and they are briefly described in the following.

Two-scale models

The Two Scale Method (TSM) approximates sea surface as a two-scale surface, with small ripples or capillary waves (small scale compared with electromagnetic waves) on the top of large-scale waves characterised by their distribution of slopes. Then, the thermal emission of sea surface is the sum of emissions from individual, slightly perturbed surface patches tilted by the underlying large-scale surface.

The geometric optics approximation is applied for long scale wavelengths, while Small Perturbation Method is used for short scale wavelengths. The problem, here, is that the division of the ocean surface into small and long scales remains an unclear process, and the parameter which divides the two scales is often arbitrarily chosen within wide limits. Different authors make different choices which range from $k_0/1.5$ to $k_0/40$ (being k_0 the electromagnetic wavelength), and the optimal wavelength for the spectrum split has been found to be incident angle dependent.

At L-band, Dinnat (2003) has however shown that small changes in this parameter do not have a significant influence on the emissivity of the sea surface.

The maximum permitted value of wind speed for this model is 19 m/s, a very unusual value to reach. Consequently, there is no practical restriction in the use of this model for sea surface emissivity simulations.

The Two-scale model that has been used in this work is developed by Yueh et al. (1997), which fix the cut-off value to $k_0/3$ and use Durden & Vesecky wave spectrum multiplied by two.

Figure 3.2 compares the sensitivity of the brightness temperature to the wind speed with the two scale method for different spectra: Elfouhaily, Durden & Veseky and Durden & Veseky×2.

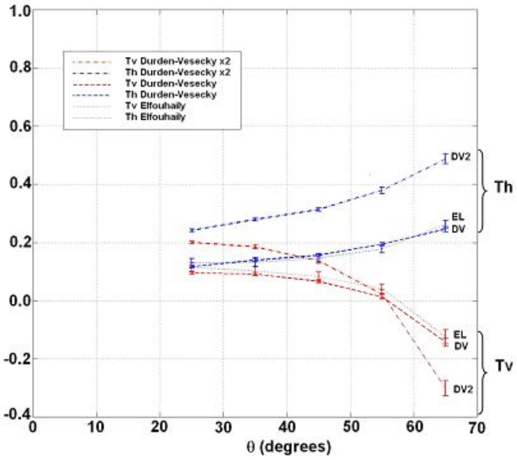

Figure 3.2: Comparison of the derivative of the brightness temperature with respect to wind speed, $\Delta T_{B\,rough}/\Delta U_{10}$, as function of the incidence angle, when Two Scale Method (Yueh et al., 1997) is used with Durden & Veseky, Durden & Veseky×2 and Elfouhaily wave spectrums (from Camps et al. (2003b)).

SSA/SPM model

Several authors have shown that expressions obtained from the SPM (Small Perturbation Method) for surface emissivity have the form of a small-slope, and not small height, expansion. Some comparisons have shown that SPM and SSA (Small Slope Approximation) are equivalent for the thermal radiation, and not for differential scattering coefficients. It has been found that errors in scattering cross-section in the near specular region are compensated by errors outside the specular region, so the integration still produces an accurate emission prediction. No artificial cut-off wavenumber is required to separate small from long waves and SSA can be applied to the entire ocean surface spectrum. Only the second order expansion is considered in this study.

The input values to the model are SSS, SST, wind speed, azimuth and incidence angle.

Figure 3.3 compares the sensitivity of the brightness temperature to the wind speed with SSA for different spectra: Elfouhaily, Kudryatsev and Durden & Veseky×2.

An exhaustive comparison of these scattering and wave spectrum models, plus others which have not been described here (Kirchhoff model, integral equation method...), is performed in Vall-llossera et al. (2003). This work reviews the

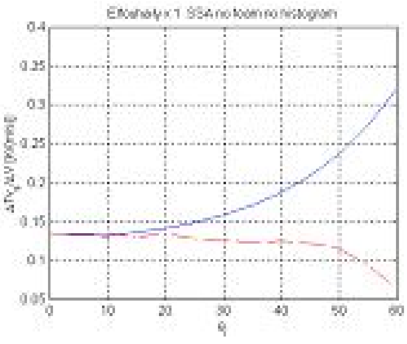

a)

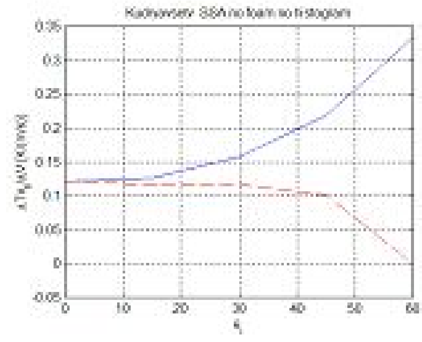

b)

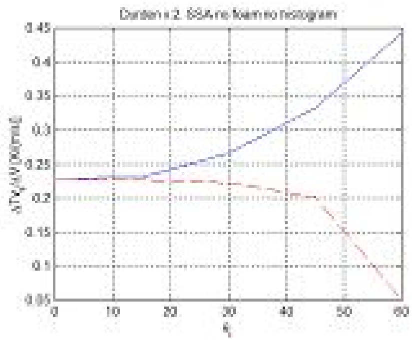

c)

Figure 3.3: Comparison of the dependence of $\Delta T_H/\Delta U_{10}$ (continuous line) and $\Delta T_V/\Delta U_{10}$ (dashed line) respect to the incidence angle predicted by SSA model when different spectra are used: a) Elfouhaily spectrum, b) Kudryavsetv c) Durden & Veseky×2 (from Vall-llossera et al. (2003)).

difference on the dependences of T_B to wind speed between the models, and compares these results with WISE campaign measurements.

Furthermore reviews on these theoretical models have been preformed in the ESA studies ITT/1-4314/02/NL/AG, WP1200 and ITT 1-4505/03/NL/Cb WP1100.

3.2 Semi-empirical models for sea surface emissivity

The semi-empirical models of the emissivity of the sea surface are obtained from experimental data. In particular the models presented below have been derived from WISE 2000 and 2001 campaigns.

The brightness temperature of the sea surface can be modelled by 3.1, composed by a term due to the emissivity of a flat surface plus another term that accounts for the effect of the sea roughness,

$$T_{B,p}(\theta_i, SST, SSS, C_n) = T_{B\,Fresnel,p}(\theta_i, SST, SSS) + \Delta T_{B\,rough,p}(\theta_i, C_n, SST, SSS) \tag{3.1}$$

where,

$$\begin{aligned} T_{B\,Fresnel,p}(\theta_i, SST, SSS) &= SST \cdot e_p(\theta_i, SST, SSS) \\ &= SST \cdot (1 - |R_p(\theta_i, SST, SSS)|^2) \end{aligned} \tag{3.2}$$

and R_p are the Fresnel field reflection coefficients with p polarisation as defined in equation 1.10, which depends on the dielectric constant.

The second term of the equation 3.1 describes the emissivity due to the roughness of sea. This term is theoretically poorly known, and it is determined by the wave spectrum, which is also unsatisfactorily known. This term is dependent on incidence angle, C_n that represent the parameters used to describe the roughness of the sea (U_{10},SWH,....), SSS and SST. The last two have not been considered in the regressions done from WISE data set since, they were very stable. However, Etcheto et al. (2004) have observed a small dependence of $\Delta T_{B\,rough,p}$ to SST with WISE and EuroSTARRS data-sets.

In this section some empirical models to describe the term $\Delta T_{B\,rough,p}$ are presented.

3.2.1 Wind speed dependence

Hollinger (1971) derived the brightness temperature sensitivity to wind speed from the measurements made at Argus Island Tower, and described it as follows:

$$\begin{aligned} \Delta T_h &\approx 0.2\,(1 + \frac{\theta_i}{55^\circ})\,U_{10} \\ \Delta T_v &\approx 0.2\,(1 - \frac{\theta_i}{55^\circ})\,U_{10} \end{aligned} \tag{3.3}$$

valid only for incidence angles (θ_i) smaller than 55°. This model was used by the National Oceanic and Atmospheric Administration (NOAA) for their experiments in 1997 with the SLFMR sensor (Goodberlet and Miller (1997)).

Camps et al. (2004a) have, also, calculated the brightness temperature sensitivity to wind speed based on WISE campaign data. A linear empirical model was obtained from fitting to the data $\Delta T_{B\,rough}$, and it is defined as follows:

$$\begin{aligned} \Delta T_h &\approx 0.23\,(1 + \frac{\theta_i}{70^\circ})\,U_{10} \\ \Delta T_v &\approx 0.23\,(1 - \frac{\theta_i}{50^\circ})\,U_{10} \end{aligned} \tag{3.4}$$

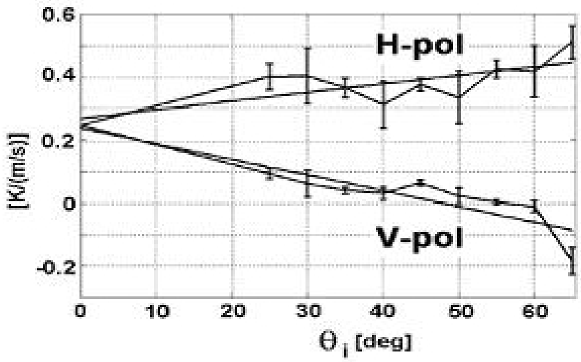

Figure 3.4: WISE 2001 derived L-band brightness temperature sensitivity to wind speed, for all data points.

The extrapolated sensitivity of T_B to wind speed is shown in figure 3.4, and at nadir is then,

$$\frac{\Delta T_{B,p}(\theta_i = 0^\circ)}{\Delta U_{10}} \approx 0.23\,K/(m/s) \tag{3.5}$$

The correlation between the data points and the linear fit is quite high, for H-pol, $r_h = 0.74$ and for V-pol, $r_v = 0.89$.

Since most of the data measured in the campaign were obtained under low wind conditions (45% of the measurements recorded with U_{10} in the range 0-5 m/s), it is evident that an error in the computed sensitivity at low winds has a very large impact in the weighted average. So Camps et al. (2004a) proposed also a new model that considers only data points that correspond to wind speed at 10 m high larger than 2m/s (below that, strange behaviours have been observed), with atmospheric instabilities corrected. Equations are written here:

$$\Delta T_h \approx 0.25\,(1 + \frac{\theta_i}{188^\circ})\,U_{10}$$
$$\Delta T_v \approx 0.25\,(1 - \frac{\theta_i}{45^\circ})\,U_{10} \quad U_{10} \geq\ 2m/s \tag{3.6}$$

The correlation coefficients between data points and the linear regression lines are: $r_h = 0.79$ and $r_v = 0.90$, which are higher than before.

3.2.2 Wave height dependence

In the same paper Camps et al. have studied the brightness temperature sensitivity to significant wave height[1] (SWH). Here it is considered that $\Delta T_{B\,rough,p}$ is expressed only through the SWH in meters. The linear fit of the measurements brings to the following model:

$$\Delta T_h \approx 1.09\,(1 + \frac{\theta_i}{142^\circ})\,SWH$$
$$\Delta T_v \approx 0.92\,(1 - \frac{\theta_i}{51^\circ})\,SWH \tag{3.7}$$

With correlation coefficient of $r_h = 0.88$ and $r_v = 0.78$, and the extrapolated sensitivity at nadir is then,

$$\frac{\Delta T_{B,p}(\theta_i = 0^\circ)}{\Delta SWH} \approx 1\,K/m \tag{3.8}$$

3.2.3 Wind speed and wave height dependence

Until the moment, most of the models (theoretical or semi-empirical) describe the brightness due to roughness of the sea as a function of wind speed only. Therefore, these models assume that the roughness of the sea is only dependent on the local wind speed. This is not completely right, since, when swell is present, some events of low local wind speed and high wave height are possible. Figure 3.5 shows the relationship between wind speed and significant wave height measured at the same time by the same buoy during WISE2001. It shows that the correlation is high between both parameters, but there are some events where high SWH were observed and U_{10} was low.

Miranda et al. (2003) showed, also, that the measured spectra frequently are not well approximated using fully developed models, since commonly situations with growing and decaying winds have been recorded.

[1]SWH is defined here as the average of the highest third of the waves.

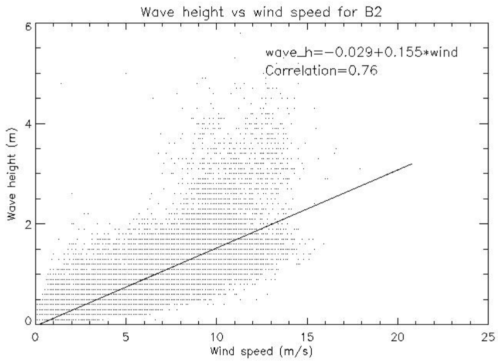

Figure 3.5: Scatter plot of SWH vs U_{10} with the liner regression line and the correlation with the data.

Being aware of this limitation, the author decided to try to find a model that takes into account also the swell events. That is to encounter a new model dependent on the local wind speed, as well as on the significant wave height. The derivation of this model, as well as test and comparison with other models, is a direct contribution of the author and it represents an important part of this thesis. This work has been published in Gabarró et al. (2004a) and has been presented in several conferences and meetings.

WISE 2001 data set was used to derive this new model. For each measurement of the radiometer, the wind speed and the wave height were obtained from the Aanderaa CMB buoy. Using 270 measurements, the curve fit IDL function was used to find the parameters that best fit the in situ measurements to the following model equation:

$$\begin{aligned} \Delta T_h &= (A + B\,\theta_i)\,U_{10} + (C + D\,\theta_i)\,SWH \\ \Delta T_v &= (A + E\,\theta_i)\,U_{10} + (C + F\,\theta_i)\,SWH \end{aligned} \tag{3.9}$$

The results obtained with their standard deviation are written in the following table:

	Result	Standard deviation
A	0.119	0.063
B	0.005	0.001
C	0.593	0.375
D	-0.012	0.008
E	0.003	0.001
F	-0.012	0.008

Finally the model derived from WISE data can be written as follows:

$$\begin{aligned} \Delta T_h &\approx 0.12\,(1+\frac{\theta_i}{24^\circ})\,U_{10} + 0.59\,(1-\frac{\theta_i}{50^\circ})\,SWH \\ \Delta T_v &\approx 0.12\,(1-\frac{\theta_i}{40^\circ})\,U_{10} + 0.59\,(1-\frac{\theta_i}{50^\circ})\,SWH \end{aligned} \tag{3.10}$$

The correlation coefficient between the data points and the model is $R = 0.761$. It should be stressed that comparing equation 3.10 with 3.6 and 3.7 at nadir, for this model, the dependence on U_{10} is almost half of the value given by the wind speed model, and that the dependence on SWH is close to the half of the sensitivity given by the model dependent on SWH.

The goodness of fit of the regression, called the *regression of determination*, is $r^2 = 60.1\%$. The absolute magnitud of the goodness of fit is the standard error of the estimate, that is defined as follows:

$$\text{Standard error of the estimate} = \left[\frac{1}{N_{data} - n_{param}} \sum_{i=1}^{N} (y-\hat{y})^2\right]^{1/2} = 1.275K \tag{3.11}$$

where N_{data} is the number of data to fit the curve, and n_{param} is the number of parameters to estimate (Emery and Thomson (1997)).

Figure 3.6 compares the $\Delta T_{B\,rough}$ measured and computed with this model for the two polarisations. The correlation at H-pol between them is 0.723, and the correlation at V-pol is 0.423, considerably lower as shown in the plot. The incidence angle of each measurement is also plotted, and it is represented through the right axis. Plot b) indicates that at incidence angles between 35 and 55 the $\Delta T_{B\,rough}$, V-pol of the model is near to zero, since the sensitivity of this to U_{10} and SWH is close to zero (the empirical model dependent on U_{10} only presents a similar behaviour). Then the high variability observed in the measurements should be due to experimental noise.

From here to the end, this new model will be called model-2P, as it is dependent on two parameters.

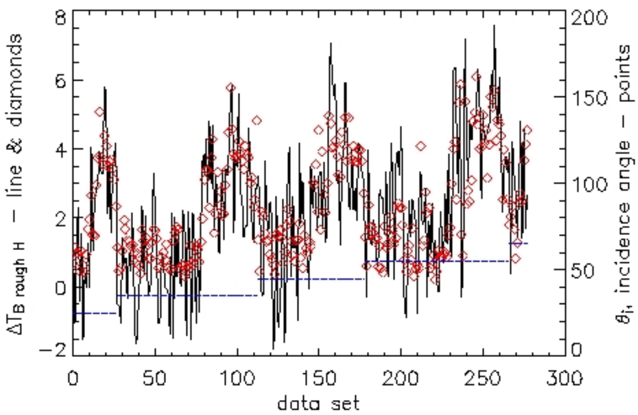

a)

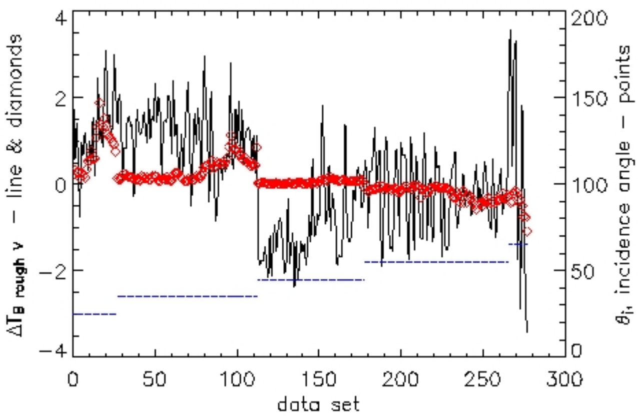

b)

Figure 3.6: a) On left axis, the black line is $\Delta T_{B\,rough}$ measured by the radiometer and the red diamonds are $\Delta T_{B\,rough}$ obtained from the model presented in equation 3.10 at H polarisation for 270 data points. Incidence angles values (25°, 35°, 45°, 55°, 65°) are plotted with blue dots, refereed at the right axis. b) The same for V polarisation.

3.3 Conclusions

Three different dielectric constant models have been presented and compared.

Also several direct models of the emissivity of sea surface at L-band have been presented. First the theoretical models have been shorty described. Later, two semi-empirical models derived by the UPC team have been presented.

Finally a new semi-empirical model, formulated by the author, that express the brightness temperature due to the roughness of the sea, is presented. The new approach in it is that sea roughness is expressed through both wind speed and significant wave height.

The advantage of this last model with respect to the others is that it considers the cases where swell is present (which is expressed in the SWH parameter) and the cases where small capillary waves are present due to local wind (which is expressed in the U_{10} parameter).

In chapter 5, these models will be compared by calculating the salinity retrieval from campaign datasets, and an analysis of the quality of them will be given, based in real data.

An interesting future work would be to try to derive other semi-empirical models using other parameters, in the way to better adjust models to real emissivity. Some other parameters that could be useful are: wave spectrum, wave edge, wind friction, etc. In section 4.4 a list of potential auxiliary parameters, that could be needed for SMOS is presented.

In chapter 6 the models will be compared using images created by the SMOS simulator.

Chapter 4

Auxiliary Parameters

This chapter presents the problem of the sensitivity of T_B auxiliary parameters, other than SSS.

Several sources of U_{10} and SWH that are currently available are introduced. Of course other sources are available, but the author has chosen few ones that are considered to have good accuracies and are representative of the whole possible sources. Hence data has been obtained from atmospheric or oceanographic models and satellite measurements.

Probably when SMOS will fly (2007) all these sources will not be available, or will be improved. But for the type of analysis done in this chapter, these sources are good enough. Finally a list of possible auxiliary parameters that could be used for SMOS is attached.

In chapter 5 the retrieved salinity errors when using different combinations of these sources will be analysed based in campaigns datasets.

4.1 Sensitivity to auxiliary parameters

The radiometer measurements at L-band are not only sensitive to salinity, but also to sea surface temperature and roughness of the sea, as has already been noted in the previous chapters.

This affirmation brings to a clear conclusion: In order to retrieve salinity it is required to know the parameters, that influence the brightness temperature. These parameters are called *auxiliary parameters*[1].

The question is now: 'How do we obtain these auxiliary parameters for SMOS?'. As explained before, the sensitivity of T_B to salinity is of the same order of magnitude or smaller than its sensitivity to SST and roughness of the sea.

Errors on T_B due to an error on an auxiliary parameter have been calculated by comparing the values measured by the radiometer with those obtained by the forward emissivity model when errors on U_{10}, SWH and SST are introduced. Figure 4.1 shows the difference $T_{B\,measured} - T_{B\,modelled}$, for different errors on the auxiliary parameters as function on the incidence angles. The plots have been done using WISE data set, and the emissivity model 2-P. The semi-empirical model that fits the dependence of T_B on both wind speed and significant wave height is used. The plots reveal that the most critical parameter is U_{10}, as pointed out by Yueh et al. (2001), and especially for the horizontal polarisation. An error on U_{10} of 3 m/s produces an error on T_B of $\approx$1.5 K. Less significant are the SWH errors, but they are not negligible at low incidence angles for V-pol.

Therefore, one can deduce that there is a need to know the auxiliary parameters with good accuracy, and as simultaneously in time and space as possible to the SMOS measurements.

One possibility is to use observations made by other sensors embarked on satellites with similar orbit, but these measurements will hardly be simultaneous. Meteorological and oceanographic marine models could also be used, with the advantage of higher temporal resolution, and that they assimilate satellite data and other sources of information. Both cases will present inaccuracies on the measurements due to instrumental errors and sampling limitations.

The advantage of SST with respect to the parameters that describe the roughness is that sea temperature has much less temporal variability than U_{10}, and so the variability is lower.

[1]Sometimes, erroneously, they are also called ancillary parameters. Ancillary parameters are those recorded by the satellite, other than radiometric, and sent to ground in the same telemetry message (e.g. platform altitude).

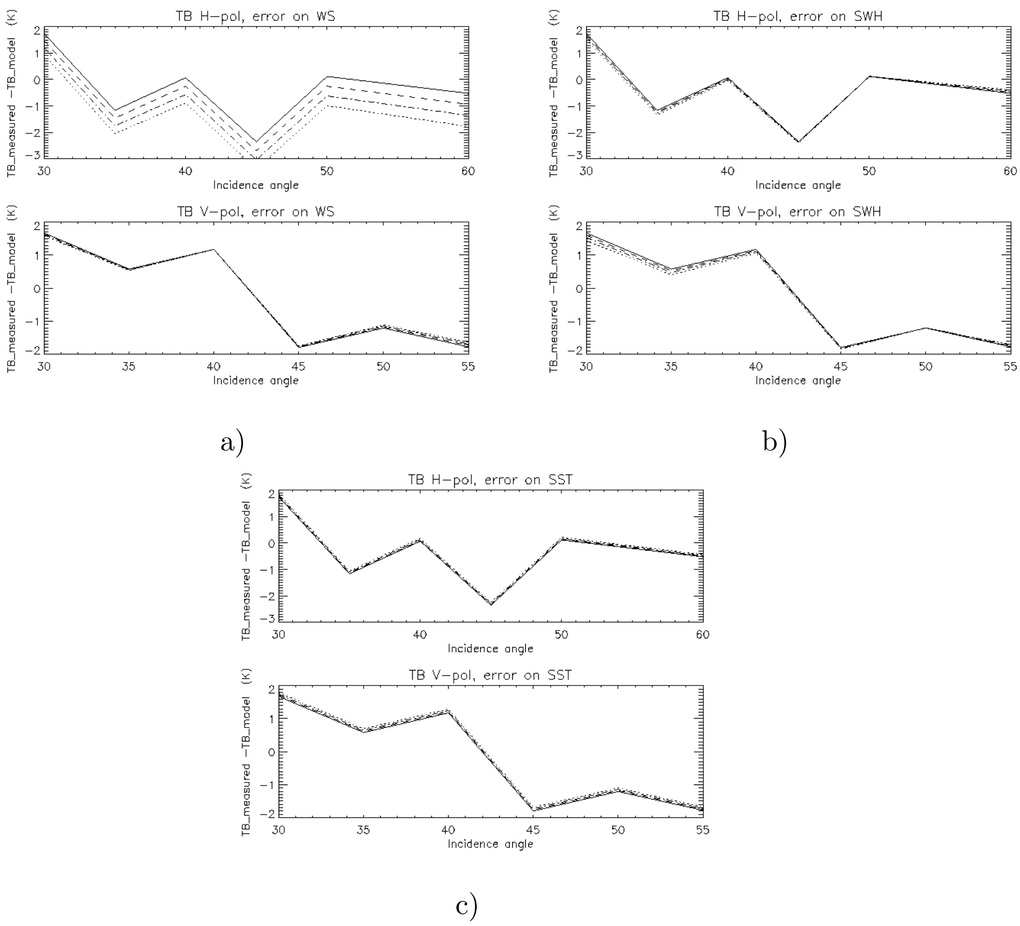

Figure 4.1: $T_{B\,measured} - T_{B\,modelled}$ as function of incidence angles, for H-pol (top) and V-pol (down). a) Case where errors on the U_{10} are added (— ΔU_{10}=0, - - - ΔU_{10}=1, -·-· ΔU_{10}=2, ··· ΔU_{10}=3 m/s). b) Case where errors on the SWH are considered (— ΔSWH=0, - - - ΔSWH=0.3, -·-· ΔSWH=0.6, ··· ΔSWH=1 m). c) Case where errors on the SST are added (— ΔSST=0, - - - ΔSST=0.3, -·-· ΔSST=0.6, ··· $\Delta SST = 1°C$).

4.2 Roughness parameter

The determination of sea roughness coincidental to SMOS overpasses is a major problem due to its high variability and accuracy limitations in satellite measurements and models.

To analyse the effect on the SSS retrieval induced by different sources of roughness parameters, the following numerical model outputs and satellite measurements of wind speed and SWH were used for the area and time of WISE 2001 campaign:

1. Wind speed information:

   - HIRLAM (HIgh Resolution Limited Area Model): A numerical short-range weather forecasting system for operational use. This is the result of a big project of cooperation between several countries (Finland, Sweden, Norway, Denmark, The Netherlands, Ireland, Iceland and Spain, plus France as collaborator), to develop numerical prediction models for short range time. The analysis is done with wind and relative humidity as well as water temperature. It does assimilation of satellite data to give the best first guess to the numerical model. It gives predictions in temporal scales of 3 hours to some years. And the spatial scale goes from the global Earth to near 10 km. The products given by the model are: surface pressure, temperature, geopotencial height, relative humidity and wind, all at surface and at several altitudes. It gives also accumulated precipitation every 6 hours.
   - ARPÈGE (Action de Recherche Petite Echelle Grande Echelle): A numerical weather prediction system developed and supported by Météo-France and the European Centre for Medium range Wethear Forecast (ECMWF) as part of the Aladin project. It is a numerical model with satellite assimilation. ARPEGE is a variable resolution spectral primitive equation system that runs with a semi-Lagrangian semi-implicit scheme.
   - QuikSCAT: The SeaWinds instrument on the QuikSCAT satellite is a specialised microwave radar scatterometer that measures near-surface wind speed and direction under all weather and cloud conditions over Earth's oceans. NASA's Quick Scatterometer (QuikSCAT) was lofted into space on June 1999 into a polar orbit. SeaWinds uses a rotating dish antenna with two spot beams that sweep in a circular pattern. The antenna radiates microwave pulses at a frequency of 13.4 gigahertz across broad regions on Earth's surface. The instrument will collect data over ocean, land, and ice in a continuous, 1800 kilometer-wide

band, making approximately 400000 measurements and covering 90% of Earth's surface in one day.

2. Significant wave height information:

    - WAM: WAM (CYCLE 4) is a third generation wave model, which computes spectra of random short-crested wind-generated waves. It is an energy balanced, spectral wave model with variable resolution. This version has incorporated improvements in the surface roughness and drag coefficients related to wave formation, as well as improved response to refraction effects from bottom topography. It defines the spectral energy of wind generated wave using 25 frequency bands and 24 direction bands. The finest resolution expected to be available, based on computer run time, input data and input wind field grid resolution is 5 minutes. The model performs best in water depths greater than 20 meters. The product generated is a gridded field that supplies wave height, period and direction for forecasts to 48 hours twice daily. WAM requires surface wind forcing from meteorological model output.
    - RA-ERS: radar altimeter on board ESA ERS-2. The Radar Altimeter is a Ku-band (13.8 GHz) nadir-pointing active microwave sensor designed to measure the time return echoes from ocean and ice surfaces. Functioning in one of two operational modes (ocean or ice) the Radar Altimeter provides information on significant wave height; surface wind speed; sea surface elevation, which relates to ocean currents, the surface geoid and tides; and various parameters over sea ice and ice sheets. Significant Wave Height (H-1/3) is derived from the slope of the return echo leading edge, which is related to the standard deviation of the heights distribution of reflecting facets on the sea surface (assumed to be gaussian). ERS-2 was launched in 1995, an putted into a near-circular, polar, Sun-synchronous orbit, with a revisit time of 35 days.

The HIRLAM and WAM model outputs have been obtained through the Spanish Instituto Nacional de Meteorología and Puertos del Estado. The wind speed information from HIRLAM is analysed data, since assimilation of satellite and buoys data has been done to run the model. On the other hand, SWH data from WAM uses HIRLAM wind speed assimilated data but does not have assimilation of SWH data.

The ARPÈGE model belongs to Météo-France, and outputs have been obtained through LODYC. The data used here are analysed data, so assimilation from satellite or buoys measurements has been done.

NASA's Quick Scatterometer Seawinds has a resolution of 25 kilometres and wind-speed measurements of 3 to 20 m/s have an accuracy of 2 m/s and an accuracy of 20 degrees on the direction measurements. It covers 90% of Earth's surface oceans in one day, but full repetition time is 3 days.

The SWH measured by the Radar Altimeter onboard ERS-2 for the Casablanca area during the WISE campaigns have been used. This instrument has an accuracy of 0.5 m or 10% whichever is higher, and a spatial resolution of 20×20 km^2. The measurement is defined as 4 times the standard deviation of the wave slope (as buoy 3 in WISE 2001) in opposition to the definition of buoy 2 (average of the highest third of the waves). To convert from one definition to the other, the value according to the first definition must be divided by $\sqrt{2}$. The problem of the radar altimeter from ERS-2 is its low temporal resolution (35 days repetition), so to have data with the required time resolution, data from a huge area (170*440 Km) were used.

SOURCE	Spatial resolution	Temporal resolution
HIRLAM	0.125°	3 hours
ARPÈGE	0.25°	6 hours
QuikSCAT	25 Km	3 days
WAM	0.125°	3 hours
RA-ERS	20 Km	35 days

Table 4.1: Comparison of different sources for wind speed and significant wave height.

Table 4.1 summarises the spatial and temporal resolutions of each data source. When accepting satellite data measured in an area (not only one point) the temporal resolution increases, since different satellite passes can be considered. Figures in 4.2 show the temporal sequence of wind speed and wave height obtained from these sources for WISE2001 time period; in situ measurements from buoys are also plotted. For wind speed, the models and satellite outputs are quite similar to in situ measurements except in some punctual occasions. The mean difference between wind speed in situ measurements and HIRLAM model output is 1.98 m/s, with respect to ARPÈGE model output is 1.93 m/s, while to satellite data is 1.59 m/s (although in this last case there are much less data points available). These differences are above the 1.5 m/s accuracy in wind speed initially required for SMOS SSS retrieval from preliminary simulations.

SWH's given by the model is similar to buoy measurements, except for high

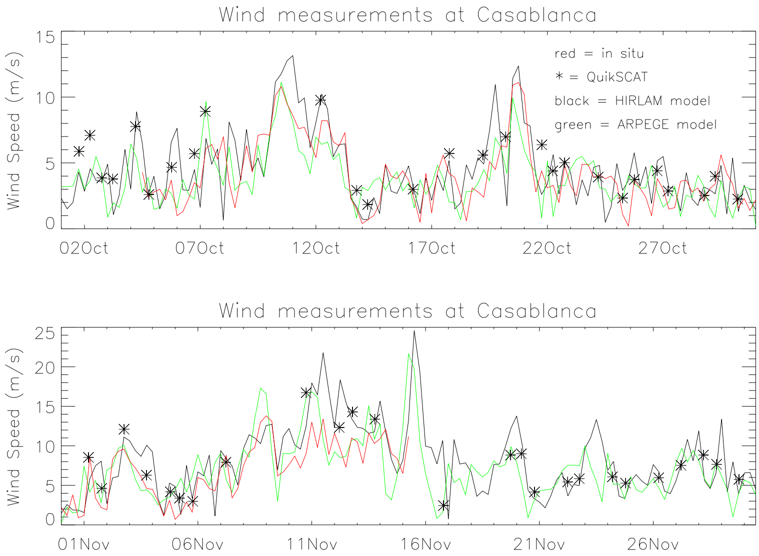

a)

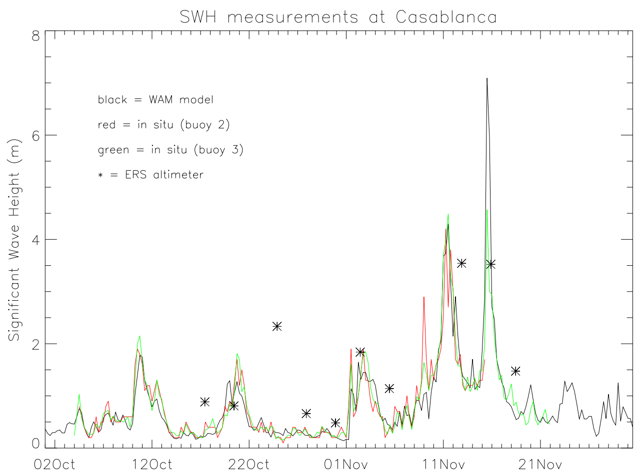

b)

Figure 4.2: a) Comparison of different sources of wind speed information during WISE 2001 campaign. In situ buoy (red line), HIRLAM model (black line), ARPÈGE model (green line) and QuikSCAT satellite (*). b) Comparison of different sources of significant wave height information during WISE 2001 campaign. In situ data buoy 2 (red line), in situ buoy 3(green line), WAM model (black line) and Radar Altimeter-ERS (*)

wave height events, where the model overestimates them. The satellite measurements are not very realistic, which is not surprising since their temporal resolution is very low and a lot of spatial averaging has to be done to cover the WISE area. The mean difference between in situ measurements and WAM model is 0.22 m, while the mean difference grows to 1.16 m with respect to satellite measurements.

4.3 SST parameter

Sea surface temperature, nevertheless, is not as critical as roughness, since its variability is much lower, the sensitivity of T_B to SST is also lower, and satellite measurements are very accurate and frequent.

The brightness temperature sensitivities to SSS and SST, for all incidence angles and flat surface, and for salinities larger than 20 psu, are the following:

- $\Delta T_B/\Delta SSS \approx 0.35 - 0.80 K/psu$ at V-pol
- $\Delta T_B/\Delta SSS \approx 0.20 - 0.60 K/psu$ at H-pol
- $\Delta T_B/\Delta SST \approx 0.02 - 0.60 K/°$C at V-pol
- $\Delta T_B/\Delta SST \approx 0.02 - 0.50 K/°$C at H-pol

SST can be obtained with good accuracy and resolution by satellite measurements. A typical accuracy from Pathfinder data-set can be of approximately ±0.3°C in clear sky conditions and ±0.5°C otherwise. This error translates to T_B errors of 0.01- 0.3 K at V-pol and 0.01-0.25K at H-pol. So these errors on T_B are not significant, and will not represent a big problem for the salinity determination.

For this reason, this thesis has been focused on the roughness auxiliary parameters problems.

4.4 Other potential auxiliary parameters

A list of all the auxiliary parameters that can be potentially used in the retrieval of salinity by the SMOS mission is presented in table 4.2 and 4.3. This includes parameters that are strictly necessary (as SST) and others that will be used depending on the parameterisation finally selected to described the surface roughness impact on T_B. The table, that also includes the present accuracy and sources for these parameters, has been compiled within an ESA study (WP1100, ESTEC ITT 1-4050/03/NL/Cb) in which the author has been participated.

Parameter	Error	Source of auxiliary data	Usage
Sea surface temperature (SST)	±0.3°C	NOAA/AVHRR, ERS/ATRS, ENVISAT/AATSR MSG, Meteosat, GOES	T_B direct model
	±0.5° C	RMM/TMI, AMSR-E, models: ECMWF, NCEP	
Wind speed (U_{10})	± 2.5 m/s	ERS-2 AMI Wind scat., QuickSCAT, ADEOS-II, SeaWinds scatterometer, METOP-1 ASCAT,ENVISAT RA-2 Altimeter, JASON-1 Altimeter, DMSP's SSM/I radiometers, RadarSat, ENVISAT/ASAR, GPS models: ECMWF, NCEP	T_B direct model
Wind direction (ϕ_{10})	±25°	ERS-2 AMI Wind scat., QuickSCAT, ADEOS-II SeaWinds scatterometer, METOP-1 ASCAT, ENVISAT RA-2 Altimeter, JASON-1 Altimeter, DMSP's RadarSat, ENVISAT/ASAR, GPS, models: ECMWF, NCEP	T_B direct model
Air temperature (T_{air})	±1° C	models: ECMWF	Wind friction velocity, Foam coverage model
Fetch (F)	-	models: ECMWF (WAM) & NCEP (WAVEWATCH III)	T_B direct model
Wave aging parameter (Ω)	-	models: ECMWF (WAM) & NCEP (WAVEWATCH III)	T_B direct model

Table 4.2: List of potential auxiliary parameters used to retrieve salinity for SMOS (from WP1100, ESTEC ITT 1-4505/03/NL/Cb).

Significant wave height (H_s)	±0.25 m	models: ECMWF (WAM) & NCEP (WAVEWATCH III), ERS2 altimeter, TOPEX/POSEIDON, ENVISAT RA, JASON-1 Altimeter	T_B direct model
Peak Wave direction	±25 m	CMWF (WAM) & NCEP (WAVEWATCH III) ERS/AMI, ENVISAT/ASAR	T_B direct model
Peak wave period (T_p)	±20%	ECMWF (WAM) & NCEP (WAVEWATCH III)	T_B direct model
$\sigma_0(dB)$	-	GPS and radar	Direct roughness correction
Currents	< 0.5 m/s	detection by AVHRR, SeaWifs, SAR imagery, models: ORCA, CLIPPER, NANSEN	
Sea surface salinity (SSS) (first guess)	±0.25 psu	models: ORCA, CLIPPER, NLOM, in situ : ARGO floats, climatologies	T_B direct model
Oil slicks	detection	ERS-2, RadarSat, ENVISAT/ASAR	

Table 4.3: Continuation of table 4.2.

Chapter 5

Salinity Retrieval

In this chapter the errors in the process of retrieving sea surface salinity from brightness temperature measurements of three campaigns are computed using different emissivity models and sources of auxiliary parameters.

The retrieved salinity errors are compared, and the discussion leads to choose a particular emissivity model, which better retrieves salinity.

Also the errors when using different sources of auxiliary parameters are presented. Since the retrieved salinity errors due to inaccuracies on the auxiliary parameters can be important, the author proposes a new method to obtain these parameters from the brightness temperatures themselves. This new method has demonstrated to retrieve salinity much better than fixing the parameters to erroneous values. However, this new method needs some adjustments and tuning.

5.1 Inversion algorithms

The *inversion* or *retrieval problem* is common for almost all satellite observations. This is how a parameter can be obtained from measured data. In the SMOS case the inversion algorithm consists of computing salinity from a set of radiometric measurements T_B, at given incidence angles and polarisations.

The so-called *forward problem* is the opposite one. This problem deals with the description of the physical laws that, given the geophysical parameter values, can predict the values that will be measured. In our case it is the law that describes the transition from SSS (among other variables) to T_B. This problem is already treated in chapter 3.

It is usually important to appreciate the degree of linearity of any given inverse problem, that is the degree to which the knowns and unknowns of the problem can be separated out into a linear equation. When dealing with linear equations, the variables to be retrieved can be calculated with some well established methods.

In our case, T_B models are not linear neither with SSS, nor SST, since dielectric constant models are clearly non-linear with those parameters. On the other hand, when using semi-empirical models, T_B is assumed linear with U_{10} and SWH.

For the SMOS case, three different inversion methods have been taken under consideration:

- Analytical inversion
- Iterative methods
- Neural network methods

A description of these methods and a comparison of the last two applied to retrieve real data can be found in the documents: 'Synergetic aspects and Auxiliary Data Concepts for Sea Surface Salinity Measurements from Space', ESTEC ITT 1-4505/03/NL/Cb Workpackage 1100 and also in the final report of the ESA 15165/01/NL/SF contract, both documents from the European Space Agency.

The iterative methods are very flexible, since the models and the auxiliary parameters can very easily be modified. This is not possible with the neural network approach because, for every modification a new database should be learnt, a procedure that could take a lot of time and effort. It is necessary, also, to know very well the properties and physical characteristics of the parameters before programming the neural networks (Hertz et al., 1991).

Furthermore, the iterative methods permits to have a clear comprehension of the physical processes and understand what is happening during the inversion process. On the other hand, neural networks can be considered as 'black boxes', since once they are trained, their characteristics and behaviour is not known (Hertz et al., 1991).

Thence, considering the advantages described above, only *iterative methods* have been used in this work.

The iterative methods follow the procedure described bellow:

1. A first-guess for SSS is chosen (or any parameter to be retrieved).

2. A weighting function is calculated by giving different weights to different observations, depending on the quality of observations.

3. Using the chosen forward model, T_B is calculated.

4. The computed brightness temperatures are compared with the measured ones.

   - If they are similar $\|T_B^{model} - T_B^{measured}\|^2 < threshold$, then the current SSS is accepted as final result.
   - If convergence has not been achieved, then a δSSS is added to the current SSS value.

5. Steps 3 through 5 are repeated until a solution is found.

When solving an overdetermined system of equations, where there are more equations (M) than unknowns (N), it can be easily handled by obtaining a "least square error solution." It consists of finding a solution which for all possible vectors of dimension N minimise the norm of $\|T_B^{model} - T_B^{measured}\|$.

Thanks to its multi-angularity capability, SMOS retrieval will be an overdetermined problem. It means that a large number of different incidence angles (from 0° to 55°) will look at the same pixel (target), so there will be more equations than unknowns. Retrievals from WISE, EuroSTARRS and FROG measurements are also overdetermined systems.

The least square error methods have been used here. The definition of the cost function (what should be minimised) is an important issue, and it can be considered with constraints or without them.

In these calculations a normal distribution of the errors is assumed. May be this is not a strictly correct assumption, but for a preliminary analysis it is a good enough approximation. Further work can be oriented on the analysis when these errors do not follow a normal distribution, but this is out of the scope of this thesis.

5.1.1 Cost function

The cost function is the function that needs to be minimised by the least square method to solve for the unknowns.

It can be defined with restrictions or without restrictions. It means that when no restrictions are considered, all possible solutions are valid. On the other hand, when dealing with restrictions, the possible solutions are constrained to within a range of values, which are already specified in the cost function.

When no restrictions are considered, the cost function is defined as:

$$\chi^2(SSS, SST, U) = \sum_{i=0}^{N-1} \frac{[\, T_{B_i}^{meas} - T_{B_i}^{model}(\theta_i, SSS, SST, U)\,]^2}{\sigma_i^2}, \tag{5.1}$$

where i is the different incidence angle, $T_{B_i}^{meas}$ is the measured brightness temperature, and $T_{B_i}^{model}$ is the modelled brightness (obtained through the forward model).

On the other hand, when considering some restrictions, then the cost function is defined as follows:

$$\chi^2(SSS, SST, U) = \sum_{i=0}^{N-1} \frac{[\, T_{B_i}^{meas} - T_{B_i}^{model}(\theta_i, SSS, SST, U)\,]^2}{\sigma_i^2} + \sum_{j} \frac{[\, P_j - P_{j\,ref}]^2}{\sigma_{P_j}^2}, \tag{5.2}$$

where P is the parameter to be found, with j possible parameters (in this case they could be: SSS, SST, U_{10} or SWH), P_{ref} is a reference value for each of the parameters (obtained from satellite or model outputs) from which the final solution should not be far, and σ_P^2 is the variance of the expected error of the reference values. The value of P at the first iteration is the so-called "a priori" or "first guess" value[1]. Then the possible solutions of P can be between $P_{ref} - \sigma_P$ and $P_{ref} + \sigma_P$. Another way to understand the importance of this parameter is the following: when a reference value of the parameters is known with low precision, then σ_P is big, then the term of this parameter is small, and have less weight in the overall equation.

Thereafter, a different number of unknowns have been considered. Sometimes only SSS is treated as unknown, while in some occasions other parameters (U_{10}

[1] Attention should be put with the names. Here we use *a priori* value for the first guess value, and *reference value* for the value of each parameter independently known with an expected error. Other authors call *a priori* the *reference value*

or SWH, SST), as well as the SSS, are dealt as parameters to be retrieved[2]. The necessity of using one or more unknowns will be argued later on.

5.1.2 Methodology

For the retrieval process the IDL software (Iterative Data Language, from RSI systems) has been used. When dealing with cases where the cost function does not have restrictions then the Levenberg-Marquardt least square algorithm has been used (Marquardt (1963)). When cost functions with restrictions are necessary, then downhill simplex method of optimisation is utilised (Nelder and Mead (1965)). For more information on those methods see appendix **??**.

The datasets that have been used for the retrieval study are from WISE, EuroSTARRS and FROG campaign. For WISE data, the best suited measurements to study the retrieval problems are the data acquired with elevation scans, and in particular data acquired with scans at 9 angles (25°, 30°, 35°, 40°, 45°, 50°, 55°, 60° and 65°), unless when specified. Regrettably not a lot of scans were performed for 9 incidence angles. On the other hand a set of elevation scans measurements were performed in steps of 10° (5 different incidence angles), but they are not as much useful as the case before. During EuroSTARRS measurements where done in 6 fix incidence angles (the radiometer has 6 beams). For FROG campaign, measurements were done with 25 incidence angles, in 1° steps.

All atmospheric corrections has been done; Up-welling and down-welling corrections and cosmic and galactic noise correction. However Faraday rotation is not necessary to correct for, since at the height of measurement, this effect is not present (this is produced in the ionosphere).

5.2 Number of incidence angles

As explained before, the acquisition strategy of WISE campaign was to measure brightness temperature in both polarisations (H and V) with three different modes of measurements:

- Mode 1, fixed observations: Long observations (1h.) at fixed incidence and azimuth angles to study the stability time scale of the sea state and its consequences on L-band emissivity.

[2]Sometimes, when some parameters other than SSS are considered as unknowns they are also called free, since they are not set to a specified value.

- Mode 2, azimuthal scan: 6 angular positions in 140° at fixed incidence angle, to study the azimuthal modulation at L-band. Measurements were 20 minutes long.

- Mode 3, elevation scans between 25° to 65°. In WISE 2001 two types of elevation scans where performed. The first was with steps of 10° pointing towards the west. The second one acquired data in steps of 5° and the radiometer was pointing towards the North, this was done during sun-shine. Mode 3 was specially selected to study the emissivity forward model at L-band.

The measurements performed in elevation scan (mode 3) are the best suited to study retrieval problems, and in consequence, these are the ones used in this work.

Figure 5.1 shows the error in the retrieved salinity (using the semi-empirical emissivity model dependent on U_{10}) as a function of the number of incidence angles. The number of incidence angles acquired (x axis) comes from five or nine different acquisitions angles per two polarisations minus the discarded measurements. Measurements were discarded when the level of radio frequency interferences (RFI), present during the whole measurement or part of it, led to too large variance in T_B values. The plot shows that the SSS retrieval quality increases with the number of acquisition angles used in the retrieval. This conclusion could be expected, since with more independent views of the same target, better will be the retrieved parameter, because the noise in each measurement has less weight.

5.3 Models comparison with salinity retrieval

In chapter 3, three groups of models have been presented: dielectric permittivity models, wave spectrum models, and scattering models. In this section the retrieved salinity results by using different combinations of them are compared and evaluated.

5.3.1 Dielectric permittivity models

The three constant dielectric models which are presented in section 3.1.1 have been used to retrieve salinity from 20 files acquired during the FROG experiment. These files were obtained for a completely flat surface, with elevation scans between 25° and 50° in steps of 1°.

In this retrieval process a cost function with restrictions is considered, and the parameters used are the following: $SSS_{ref} = SSS_{insitu} + 0.5$, $\sigma^2_{SSS} = 1.0$

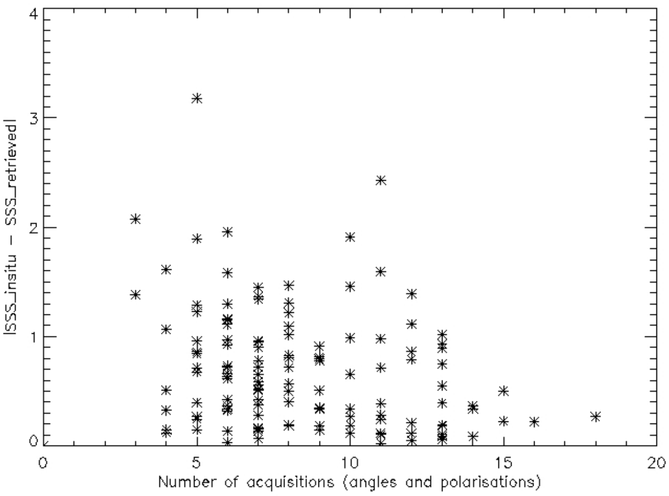

Figure 5.1: Retrieved salinity errors as function of the number of acquisition angles. The computations were performed with the semi-empirical model dependent on U_{10}.

psu and the initial guess for SSS was set to 37.5 psu. The model that has been used is the Fresnel reflection with the $\Delta T_{B\,rough}$ equal 0, since no roughness was present (flat surface).

Table 5.1 summarises the mean and the variance of the retrieved salinity results ($\Delta SSS = |SSS_{insitu} - SSS_{retrieved}|$) for the 20 files, for the three models. The retrieved salinities are compared with the salinity measured in situ by the MICROCAT instrument which has an absolute accuracy of 0.02 psu. The table shows that the model that makes a prediction of T_B closer to the measurements is the Klein & Swift model. Blanch & Aguasca shows relatively close behaviour, while Ellison model gives seriously biased results.

Dielectric const. model	$\overline{\Delta SSS}(psu)$	$\sigma^2_{\Delta SSS}$
Klein & Swift	0.261	0.025
Ellison	2.125	0.511
Blanch & Aguasca	0.596	0.061

Table 5.1: Comparison of retrieved salinity errors when using different dielectric constant models and FROG data set.

For the following calculations the Klein & Swift dielectric constant model has been used, except when explicitly stated.

Only the FROG data set has been used in this study, because only this one permits to isolate the problem of the dielectric constant from other issues which are not well known (for example the effect of roughness in emissivity). This is because during FROG the measurements were done with completely flat water surface.

5.3.2 Scattering and wave spectrum models

Results from WISE data set

Four different combinations of scattering and wave spectrum models have been used to retrieve salinities from the WISE 2001 data set. The four combinations used are dependent on the wind speed only and are the following:

- Two-scale Method with Durden and Vesecky spectrum $\times$ 2.
- SPM/SSA scattering model with Elfouhaily wave spectrum
- Semi-empirical model with Hollinger's linear regression model (equation 3.3)
- Semi-empirical model with WISE's derived linear regression model, which depends on wind speed (equation 3.4).

These models have been run over 25 different files obtained during WISE2001 with 9 different elevation angles. They were acquired on different days and therefore under different wind and temperature conditions. In order to run the algorithm to retrieve salinity, in addition to the measured T_B, it is necessary to introduce as input the wind speed and sea surface temperature. For that, data measured by oceanographic and meteorological buoys and have been used.

Figure 5.2 shows the difference between the in situ salinity (with an absolute accuracy of 0.02 psu) and the retrieved salinity for the models under study, when no restrictions were considered. It shows that the model that best fits in situ measurements is WISE-derived model, as was expected since a model function derived from the same data set is used. The mean and the variance of the errors in the retrieved salinities for the 25 files have been calculated and are presented in table 5.2.

The retrieved salinities have also been obtained using the individual points of the WISE-derived model, measured T_B for a specific U_{10} instead of the linear

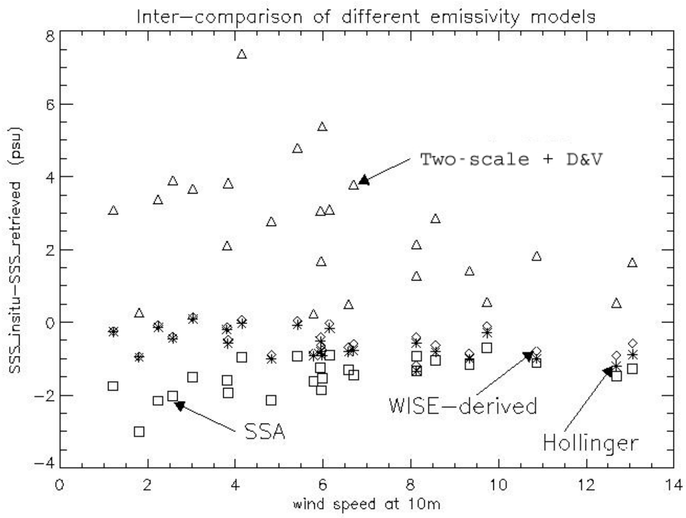

Figure 5.2: Error on the salinity retrieved using different emissivity models.

fit. The results demonstrate that the approximation made with the linear fit produces the errors in the retrieved salinity by less than 0.01 psu.

The Two-Scale model always highly underestimates the salinity. This problem could be due to a bias on the modelled T_B of about 1-1.5K that produces a negative bias of 2-3 psu in the salinity. It may also be due to a weak wind dependence that forces the algorithm to decrease salinity in order to increase T_B.

The SSA model overestimates salinity, i.e. the wind dependence is too high. In figure 5.3 it can be observed that the accuracy on the retrieved salinity is poorer for events with low wind speed and small waves than in other conditions. This is in agreement with Voronovich and Zavorotny (2001), because they conclude

Model	$\overline{\Delta SSS}$ (psu)	$\sigma^2_{\Delta SSS}$
Hollinger's model	0.63	0.15
WISE-derived model	0.52	0.12
Two-scale + Durden & Vesecky ×2	4.28	3.18
SSA + Elfouhaily	1.48	0.27

Table 5.2: Mean and variance of the retrieved salinity errors for different models, considering $\Delta SSS = |SSS_{insitu} - SSS_{retrieved}|$.

that the Elfouhaily spectrum overestimates the probability of having short waves by 2-4 dB in the cross-wind direction. The results show that this model is not recommended for low wind events.

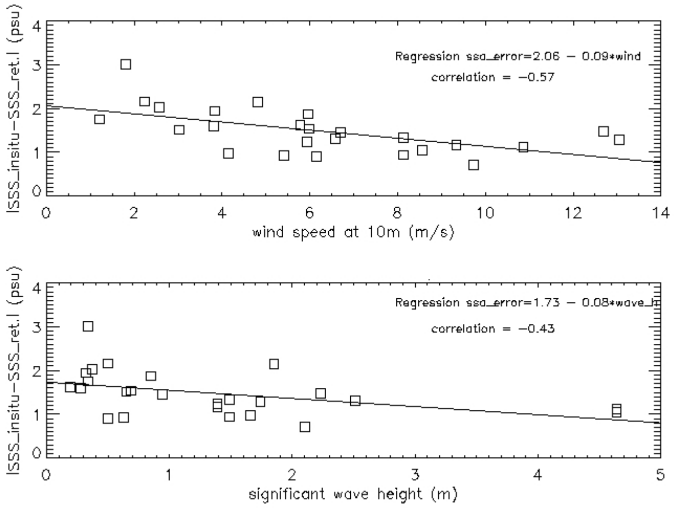

Figure 5.3: Error on the salinity retrieved when using the SSA + Elfouhaily model as function of the wind speed and significant wave height.

From these results it can be concluded that semi-empirical models seem to recover salinity better than the analytical ones, and that the best model to use in order to retrieve salinities from WISE data is the WISE-derived model.

Figure 5.4 shows that the error in the retrieved salinities using the WISE-derived model tends to increase linearly with increasing wind speed and wave height. This effect can be explained by the fact that the influence of foam has not been taken into account in the models. Normally, the foam coverage increases with wind speed (or wave height) and its effect can be considered negligible only with wind speeds below 10m/s. The foam increases the brightness temperature. If this $\Delta T_{B\,foam}$ is not expressed in the model equations, the inversion algorithm will decrease the salinity to compensate for this increase in T_B. On the other hand, as the model was derived from measurements, and more measurements for low wind speeds than strong wind speeds were acquired, higher uncertainties appear for the high wind speed region.

Vall-llossera et al. (2003) showed that models and WISE measurements have some disagreements with $\Delta T/\Delta U$, especially at low wind speeds. Figure 5.5 plots the sensitivity of T_B to U_{10} respect to U_{10} and θ_i for Durden and Vesecky×2, Elfouhaily×2 and Kudryavtsev. It can be seen that their behaviour mainly differ

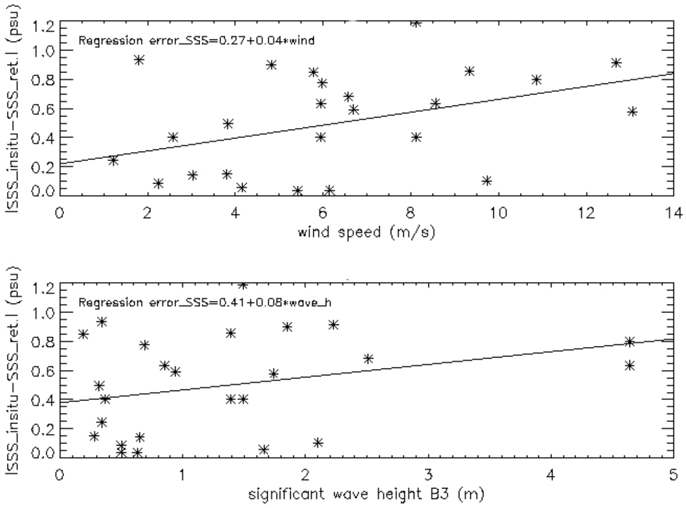

Figure 5.4: Error on the salinity retrieved when using the WISE-derived model as function of the wind speed and significant wave height.

for low wind speeds, since for that range the sensitivity is high non-monotonic. Therefore, since 45% of measurements in WISE 2001 campaign were performed in the range of 0-5m/s, 34% in the range 5-10m/s and only 21% for higher winds than 10m/s, it is clear that an error in the computed sensitivities at low wind speeds has a large impact in the mean salinity error values.

This different behaviour of the sensitivity of T_B for low wind speed with respect to higher values has also been observed with WISE 2001 measurements by Etcheto et al. (2004). They observed that $\Delta T_{B\,rough}$ abruptly decreases for wind speed lower 3 m/s, as shown in figure 5.6. This behaviour was observed at 2.65 GHz by Blume et al. (1977) during a flight above Chesapeake Bay. It is known that the scatterometer measurements are very inaccurate below 3 ms^{-1}. The reason for this decrease is probably the threshold effect in the generation of capillary waves: the wind speed needs to be above a threshold for the friction to overcome the viscosity effects of the water.

For these calculations the WISE-derived model used to retrieve salinity, is the one which is computed when all that points are used.

Another way to retrieve salinity is to use a model that considers the sea surface roughness term as a function of the significant wave height instead of the wind

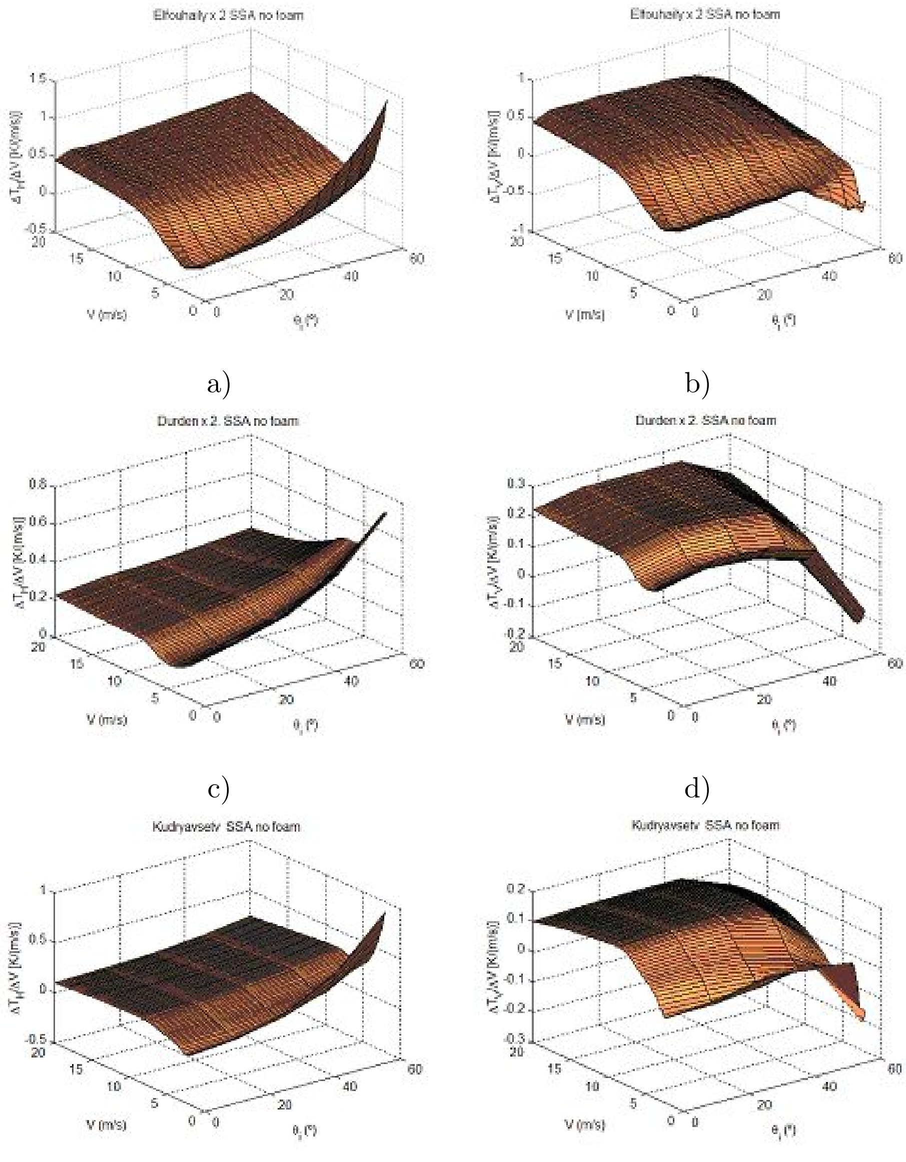

Figure 5.5: $\Delta T_h/\Delta U_{10}$ respect to U_{10} and θ_i predicts by SSA for a) Elfouhaily×2 c) Durden and Vesecky×2 e) Kudryavtsev. $\Delta T_v/\Delta U_{10}$ respect to U_{10} and θ_i predicted by SSA for b) Elfouhaily×2 e) Durden and Vesecky×2 f)Kudryavtsev (from Vall-llossera et al. (2003)).

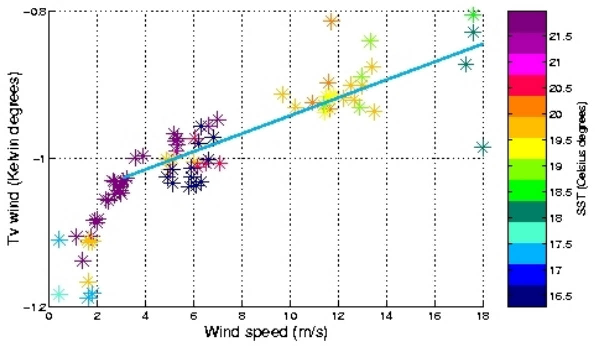

a)

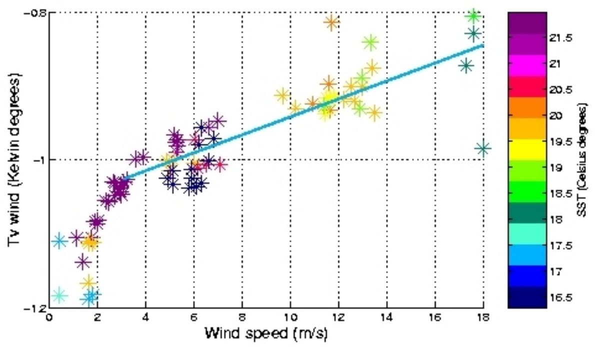

b)

Figure 5.6: $T_{B\,rough}$ in vertical (a) and horizontal (b) polarisations measured at 44° incidence angle from WISE 2001 measurements. (from Etcheto et al. (2004)).

speed. The advantage of this dependence should be that the wave height is not as variable as the wind. In addition, surface roughness may be due to the swell and not only to wind waves. The theoretical spectrum models usually consider fully developed seas dependent only on the actual local wind (they usually neglect the swell effect).

Salinity retrieved errors have also been calculated when using the WISE-derived semi-empirical model, presented in section 3.2.2, which is dependent on significant wave height.

In addition, model-2P, which depends on both wind speed and significant wave height presented in section 3.2.3, has been used to compute the retrieved salinities as well.

Table 5.3 compares the errors on retrieved salinities when using the three WISE-derived models: the U_{10} dependence model, the SWH dependence model and model-2p that depends on both. The data used here are the measurements acquired at 9 different incidence angles that where pointing towards north. The buoys measurements of U_{10} and SWH have been used. The model of SWH dependence does not give satisfactory results, probably due to the fact that the dominant wind during WISE 2001 was from the North. Then some reflection waves produced by the platform legs were observed when using observations from this direction. Of course, the most sensitive model to these roughness deformations is the SWH dependence model. The table shows that the model dependent on the two parameters is the one that better retrieves salinity from radiometric measurements.

Model	$\overline{\Delta SSS}$ (psu)	$\sigma^2_{\Delta SSS}$
U_{10} dependence	0.52	0.12
SWH dependence	0.80	0.34
U_{10} & SWH dependence	0.33	0.05

Table 5.3: Mean and variance of the retrieved salinity errors using three WISE-derived models, considering $\Delta SSS = |SSS_{insitu} - SSS_{retrieved}|$. Measurements were done with scans of 9 incidence angles, pointing towards north.

Also a comparison of the three WISE-derived model has been performed, using not only the 25 mentioned data files but a total of 132 measurements from WISE with incidence angles varying from 2 to 9 values. The results of comparing the three models are shown in table 5.4. These values are worse than in the case above, since all the recorded data have been now considered, even though corresponding to cases were few incidence angles were acquired, and so this produces a reduction on the quality of retrieved salinities.

Model	$\overline{\Delta SSS}$ (psu)	$\sigma^2_{\Delta SSS}$
U_{10} dependence	0.68	0.30
SWH dependence	0.69	0.39
U_{10} & SWH dependence	0.56	0.26

Table 5.4: Mean and variance of the retrieved salinity error using three WISE-derived models considering $\Delta SSS = |SSS_{insitu} - SSS_{retrieved}|$. 132 files measurements, with incidence angles from 2 to 9 have been used.

The average error on the retrieved salinity obtained with this derived model-2P is considerably smaller than using other models that considers only local wind speed or wave height. The standard deviation has also been reduced. A reduction in the error budget is expected in any regression when the degree of freedom is increased. However, in this case it has a physical meaning since SWH data contain information from processes that modify the sea surface spectrum other than contemporaneous local winds. Considering only SWH is not enough (as shown in the results), since it does not provide information on the wind-induced capillary waves. The substantial reduction on the SSS error (about 35%) when using this model confirms that swell and varying winds play an important role in the final balance of sea emissivity.

Results from EuroSTARRS dataset

These models have also been applied to retrieve salinity from the EuroSTARRS data set, although the radiometric data happened to be very noisy and some beams were affected by calibration problems.

If only one measurement, of six beams, is used to retrieve salinity, the error on the SSS retrieved is large (~ 3 psu), since noise and other errors are present on the measured value. On the other hand, if several T_B measurements are averaged, before doing the retrieval process, better salinity values are retrieved. This is because the averaging performs a reduction of the uncorrelated noise by a factor of $\sqrt{N}$ (being N the number of averaged data). This technique can only be used when very similar conditions are present. For example, a change on SSS would produce a change on T_B, and by averaging it could be masked.

A sequence of 762 T_B measurements along a straight line over relatively homogeneous fields has been averaged to retrieve salinity. The flight height for this line was 2700 m. Table 5.5 shows the errors on the retrieved salinities from this averaged value. These confirm that the new model-2P retrieves salinity better than the models only dependent on U_{10}. Results underline, again, that semi-empirical models give better results than theoretical ones. The table shows up, also, the tendency of the two scale model to underestimate the retrieved salinity and the tendency of the SSA model to overestimate it, since during this campaign the wind speed was low, and then the error important, as also observed for the WISE data sets.

These EuroSTARRS results are highly improved with respect to WISE results due to the large number of radiometer snapshot measurements averaged before retrieval.

Model	ΔSSS (psu)
Hollinger's model U_{10} dependence	0.24
WISE-derived U_{10} dependence	0.35
Two-scale + Durden & Vesecky × 2	-3.07
SSA + Elfouhaily	5.17
WISE-derived U_{10} & SWH dependence	0.13

Table 5.5: Retrieved salinity error using WISE-derived U_{10} dependence and U_{10} + SWH dependence, considering $\Delta SSS = SSS_{retrieved} - SSS_{insitu}$ from EuroSTARRS data.

Part of this work has been published in Gabarró et al. (2003) and Gabarró et al. (2004b).

5.4 Impact on retrieved salinity of auxiliary parameters errors

To retrieve salinity from SMOS good quality auxiliary variables (wind speed, wave height and SST) are needed as simultaneous both in time and space as possible to the spaceborne radiometer measurements.

A theoretical study of the impact on the retrieved SSS of errors on the auxiliary variables is shown in figure 5.7. The semi-empirical model-2P has been used. The results are calculated by averaging 25 retrieved salinities from different measurements, and the standard deviations are expressed in the vertical bars of the plots. X-axis expresses the error on the auxiliary parameters, and Y-axis plots the salinity retried error, when using the corresponding U_{10} error. When U_{10} error equals zero, salinity errors are not zero, since other sources of error are present in the brightness measurements.

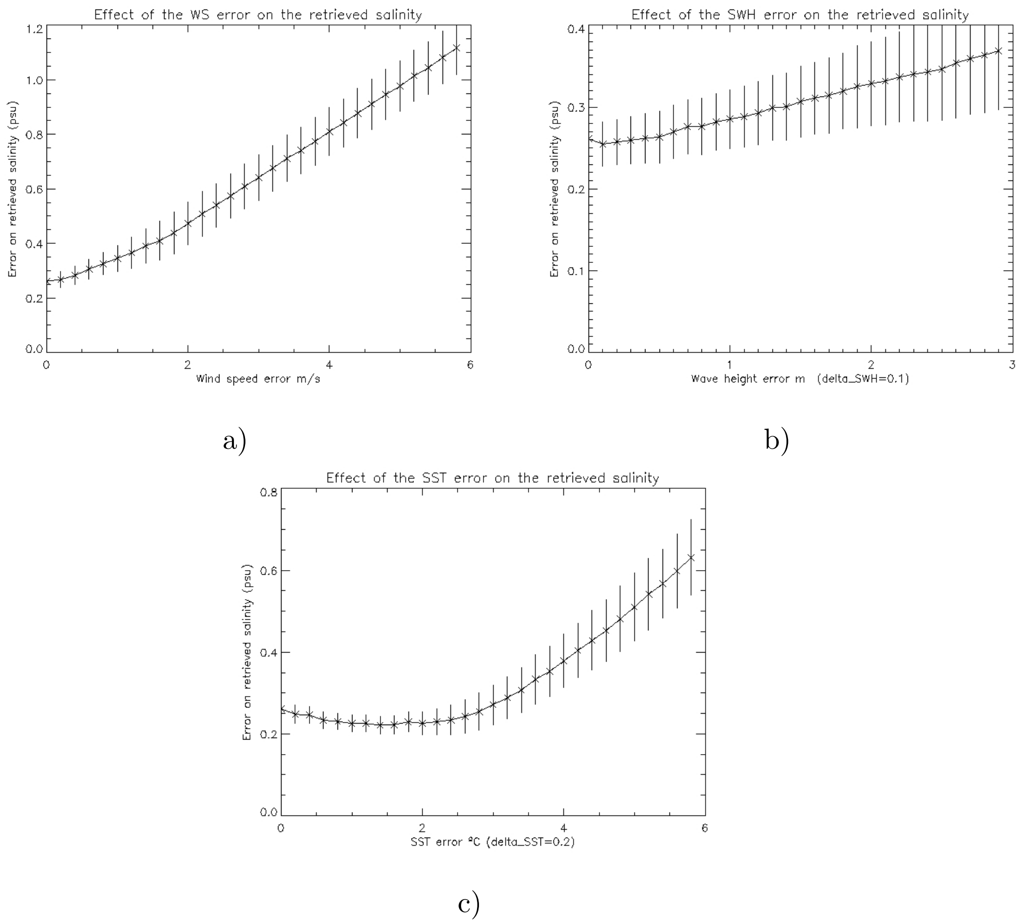

Figure 5.7: Errors on the retrieved salinity as function of errors on the auxiliary parameters, by using the model dependent on U_{10} and SWH. a) error on U_{10}, b) error on SWH and c) error on SST.

These plots show again that the auxiliary parameter that requires higher accuracy is the wind speed. For example, 2 m/s error on U_{10} produces an extra error (additional uncertainty over the case with zero U_{10} error) on the retrieved salinity of about 0.2 psu, and an error on SWH of 1 m brings to an extra error on salinity of less than 0.025 psu. On the other hand figure 5.7c shows almost no influence of the SST errors below 2.5 °C, and even an improvement on retrieved SSS for

SST 1.5 ºC above in situ values. This apparently anomalous behaviour (results in fact are indistinguishable within error bars) requires additional investigation.

This section also studies the salinity retrieved errors when using different existing sources of auxiliary parameters, in particular wind speed and significant wave height. In chapter 4 some sources have been presented, the theoretical accuracies have been discussed, as well as the time and space resolutions for each source.

The errors on the retrieved salinities, from WISE 2001 dataset, when setting the parameters to different combinations of U_{10} and SWH sources are presented in table 5.6. These values have been computed using the semi-empirical model-2P, since in the above sections it has been shown to be the best model to retrieve salinity from WISE and EuroSTARRS dataset. Cost functions without constrains is considered.

Source U_{10}	Source SWH	ΔSSS	ΔU_{10}	ΔSWH
In situ	in situ	0.33	–	–
HIRLAM	WAM	0.59	1.98	0.22
ARPÈGE	WAM	0.49	1.94	0.22
QuikSCAT	ERS	0.61	1.59	0.46

Table 5.6: Retrieved salinity error using WISE-derived model-2P, considering $\Delta P = |P_{insitu} - P_{retrieved}|$, being P each parameter, from WISE 2001 data set.

The table shows that that an important deterioration is suffered by the retrieved salinity when fixing the auxiliary parameters to data obtained from external source.This is because these data have some accuracy errors as well as a spatial and temporal lack of simultaneity between its acquisitions and radiometric measurements. It also manifest that the usage of meteorological (HIRLAM, ARPEGE) and oceanographic (WAM) model data (with assimilation of spaceborne observations) is better than to use satellite data directly, since the latter have much worse temporal resolution.

5.4.1 Auxiliary parameters obtained from the T_B

With the above situation in mind other possible ways for obtaining the parameters information have been studied in this thesis.

As explained before, SMOS, as well as WISE and EuroSTARRS measurements form overestimated systems, since there are more measurements than unknowns. Then the possibility of retrieving the auxiliary parameters from brightness temperature measurements themselves as well as the salinity has been investigated.

The model-2P is used in the retrieval algorithm. Firstly the cost function without restrictions has been employed to retrieve salinity, wind speed and wave height. The sea surface temperature has been fixed by in situ measurements. The inversion algorithm has been modified now to consider U_{10} and SWH as parameters to retrieve as well as salinity. The first guess values given to the inversion algorithm are: for salinity 37.5 psu, for U_{10} the HIRLAM output data and for SWH the WAM output data. After some iterations the algorithm converges.

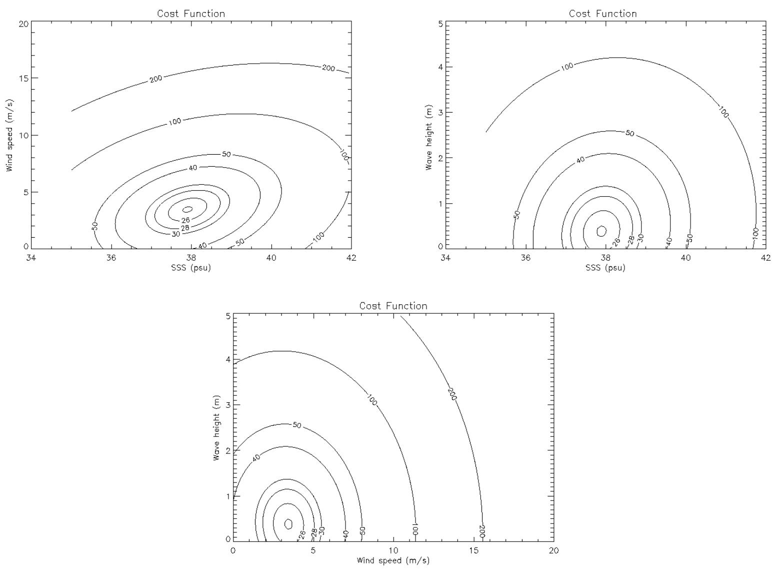

Figure 5.8: Cost function contour plot when varying SSS, U_{10} and SWH parameters.

Figure 5.8 plots the cost function behaviour when varying SSS, U_{10} and SWH. It shows that it is a convex function and consequently only one minimum is present, i.e. there is not the possibility that the solution falls down into a local minimum. This situation persists for both cases: when restrictions and no restrictions are considered in the cost function.

When performing the inversion algorithm with the cost function without constrains from the WISE 2001 data, the retrieved parameter errors are $\overline{\Delta SSS} = 0.40$, $\overline{\Delta WS} = 1.22$ and $\overline{\Delta SWH} = 2.44$.

The comparison of these results with the ones presented in table 5.6 (lines 2 to 4), reveals that better results are obtained when considering the auxiliary parameters as variables to be optimised, than fixing them with excessively erroneous values (those provided by models). Furthermore, the error on the wind speed retrieved with the optimisation process is smaller than model outputs and satellite errors. Figure 5.9 compares the results of retrieved U_{10} with in situ measurements and HIRLAM output model for several measurements. It shows that the retrieved U_{10} is closer to in situ measurements than the HIRLAM output, even though these values were used as first guess values. So it seems that by leaving U_{10} as parameter to be retrieved, the algorithm can improve its initial values. On the other hand, the significant wave height has not been retrieved with good quality.

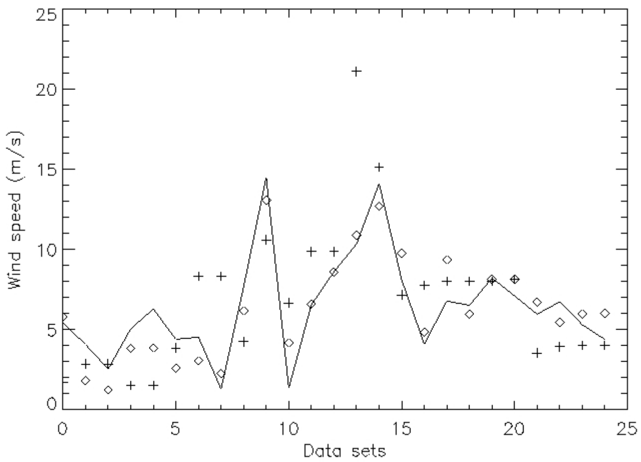

Figure 5.9: Comparison of the wind speed measurement determinations: measured in situ (diamonds), output from HIRLAM (crosses) and retrieved by the algorithm when it is set to retrieve wind speed (line).

In a second step, a cost function with constrains has been used to retrieve all these parameters, and has been shown to obtain better results than when no constrains are considered, as it is explained below.

The cost function with restrictions requires to have a reference value for each parameter to calculate and its expected error (σ_p^2). For the case study, the cost function results as follows:

$$\chi^2(SSS, SST, U_{10}, SWH) = \sum_{i=0}^{N-1} \frac{[\, T_{B_i}^{meas} - T_{B_i}^{model}(\theta_i, SSS, SST, U_{10}, SWH)\,]^2}{\sigma_i^2} + \frac{[\, SSS - SSS_{ref}]^2}{\sigma_{SSS}^2} + \frac{[\, U_{10} - U_{10\,ref}]^2}{\sigma_{U_{10}}^2} + \frac{[\, SWH - SWH_{ref}]^2}{\sigma_{SWH}^2} \quad (5.3)$$

A comparison of retrieved salinities with insitu measurements when using several auxiliary parameters combinations has been performed. Calculations have been done considering the following parameters: $\sigma_{T_B} = 1.0$ K, $\sigma_{SSS} = 0.5$ psu, $\sigma_{U_{10}} = 2.0$ m/s, $\sigma_{SWH} = 0.5$ m, $SSS_{ref} = 37.7$ psu, $U_{10\,ref} = HIRLAM$, $SWH_{ref} = WAM$. The emissivity model-2P has been used for the calculations.

The new method of permitting the auxiliary parameters to be retrieved from radiometric measurements has been used, also. Table 5.7 summarise all these results, and it reveals the same conclusions as before: It is much better to retrieve all these parameters from radiometric measurements themselves than fixing them to an erroneous value.

Source U_{10}	Source SWH	$\overline{\Delta SSS}$ (psu)	$\sigma^2_{\Delta SSS}$
In situ	in situ	0.13	0.01
HIRLAM	WAM	0.33	0.06
ARPÈGE	WAM	0.26	0.06
QuikSCAT	ERS	0.30	0.08
Free	free	0.16	0.02

Table 5.7: Retrieved salinity errors using model-2P, and cost function with restrictions, from WISE 2001 data-set.

The comparison between tables 5.7 and 5.6 shows that better results are obtained when considering constrains in the cost function, since in the latter more information is given to the algorithm.

Quality of the reference parameters

Since by enhancing the quality of the reference values the quality of the retrieved salinity is improved. To try to understand a little bit better this problem, an analysis of three different conditions on the reference value qualities has been done. The considered conditions are the following:

1. Good conditions: The reference values of the parameters are known with good quality, then their variance are low. The values are: $\sigma_{T_B} = 1.0$ K, $\sigma_{SSS} = 0.5$ psu, $\sigma_{U_{10}} = 2.0$ m/s, $\sigma_{SWH} = 0.5$ m, $SSS_{ref} = 37.7$ psu, $U_{10\,ref} = HIRLAM$, $SWH_{ref} = WAM$.

2. Relaxed conditions: The reference values of the parameters are considered to be a little bit worse than in the case before. The values are: $\sigma_{T_B} = 1.0$ K, $\sigma_{SSS} = 1.0$ psu, $\sigma_{U_{10}} = 2.5$ m/s, $\sigma_{SWH} = 1$ m, $SSS_{ref} = 37.7$ psu, $U_{10\,ref} = HIRLAM$, $SWH_{ref} = WAM$.

3. Bad conditions: The reference values of the parameters are not known with good accuracies. This is a similar situation to the SMOS situation, since it will be impossible to have these reference values coincident in time and space to the SMOS track. The values chosen here are: $\sigma_{T_B} = 1.0$ K, $\sigma_{SSS} = 2.0$ psu, $\sigma_{U_{10}} = 3.5$ m/s, $\sigma_{SWH} = 2.0$ m, $SSS_{ref} = 37.7$ psu, $U_{10\,ref} = HIRLAM$, $SWH_{ref} = WAM$.

For the above conditions, the reference values are the same for the three cases but the expected quality σ_P of them are different. Following these conditions the three parameters have been retrieved from WISE 2001 dataset, by using only the files with 9 incidence angles.

Table 5.8 summarises the retrieved values of the parameters (SSS, U_{10}, SWH) and shows that, as expected, better knowledge of the reference values leads to better retrieved parameters. For each condition, the table shows two results. The first one represents the case of knowing exactly the SST value, by using in situ measurements, while the second one is the case of having a bias on the SST of 1°C. Results also indicate that an error on the SST measurement of 1°C does not introduce significant additional errors on the retrieved parameters, and in particular to the retrieved salinity, that is the most important parameter to retrieve.

Figure 5.10 plots the SSS, U_{10} and SWH retrieved for the case of good conditions. The plot shows that the retrieved values are closer to the in situ measurements than the model output, which have been used as references values. It means that this method can improve the given reference values.

Conditions	$\overline{\Delta SSS}$ (psu)	$\overline{\Delta U_{10}}$ (m/s)	$\overline{\Delta SWH}$ (m)
Good conditions with in situ SST	0.16	1.05	0.37
Good conditions with in situ SST+1°C	0.17	1.09	0.37
More relaxed conditions with in situ SST	0.28	1.11	0.48
More relaxed conditions with in situ SST+1°C	0.32	1.08	0.48
Bad conditions with in situ SST	0.35	1.15	1.14
Bad conditions with in situ SST+1°C	0.41	1.13	1.13

Table 5.8: Retrieved salinity error using model-2P, for the three conditions and using restrictions on the cost function.

Also, a study to understand the dependences of the retrieved salinity on the quality of the reference values, when fixing the σ_p of the parameters, has been developed.

Plots in 5.11 show the retrieved salinity errors as function of errors on reference salinity value (x axis), for the same σ_{SSS}, and errors on reference wind speed values (c). The errors of the reference salinity values are calculated by the differences between the SSS_{ref} and the in situ measurements. Errors on two different conditions have been calculated, plot (a) is for good conditions, and plot (b) is for relaxed conditions. The plots show that by deteriorating the SSS reference value (always obeying the σ_{SSS} condition) the retrieved salinity is worse, and the standard deviation increases. The plots also compare the results when restrictions and no restrictions are considered, and in general better results are obtained with the former case. When worsen the U_{10} and SWH references values (figures c) and d)), the impact on the SSS retrieved is ≈ 0.02 psu, which is negligible.

Further work should be done to study the required quality of the SSS_{ref} for SMOS, and to find the way of obtaining this best reference value for SSS.

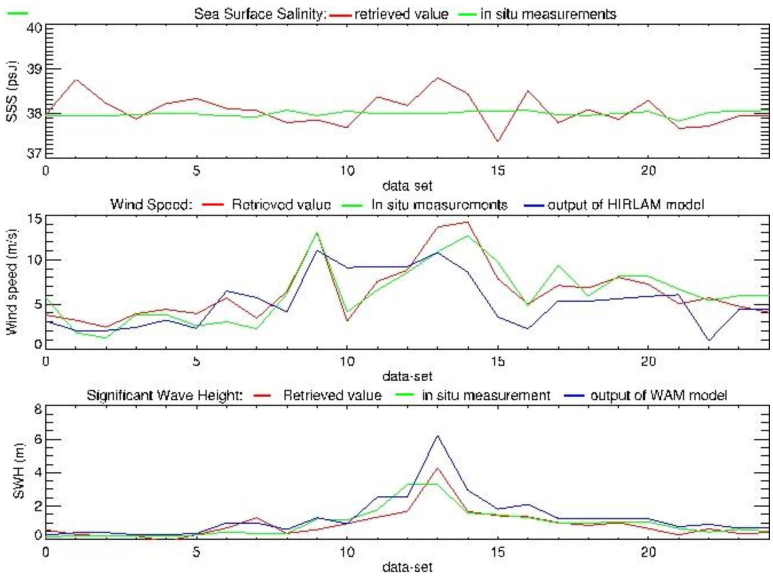

Figure 5.10: Comparison of the SSS, U_{10} and SWH calculated from different methods: measured in situ (green), output models (blue) and retrieved from radiometric measurements with restrictions (red).

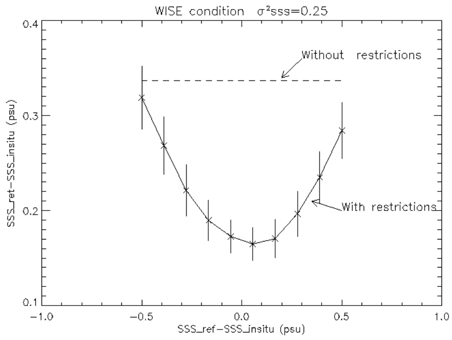

a)

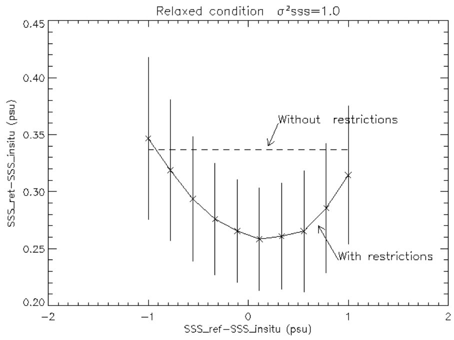

b)

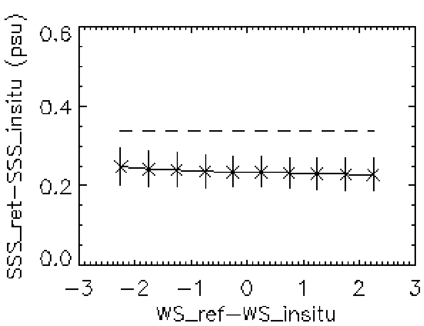

c)

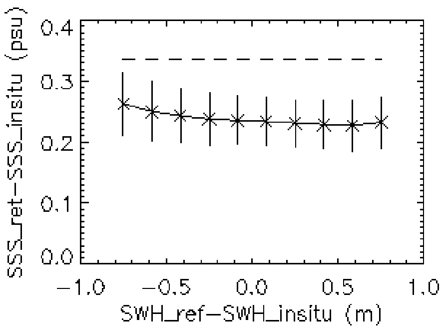

d)

Figure 5.11: Plots of the retrieved SSS error (y axis) as function on the reference error (x axis). a) Calculations done with good conditions, b) calculations done with relaxed conditions. Vertical lines are the standard deviations. c) Retrieved SSS errors when the reference value of wind speed varies, for the case of relaxed conditions. d) Retrieved SSS errors when the reference value of SWH varies. This is done for two cases, when cost function with constrains are considered and when no constrains are considered.

SST parameter

The possibility of allowing the SST to be retrieved also with the inverse algorithm instead of setting it to a fixed value has been analysed as well.

Figure 5.12 shows the aspect of the cost function when varying SSS and SST values. Firstly it has been computed using no restrictions, and it shows that the function does not have a clear minimum (left plot). This is because T_B is highly non-linear with SSS and SST. On the other hand, when using restrictions, i.e. allowing only some possible solutions, the cost function presents only one minimum (right plot).

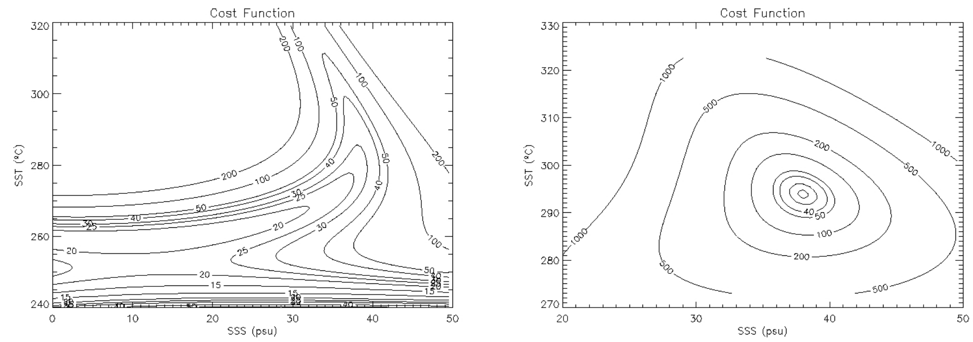

a) b)

Figure 5.12: Cost function contour plot when varying SSS and SST parameters. a) when no restrictions are considered in the cost function, b) when restrictions are considered.

The results of the 4 retrieved parameters are summarised in table 5.9, when restrictions are considered.

Conditions	$\overline{\Delta SSS}$ (psu)	$\overline{\Delta U_{10}}$ (m/s)	$\overline{\Delta SWH}$ (m)	$\overline{\Delta SST}$
Good conditions	0.16	1.08	0.28	0.66
More relaxed conditions	0.25	1.13	1.48	0.64

Table 5.9: Retrieved salinity error using WISE-derived model-2P, when SST is a parameter to retrieve.

Comparisons of the above table with table 5.8 shows that a small improvement (0.01-0.06 psu) occurs when considering SST as a parameter to retrieve with respect to fixing SST to a value with 1°C of error. Since SST measurements are obtained from satellites and models with an accuracy better than 0.5°C and high temporal resolution, this parameters does not represent a problem for the SMOS retrieval process.

5.5 Retrieved salinity from the Plata survey

For the Plata campaign the STARRS instrument calibration was clearly improved with respect to EuroSTARRS campaign, and several tests shown that radiometric measurements suffered fewer noise than during EuroSTARRS measurements. Another advantage that presents this survey with respect EuroSTARRS is that the sea in La Plata delta area presents important variations on salinity, which ranges from 28 psu to 36 psu, since La Plata river brings an important amount of fresh water to the ocean. This will allow to investigate if salinity changes are detectable with the STARRS instrument.

A draw back of this data-set is that in situ measurements performed by the oceanographic ship were, most of the time, not simultaneous with the plane track. The lack of precise auxiliary parameters makes more difficult the validation of the retrieved salinity.

Figure 2.14 shows the ship and the plane tracks over the area of LaPlata Delta. For the retrieval process analysis, only data of LEG2 transect called 'Rio Grande' has been used. This transect starts near the coast and finishes at 185 km (100 nautical miles) offshore, and is located in the North of the delta of the river. Since the currents in the area follow a South-North direction near the coast, the transect traverses an important gradient of surface salinity, being fresher water near the coast and saltier offshore (see figure 2.14c). Three areas of this track have been selected to perform the retrieval process, as they present different salinities and few variation on pitch and roll of the plane.

Figure 5.13 shows the salinity measured by the thermosalinograph and the interpolated wind speed measured in the CTD stations as function of time, for the whole LEG2 transect. It has to be remarked that the ship survey wan in the area 4 days before the STARRS plane measurements. Therefore the wind speed data is not reliable any more after 4 days, but in the other hand, SSS is not suppose to suffer large changes in that period of time. The three areas used for the analysis are marked as A, B and C. Each part has been chosen to be 300 radiometric measurements long, to be comparable with WISE measurements, in which each angle measurement was averaged during 5 minutes, and one measurement was done every second (i.e. 5*60=300).

Bias on the pitch and roll of the plane produce an increment/decrement on T_B measured, depending on the incidence angle. For example 1° of roll produce an increment on T_B of 1.23 K at the 38.5° incidence angle beam. Corrections for that misalignment of the plane have been performed. On the other hand, the galactic noise has not been corrected for, since that data are not available at the time of writing this document, so a fixed value of 3.8 K has been considered. The up-welling, and down-welling atmospheric corrections have been done as well as the correction for the cosmic noise.

The cost function with constrains has been used to retrieve salinity from STARRS data over the Plata area. Three semi-empirical models have been compared; Hollinger and WISE 2001 models, which only depend on U_{10}, and the WISE derived model-2P, which depends also on the SWH. Since this last variable was not recorded in the campaign, the regression obtained from WISE2001 dataset ($SWH = -0.29 + 0.155U_{10}$) has been used to compute SWH as a very rough approximation.

The reference values used for the inversion algorithm with constrains were: $SSS_{ref} = SSS_{insitu} + 4.5$ psu, $U_{10\,ref} = U_{10\,insitu} + 3.5$, $SWH_{ref} = SWH_{calc} + 1$. The variance of those reference parameters have been fixed to: $\sigma_{T_B} = 1.0$ K, $\sigma_{SSS} = 5.0$ psu, $\sigma_{U_{10}} = 4.0$ m/s, $\sigma_{SWH} = 2.0$ m, therefore they are considered to be very poorly known, since salinity suffer big variations in a small area.

For this study three different methods of retrieval have been used. The first one considers only the SSS parameter to be retrieved, while U_{10} and SWH are fixed to the measured (or computed for SWH) values (this is called M1). The second method allows the algorithm to retrieve SSS and U_{10} while SWH is fixed to the computed value (M2). The last case is when all three parameters are considered to be retrieved from brightness temperature (M3). When using the models only dependent on WS then of course M3 is not used, and the comments on SWH do not apply.

Firstly the retrieved salinity has been calculated directly for individual T_B measurements, without performing any averaging. Figure 5.14 shows the retrieved SSS for each of the areas (300 points each) when using the model-2P for M1 and M2 methods. The variable line is the retrieved salinity while the stable line is the measured one. The plots show that the retrieved salinity follow the increments on SSS, except on area C, where retrieved salinity is highly underestimated. An explanation for that behaviour can not be found, since local wind speed or SWH at the time of radiometric measurements were not available.

However, by performing the average of several T_B measurements, the white noise of the measured value can be reduced. Therefore the average of 300 T_B measurements of each area has been done and a slight improvement on the retrieved values has been observed. The in situ measurements for each area are presented bellow, but it should be retained that the wind speed was measured 4 days before the radiometric measurements:

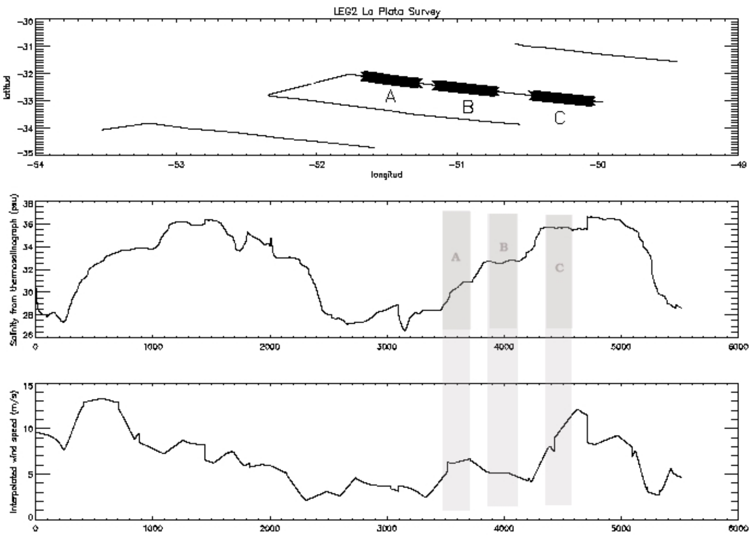

Figure 5.13: Top, LEG2 track map, middle, salinity measured by the thermosalinograph and bottom, interpolated U_{10} measured in the stations. The three study areas are marked by A, B and C.

- Area A : The in situ mean values are: $\overline{SSS_{insitu}} = 30.183$, $\overline{U_{10\,insitu}} = 6.022$ and $\overline{SWH_{calc}} = 0.645$
- Area B : the in situ mean values are: $\overline{SSS_{insitu}} = 32.692$, $\overline{U_{10\,insitu}} = 5.028$ and $\overline{SWH_{calc}} = 0.489$
- Area C : the in situ mean values are: $\overline{SSS_{insitu}} = 35.642$, $\overline{U_{10\,insitu}} = 9.987$ and $\overline{SWH_{calc}} = 1.258$

Retrieved results are summarised in tables 5.10, 5.11 and 5.12, for area A, B and C respectively. The inversion analysis has been performed for the three semi-empirical models and for the three methods explained above. Tables show the retrieved SSS, U_{10} and SWH.

Quite good salinity retrievals have been obtained from STARRS measurements from the Plata campaign. They show that the instrument is capable to distinguish between different waters with different salt concentration. Retrieved salinity errors better than 0.5 psu have been obtained for A and B areas.

A comparison of tables 5.10, 5.11 and 5.12 shows up that in general, better results are achieved when using the emissivity model-2P which is dependent on WS and SWH even though not significant differences are observed.

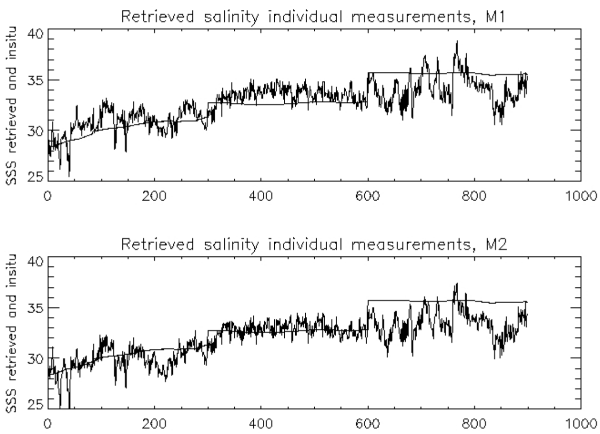

Figure 5.14: Retrieved salinity (variable line) for the three areas (each area is 300 measurements), when using the model-2P comparing with measured salinity (stable line). Top when fixing U_{10} to the measured values (M1), bottom when allowing U_{10} to be retrieved (M3)

Another important conclusion that can be derived is that much better results are obtained when allowing the inverse algorithm to retrieve WS as well as salinity than fixing it to an erroneous value. On the other hand, when allowing the algorithm to retrieve also SWH (M3) results get degraded. A possible explanation for that could be that few independent observations are obtained for each measurements, they are only 3 different incidence angles, since the instrument was mounted without tilt. Then the case of having 3 unknowns can not properly be resolved.

Bad retrieval results are obtained from area C, salinity is always underestimated. This area is the most offshore region from the transect analysed. May be the U_{10} was very high and important roughness was present for that period of time, but since this information is not available, a clear conclusion on why this SSS is poorly retrieved can not be given by the author.

A study of the errors on the retrieved salinity due to inaccuracies on the auxiliary parameters can not be done with this data set, since in situ data simultaneous with radiometric measurements have not been measured.

This analysis of the Plata campaign indicates again, that the model-2P, which depends on U_{10} and on *SWH* is the one that better retrieve salinity from radiometric measurements. Furthermore this analysis confirms the robustness of this model, even it was obtained under very different conditions from La Plata Delta area.

Area A	SSS_{ret}	ΔSSS	$U_{10\,ret}$	SWH_{ret}
Method	Model-2P			
M1	30.656	-0.473	-	-
M2	29.781	0.402	2.368	-
M3	27.804	2.379	5.924	-1.723
	Hollinger model			
M1	30.851	-0.668	-	-
M2	29.438	0.745	2.495	-
	WISE 2001 model			
M1	31.340	-1.157	-	-
M2	28.934	1.249	1.018	-

Table 5.10: Retrieved parameters for three different emissivity models and three different methods for area A. $\Delta SSS = SSS_{insitu} - SSS_{ret}$

5.6 Conclusions

Results show up that better predictions of brightness temperature can be achieved by semi-empirical models than using theoretical ones. This behaviour is observed for two campaigns with independent radiometers, but both located on the same area.

An important conclusion that can be also extrapolated from this chapter is that to retrieve salinity from WISE and EuroSTARRS data sets, the model dependent on wind speed as well as on significant wave height is better than other models only dependent on wind speed, or only SWH.

From the auxiliary parameters work, one can conclude that using data from meteorological models to retrieve salinity is better than using direct satellite data, since the former have smaller temporal resolution. Even though, the necessary accuracy of U_{10} is high (of the order of 1 m/s to obtain an extra salinity error lower than 0.1 psu), and this is impossible to achieve nowadays by using satellite data (the temporal resolution is low), and probably neither using atmospheric models.

From the analysis of WISE data set it appears that, in absence of accurate in situ measurements, the best method to retrieve salinity is to leave U_{10} and SWH

Area B	SSS_{ret}	ΔSSS	$U_{10\,ret}$	SWH_{ret}
Method	Model-2P			
M1	33.468	-0.776	-	- 3
M2	32.800	-0.108	2.136	-
M3	31.172	1.520	5.279	-1.540
	Hollinger model			
M1	33.674	-0.982	-	-
M2	32.586	0.106	2.240	-
	WISE 2001 model			
M1	34.084	-1.392	-	-
M2	32.154	0.538	0.930	-

Table 5.11: Retrieved parameters for three different emissivity models and three different methods for area B. $\Delta SSS = SSS_{insitu} - SSS_{ret}$.

as free parameters, and let the inverse algorithm to retrieve them as well as SSS from the radiometric measurements, taking advantage of the multi-angular view capability of SMOS imaging configuration. Using this method, the U_{10} is retrieved with a mean error of the order of 1 m/s, and SWH of 0.3 m.

However, in this case, it is necessary to find the best reference values and to characterise very well their errors. Then, it is needed to tune very well these values in the cost function. When SMOS will be flying, the reference values for WS and SWH could be obtained from analysed models, and the reference value of SSS could be the SMOS measurement of that area obtained during the previous pass of the satellite.

Errors on SST of 1° C produce minimum errors on the retrieved SSS (less than 0.06 psu). Since the actual knowledge of SST parameter measured by satellites or models is better that that value, SSS errors due to SST inaccuracies can be neglected in the future SMOS operational procedures.

Results with the Plata experiment dataset show that the L-band radiometer, STARRS, is capable to detect variations on SSS in an area with strong surface salinity gradient. The study demonstrates that better results are obtained when allowing the algorithm to retrieve wind speed, as well as SSS, than fixing it to possibly erroneous values. Another conclusion is that when the model-2P,

Area C	SSS_{ret}	ΔSSS	$U_{10\,ret}$	SWH_{ret}
Method	Model-2P			
M1	34.113	1.529	-	-
M2	33.425	2.217	6.927	-
M3	31.762	3.880	10.175	-0.890
	Hollinger model			
M1	34.191	1.451	-	-
M2	33.323	2.319	7.639	-
	WISE 2001 model			
M1	34.973	0.669	-	-
M2	32.946	2.696	5.506	-

Table 5.12: Retrieved parameters for three different emissivity models and three different methods for area C. $\Delta SSS = SSS_{insitu} - SSS_{ret}$.

which is dependent on U_{10} and SWH, is used in the retrieval process, slightly better results are obtained than using other semi-empirical models. However, as the model-2P was derived from western Mediterranean conditions, better results should be expected by deriving one model for each ocean conditions. It would be interesting for further work to derive a model from the Plata data-set (if enough in situ data are available) and compare it with the WISE derived models.

The accuracy and resolution of meteorological models can also vary in other regions, as well as the accuracy of satellite data. This work is a regional study, but could be a first step for a global scheme applicable to SMOS observations.

Chapter 6

Salinity retrieved from images generated by the SMOS End-to-End performance simulator

In this chapter some aspects of the salinity retrieval are analysed using the SMOS End-to-end Performance Simulator (SEPS), which simulates the performance of MIRAS instrument very accurately.

This tool has been used to create three different brightness temperature scenes, as would be measured by MIRAS, after 78 consecutive SMOS snap-shots. These permit to have views from up to 78 different incidence angles in some pixels of the FOV. The three scenarios are representative of different ocean conditions.

Salinity has been retrieved from the pixels of the FOV using a Level2 processor prototype, created by UPC. First, a theoretical study of the effect of noise and bias in the retrieved salinity has been performed. Secondly salinity has been retrieved from the scenarios created by SEPS, with some limitations.

The approach of allowing the inversion algorithm to obtain the auxiliary parameters is also analysed.

6.1 Introduction to SEPS

The SMOS End-to-end Performance Simulator (SEPS) is a tool that allows the design engineers and scientists to simulate the full operation of the MIRAS instrument in a reliable and highly representative way (Corbella et al., 2003, Camps et al., 2003a). SEPS is based on the existing MIRAS End-to-end Performance Simulator created at the Polythecnical University of Catalonia (UPC) by Camps (1996), and has been implemented for ESA by a consortium led by EADS-CASA, with GMV, DLR and UPC.

It is a flexible software tool, modular and open to the integration of new routines and processing steps. It performs the simulation of all the aspects that are present in the process of imaging brightness temperature maps.

SEPS calculates the brightness temperatures of the FOV of SMOS for each snap-shot while orbiting, for land and ocean areas. It includes the following blocks:

- A detailed hardware modelling. It is based on MIRAS breadboard parameters and on the design experience obtained during the development of a X-band interferometric radiometer prototype, performed in the UPC.
- The implementation of the calibration and image reconstruction procedures.
- The implementation of an orbit propagator to generate the sequence of satellite positions at different times.
- The implementation of an L-band brightness temperature generator. Vertical and horizontal brightness temperatures are computed from emissivity models and the following physical parameters: soil and snow albedos, snow depth, soil roughness, vegetation albedos, soil moisture, soil surface temperature, ocean salinity, zonal and meridional winds over the oceans, vegetation height, ocean surface temperature and ocean ice cover.

Since the "vertical polarisation" antennas are oriented in the along-track direction, the brightness temperature that would be measured along the vertical line (ξ=0) would be the vertical one, and, since the array is tilted 31.2° with respect to nadir, the brightness temperature that would be measured along the horizontal line (η=0), would be a linear combination of the vertical and the horizontal ones.

The direct models used in SEPS to compute the emissivity of the sea surface is the Fresnel equation for the emissivity of a flat surface, and a linear approximation of Hollinger (1971) measurements for the roughness of the surface due to wind speed. The dielectric permittivity of sea water is computed using the Klein and

Swift (1977) model, however the tool allows to change this model to the Ellison et al. (1998) one.

Tables of geophysical parameters (SSS, U_{10} and SST) have been used to generate the brightness temperature maps over the sea. These tables have a spatial resolution of $1^\circ \times 1^\circ$ and are linearly interpolated.

Each pixel in the alias free field of view is seen under different incidence angle, radiometric sensitivity and spatial resolution. As the satellite moves, the projection of the FOV in cross-track/along-track Earth coordinates is displaced from snap-shot to snap-shot, and pixels are then seen in different positions in the FOV, so under different incidence angles, as shown in figure 6.1. This characteristic will allow us to do the retrieval process from T_B for each pixel when it is seen from different incidence angles (different snap-shots).

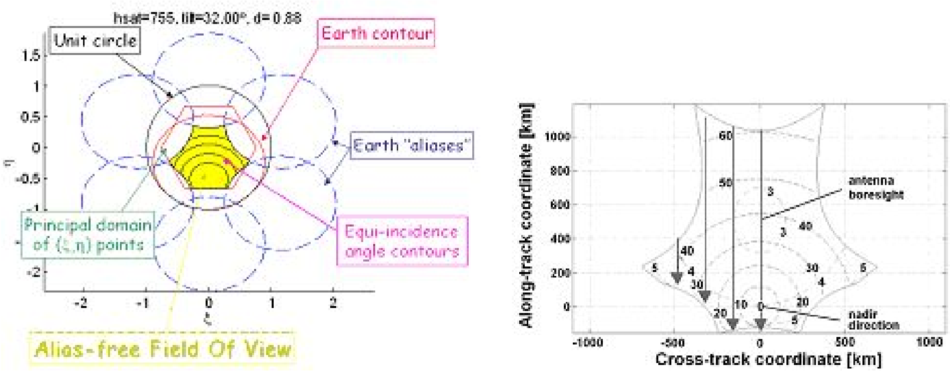

a) b)

Figure 6.1: a) SMOS observation geometry, mapped into the unit circle in (ξ, η). b) Imaging of a pixel through the alias free FOV under incidence angles (0°-60°, dashed contour centred at nadir), with different spatial resolution and radiometric sensitivities (from 3 K - 7 K, dashed-dot line centred at boresight). Parameters: 21 antennas per arm, d=0.875 λ antenna spacing, $\beta = 32^\circ$ tilt angle, and h=755 Km platform hight (from Camps et al. (2003b)).

SEPS is the tool that the SMOS community has to perform the analyses and studies necessary to solve the open issues of the project that are related to the instrument functioning under the specific configuration selected for SMOS.

6.2 Retrieval process

A complementary tool called Level 2 processor has been used to retrieve salinity from SEPS generated images. This tool has also been developed at the Polythecnical University of Catalonia, under the grant "MIDAS-2: Definición del proceso de datos de la misión espacial SMOS en la estación de Villafranca del Castillo (SMOS-GS-B) PARTE UPC", sponsored by Plan Nacional del Espacio ESP2002-11648-E.

The formulation of the retrieval problem has been done in terms of the first Stokes parameter (I) :

$$I = T_{xx} + T_{yy} = T_{hh} + T_{vv} \tag{6.1}$$

By this method the Faraday and the geometric rotations are avoided, while the radiometric sensitivity is not degraded since T_{xx} and T_{yy} can be computed in the dual-pol mode and not in the full-pol one. This alternative approach was first proposed in Camps et al. (2001).

The process to retrieve SSS from images generated by SEPS using the UPC tool is sketched below:

- Determine if a pixel is a land, sea or mixed pixel.
- Track the pixel as it moves in the alias-free FOV in a series of consecutive snap-shots. Tracking can be performed in the along-track/cross-track coordinates (figure 6.1b), or in the (ξ, η) director cosines coordinates (figure 6.1a).
- For each snap-shot, interpolate T_{xx} and T_{yy} from the (ξ, η) grid where the image reconstruction is performed to the geographical position of the pixel being tracked at that particular snap-shot. This process can be performed with the same window for all pixels, providing the same angular resolution in all directions, but different spatial resolution on ground, or with a "strip adaptative" processing window (Ribó, 2003) tailored to provide the same spatial resolution at all directions.
- Correct for sky (cosmic and galactic noise) and atmospheric/ionospheric effects: signal attenuation, upwelling brightness temperature, downwelling brightness temperature scattered in the direction of observation.
- For each snap-shot, the error (variance) between the model and the measured data at all incidence angles must be minimised, obtaining a set of estimated parameters (Camps et al., 2002a).

The inversion method selected is the Levenberg-Marquardt method with a cubic polynomial line search and Gill-Murray Hessian update methods.

First a theoretical analysis has been done. A scene with homogeneous salinity, wind speed and SST has been used to retrieve salinity with the level2 processor. This scene is an ideal scene, without any noise, bias nor perturbation, and follows the SMOS configuration with 78 snap shots. The original values are set to: SSS= 35 psu, wind speed=10 m/s and SST=15°. Afterwords, controlled noises and biases have been added to the computed brightness temperature , and the retrieved salinities have been calculated.

Figure 6.2 shows the number of incidence angles for each pixel of the image, the maximum is 78 since the image has been created with 78 snap-shots.

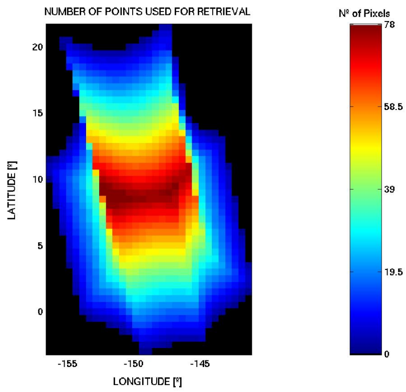

Figure 6.2: Number of incidence angles for each pixel.

Table 6.1 shows the mean and the variance of the retrieved salinity of the image for several combinations of noise and bias on T_B, as well as the case when a different emissivity model is used in the retrieval process (remember that the T_B images have been created using Hollinger's model).

Table shows up that when random added noise is present, the mean retrieved salinity does not suffer important errors, but the standard deviation (dispersion) increases. However, when bias is added to the brightness temperature, the retrieved salinity presents an important bias as well, but the dispersion is very low. Small deterioration of the retrieved salinity is observed when different emissivity models for the direct and the retrieval process are used. It should be pointed out that both models are very similar.

With an error on the auxiliary parameters of 2.5m/s on the wind speed and of 0.5° on the SST, and a random noise of 10K on T_B, the salinity is retrieved with an error of $\approx$ 0.15 psu. However, better results are obtained when the three parameters (SSS, U_{10} and SST) are left to be retrieved by the inversion algorithm (error of $\approx$ 0.08 psu).

Case of study	$\overline{SSS}$ (psu)	σ_{SSS}
Ideal	34.997	0.009
T_B+5*rand	34.953	1.126
T_B+10*rand	34.930	2.343
T_B+5 (bias)	29.405	0.050
T_B+10*rand+5	29.314	2.429
WISE-derived model	35.048	0.194
T_B+10*rand / error on aux. param.	34.852	2.554
T_B+10*rand three param. free	34.922	2.575

Table 6.1: Mean and standard deviation of the retrieved salinity errors using different combinations of added noise and bias, and different models. The original salinity is 35 psu.

Figure 6.3 shows the results of retrieving salinity for the combinations of noise and biases added to the brightness temperature shown in the table. They show that the best retrieved values are found in the middle of the FOV, where more independent measurements are acquired (more incidence angles).

The second part of the study consisted of retrieving salinity from scenes created by SEPS, which are SMOS-like images. In this part all the effects involved in the creation of a brightness temperature image, as in the SMOS satellite, are considered. They considered errors on the receivers, on the antennas, and image reconstruction limitations. They also considered the atmosphere and ionosphere effects, as well as the extraterrestrial noises, and the Sun and the Moon direct and reflected contributions.

This is in opposition to what has been done in part one, that was an ideal case, without any of these effects.

Of course, when all these effects are considered, the brightness temperature measured differs from the ideal one. The bias and noise effecting to the T_B makes less effective the retrieval process, and will bring to a poorer retrieved salinity.

Camps et al. (2004b) identify three sources of bias. The first is the instrumental inaccuracies in the Noise Injection Radiometers used to measure the antenna temperature (thermal noise, offset, linearity). The second source is the inherent

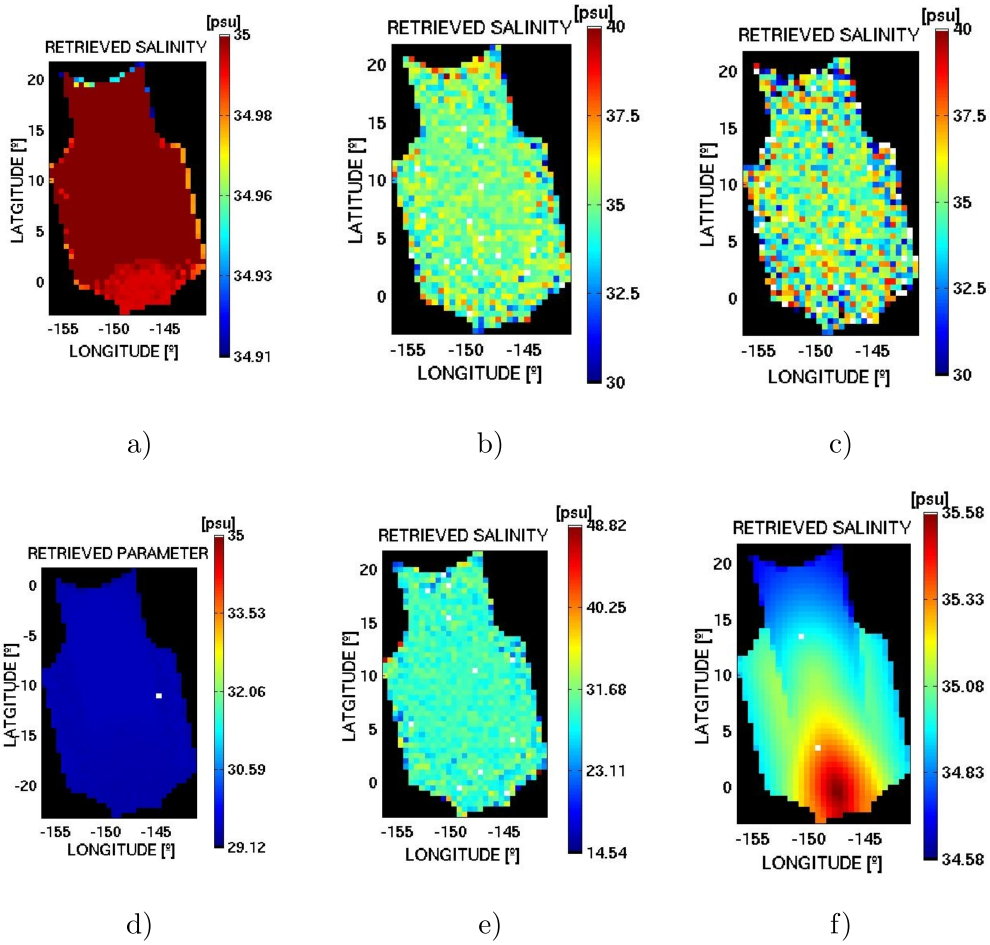

Figure 6.3: Retrieved SSS when the scene is homogeneous to SSS=35 psu. a) Ideal case (no noise neither bias) b) when a random noise of 5K is added to T_B c) when a random noise of 10K is added to T_B d) when a bias of 5K is added to T_B e) when a random noise of 10K and a bias of 5K is added to T_B f) when using WISE-derived model in the retrieval process (and no noise neither bias).

difference between the antenna temperature (measured in the whole unit circle) and the average brightness temperature in the alias free FOV, since in the last one, smaller area is considered (see figure 6.1a). Inhomogeneous scenes (near the coastline) produce more important bias of this kind. The third source is the Sun contribution which is not perfectly cancelled.

(Camps et al., 2004b) propose to correction for the bias with an external calibration. This calibration consists of, having an in situ measurement of SSS, U_{10} and SST for each scene, to calculate the brightness temperature at nadir for each snap shot. Later the first Stokes parameter is calculated by adding both polarisations of T_B. Therefore the bias can be calculated by performing the mean of the subtraction of the predicted first Stokes from the measured image. Finally this bias is deduced from the measured first Stokes parameter of each pixel. This would flap the level of brightness temperature to the correct one.

Three scenes have been generated with SEPS, on different ocean scenarios, to study the effects of meteorological and oceanographic conditions on the retrieved parameters. For the analysis 78 snap-shots are used. The different scenes are called A, B and C.

Scene A is located in the North Atlantic ocean, just south of Greenland, as shown in figure 6.4a. It is a region with very cold waters; sea surface temperatures in the FOV range from 7.5° (North area) to almost 20°. Salinity is 34.8 psu in the colder area, and increases until 36 psu. Figure 6.4e, shows the number of times each pixel is seen by the SMOS FOV, while satellite moves. This image was generated in an area with coordinates: latitude=[45,50], longitude =[-35,-30].

Scene B is located in the equatorial Pacific. This is a region with hot waters, as shown in figure 6.5. Sea surface temperatures range from 24° to more than 28°, in the FOV. Salinity ranges from 34.4 psu to near 35.6 psu. This image was generated in the area with coordinates: latitude=[0,5], longitude =[-150,-145].

Scene C is located over the Gulf Stream area, and present a big range of temperature and salinity, as shown in figure 6.6. Sea surface temperatures range from 3° to 26° and salinity ranges from 32.0 to 37.5 psu, in the field of view. This image was generated in the area with coordinates: latitude=[25,30], longitude =[-55,-50].

Figure 6.7 shows the retrieved salinity for each scene in two different scales. The results show a clear underestimation of the retrieved sea surface salinity from SEPS images. These results could be due to biases on T_B, therefore the inversion algorithm to compensate for this bias needs to decrease the salinity. If the bias is the same for the whole image, an increment on SSS should be added on the retrieved salinity images. Thereafter, the worse retrieval values would be located in the edge areas, as expected. The large variability of the retrieved salinity should be due to random noise, which increases the variability.

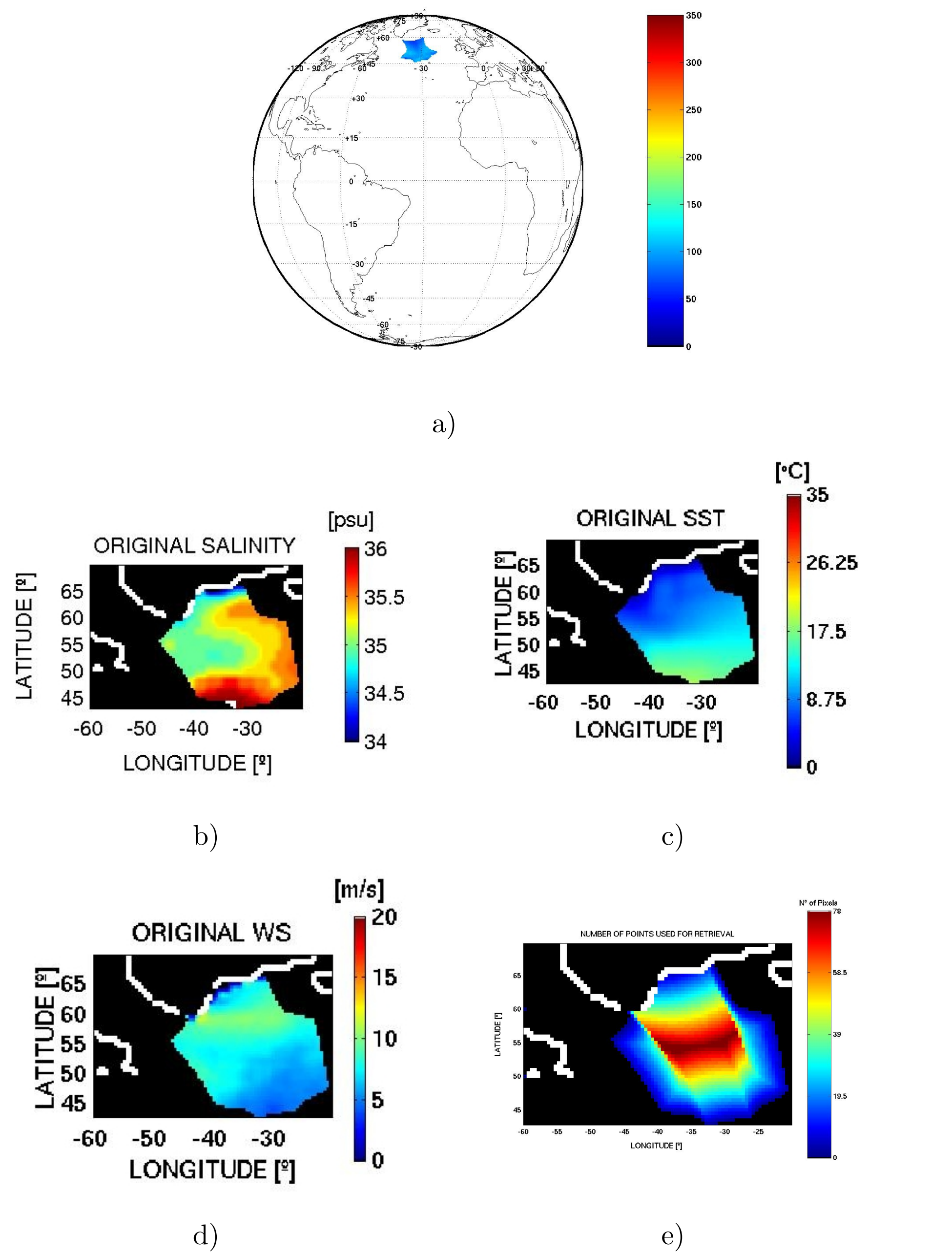

Figure 6.4: Scene A. a) Location of the scene. SSS insitu (b), SST insitu (c), and wind speed in situ (d) data used by the direct model to create T_B. e) Number of independent views of each pixel.

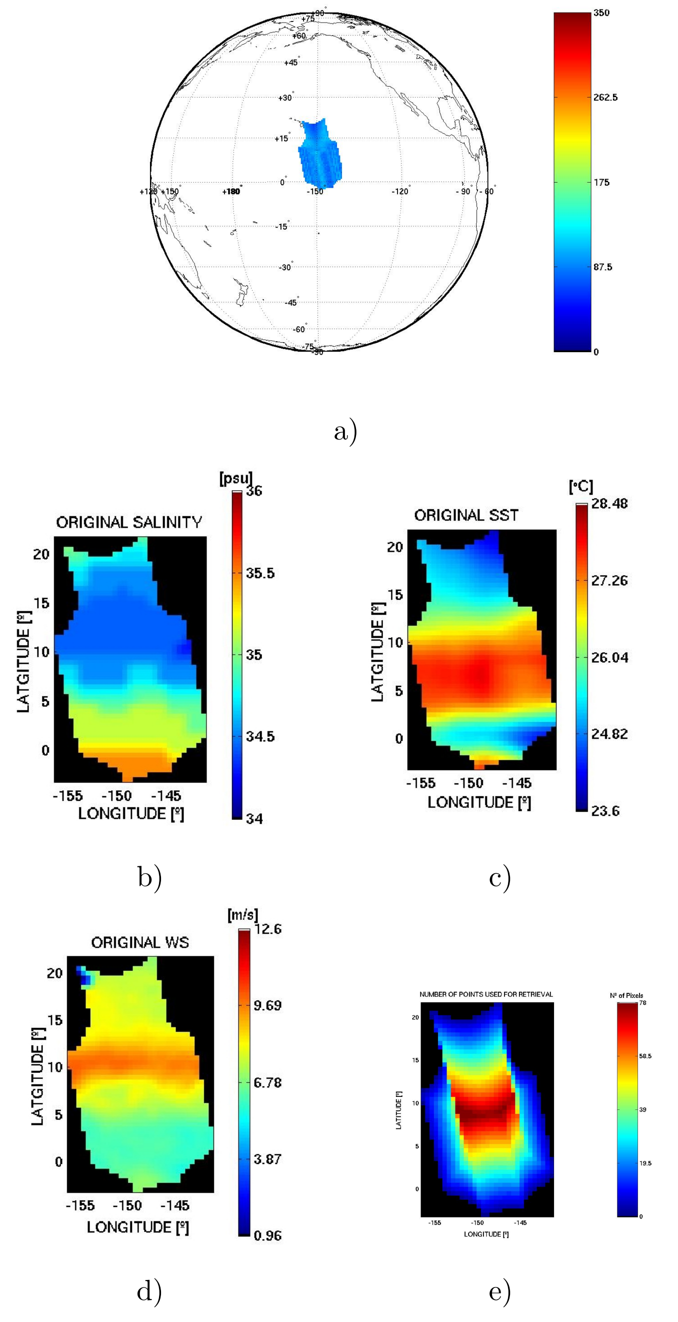

Figure 6.5: Scene B. a) Location of the scene. SSS in situ (b), SST in situ (c), and wind speed in situ (d) data used by the direct model to create T_B. e) number of independent views of each pixel.

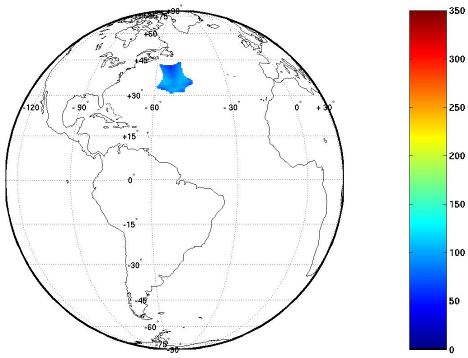

a)

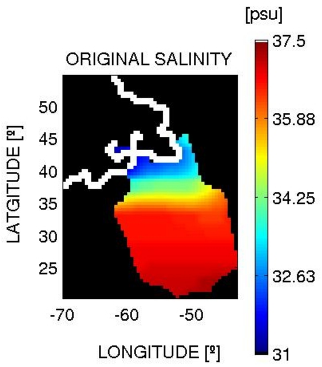

a)

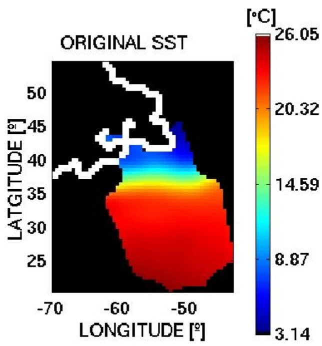

b)

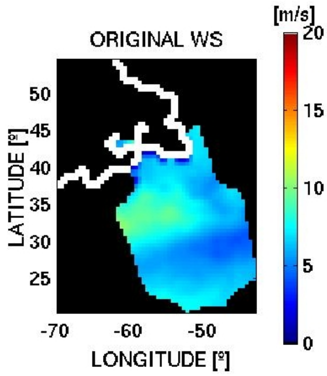

c)

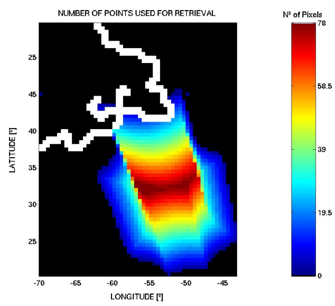

d)

Figure 6.6: Scene C. a) Location of the scene. SSS in situ (b), SST in situ (c), and wind speed in situ (d) data used by the direct model to create T_B. e) Number of snap shots for each pixel.

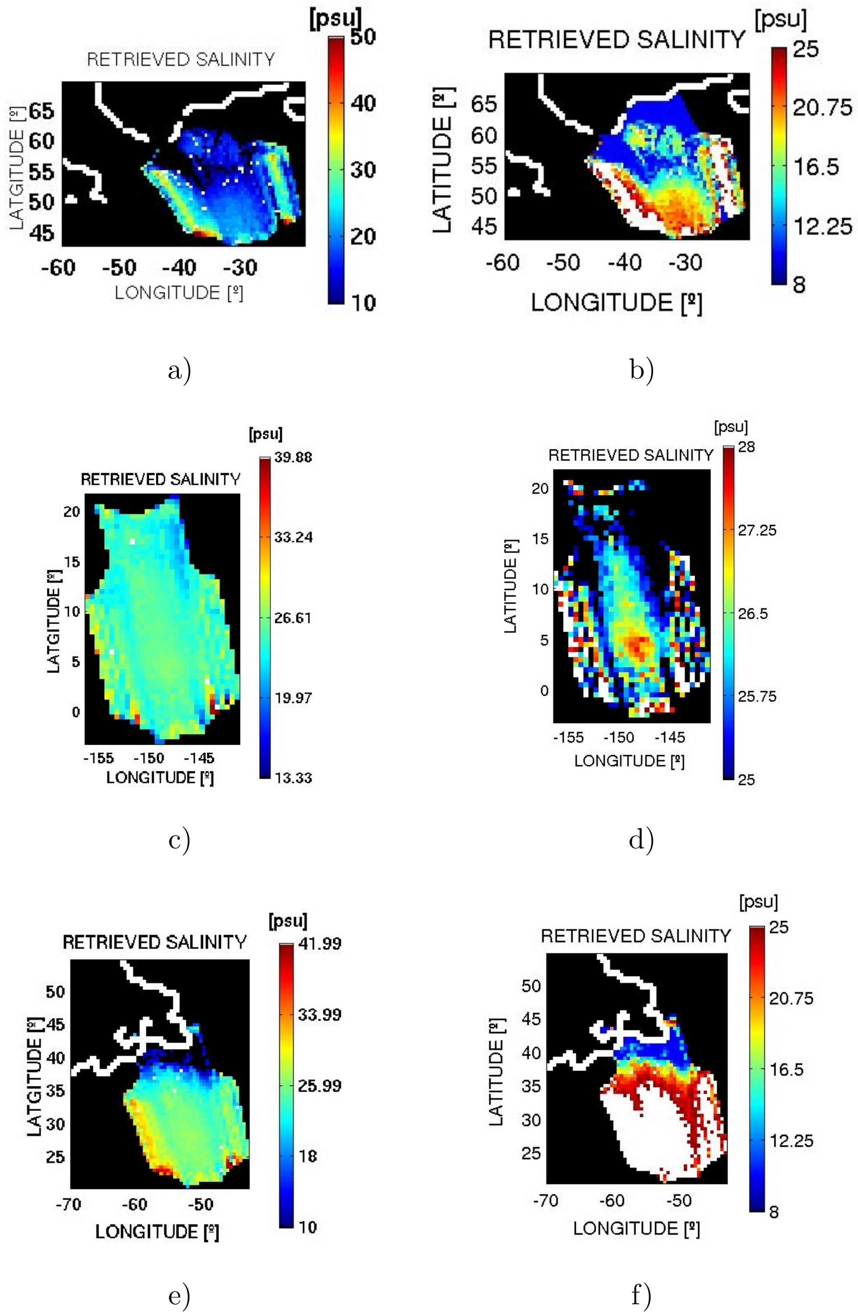

Figure 6.7: a) Retrieved SSS for scene A (b) and the error as $error = SSS_{original} - SSS_{retrieved}$ for scene A (c) Retrieved SSS for scene B (d) and its error (e) Retrieved SSS for scene C (f) and its error.

From figure 6.7 one can observe that scenes A and C present higher biases than scene B. These could be due to the second source of bias above explained, since scenes A and C are nearer to the coast, while B is in the middle of the Pacific.

However the figures also show a large dispersion of the retrieved values. This important dispersion can be due to random noise errors which effect the brightness temperature measurements. These random noises could be reduced by applying some statistical treatment. Scene B (figure 6.7d) is the one which presents less dispersion of the images. This is probably because the measurements have been done far away from coast.

Scene C is the one that presents more variability of SSS and SST. In the North area of this scene there is a front that shows a rapid decrease on SSS from ≈ 37 psu to near 34 psu. This variation of salinity in the area is also visible in the retrieved salinity image (figures 6.7e,f). Therefore it seems that the system is capable to detect variances on SSS, even though the absolute values are not correct.

These results are obtained with data of only one pass of the satellite and therefore pixel averaging has not yet been performed. Better results should be expected for the SMOS case, since temporal and spatial averaging will be performed, and thereby noise will be reduced.

Other works performed using these tools can be found in Camps et al. (2002a) and Camps et al. (2004c).

6.3 Conclusions

From the above work, it can be concluded that small errors on the retrieved salinity can be expected due to random noise on the brightness temperature. However, biases on the brightness temperature (for example 5K) produce important errors on the retrieved salinity (5.5 psu).

Errors on the auxiliary parameters, produce errors on the retrieved salinity which are not negligible. An important conclusion is that better salinity retrievals are obtained when the auxiliary parameters are left to be retrieved from the inversion algorithm, instead of fixing them to erroneous values . This is in accordance with what was concluded when experimental data set has been used (chapter 5).

From the SMOS images analysis, one can conclude that a lot of work is needed to investigate how to reduce the noise and biases that effects the measured T_B. May be, a statistical treatment should be used to decrease as much as possible the errors. Results, also, underline that probably an external calibration will be necessary to correct the brightness temperatures from biases which are not controlled.

Results show that the system is capable to detect steps on SSS in one satellite overpass, when they are high (≈ 3 psu), and therefore to detect fronts.

Chapter 7

Conclusions and recommendations

This thesis has been performed in the framework of the SMOS mission. The ICM has actively participated in two experiments sponsored by ESA, and has also participated in some ESA study contracts related with the SMOS mission.

In this thesis, errors on the sea surface salinity retrieved from L-band radiometric measurements have been investigated. This work has been done based in measurements acquired during campaigns organised by ESA as preparatory activities for the SMOS mission.

The study is a first step to understand which issues are more critical on the inversion process. Of course campaign measurements were not acquired exactly as SMOS will do, but the results can bring some insight on how the SMOS level 2 (geophysical products) processing chain should be developed.

The work has analysed two important issues that are still open for SMOS: the emissivity models and the auxiliary parameters.

7.1 Conclusions on emissivity models

The analysis of three dielectric constant models performed using the FROG campaign data-set, has shown that Klein and Swift (1977) model is the one that best retrieves salinity, while Blanch and Aguasca (2004) has a quite similar behaviour. Ellison et al. (1998) model gives biased results.

Salinity is properly retrieved from radiometric measurements obtained in different campaigns with an accuracy of 0.13-0.5 psu, depending on the emissivity models and the auxiliary parameters used. Therefore, it is possible to detect important gradients of salinity (the Plata campaign).

Retrieval salinity analysis from WISE and EuroSTARRS campaigns has shown that better results are obtained when using semi-empirical models to describe the emissivity of the sea than using the two tested theoretical models.

A new sea roughness semi-empirical model derived by the author from WISE 2001 data set has shown to retrieve salinity better than the other models, which depend only on wind speed. This conclusion is valid for the three campaigns tested in the study: WISE, EuroSTARRS and Plata. The new approach of this semi-empirical model is that the roughness of the sea is expressed as function of wind speed and also of the significant wave height, and therefore the swell events are considered. This model, derived from Mediterranean data (WISE), has been validated for completely different sea conditions (South Atlantic, Plata).

7.2 Conclusions on auxiliary parameters

An analysis of the auxiliary parameters used in the retrieval process has shown that important errors are introduced in the retrieved salinity due to imprecisions in these auxiliary parameters.

Comparisons of retrieved salinity have shown that better results are obtained when atmospheric and oceanographic models are used to obtain U_{10} and SWH parameters than using directly satellite observations. This is probably because this models have higher temporal resolution. However, this conclusion can not be directly extrapolated to other ocean conditions since this analysis has been performed in a determined area only.

A new method to obtain the auxiliary parameters has been proposed in this thesis. It consists of obtaining them (or some of them) from the radiometric measurements themselves. This is possible thanks to the multi-angular capability of SMOS, that allows each pixel to be repeatedly observed from several incidence angles. Therefore, having several measurements of the same pixel permits to retrieve several unknown parameters, since the system is overdetermined.

The introduction of constrains in the cost function (reference values for the parameters and their expected uncertainties) improves the quality of the salinity retrieval.

A better retrieval of the parameters is obtained when better quality reference values are used. However, the reference value for SSS is the one that has more impact on the retrieved salinity.

Following this new insight, wind speed can be retrieved with an error of 1 m/s, an accuracy that, until the present, no satellite measurement or model output can achieve simultaneous to SMOS measurements. When using this method, since the parameters are not fixed to any specific value, the inversion algorithm can properly converge to good results.

The same analysis has been done using SMOS-like images generated by SEPS, and the best results are obtained when leaving the auxiliary parameters to be retrieved from the inversion algorithm also.

The usage of this method to retrieve sea surface temperature does not show big improvements on the quality of the retrieved salinity. This is because this parameter can be measured by other sources with enough good accuracy.

7.3 Recommendations

In many satellite missions, when the knowledge of the physical mechanisms responsible for the signal measured by a sensor in function of a geophysical variable is not sufficiently detailed, empirical approaches are often developed to obtain a practical algorithm to retrieve the geophysical variable. This is the case for example of the CMOD algorithm (Stoffelen and Anderson, 1993) to derive wind velocity from the ERS scatterometer.

For the case of SMOS, as nowadays few experimental data exist at L-band, it is difficult to validate the models. Thereby, maybe the emissivity model should be decided during the first period of SMOS live (commissioning phase), in which data validation will be performed. During this period, SMOS measurements will be compared with in situ salinity measurements obtained from thousands of floats that will be diving over the oceans (ARGO floats), as well as other in situ measurements. The large amount of data acquired will also permit to derive several semi-empirical models for different sea conditions, which might improve the retrieved salinity from SMOS measurements, since the model will be optimised for each area conditions.

A good approach for study this issue is to derive a new semi-empirical model of emissivity from the Plata data set, and to analyse if significant differences appear between models from different sea conditions.

Another interesting study would be to analyse if other auxiliary parameters could add important information to the emissivity model, as for example wave age or fetch.

An analysis similar to what has been done in this thesis, should be done considering the first Stokes parameter. As explained at the beginning of this document, when this parameter is used ($I=T_{BH}+T_{BV}$), besides using them separately, the Faraday and geometrical rotations are cancelled out. Nevertheless the number of independent measurements is reduced to the half, which produces a small degradation on the quality of the retrieved salinity. During this thesis, preliminary analysis have been done using experimental data, and results show that the deterioration of the retrieve salinity is not large. However more exhaustive analysis should be performed.

A strong recommendation is done to SMOS community to use the method that permits the auxiliary parameters to be retrieved from SMOS measurements themselves. For SMOS, the last orbital pass of the satellite over the same pixel could be used as reference for SSS value to be used in the retrieval, since salinity does not present fast variations.

More work should be done to investigate how to reduce the noises and biases that effect the images measured by SMOS. The work done with the SMOS simulator images show that good quality salinity maps are not possible to obtain due to the important artifacts (specially bias) that affect the brightness images.

We are still far from closing all the open issues on the salinity retrieval from SMOS measurements, but several theoretical studies and experimental work performed during the last years have permitted to improve our understanding of the physical laws and the retrieval concepts. The work presented in this thesis gives some new insights to the SMOS level 2 data processing chain.

Appendix A

Compilation of articles

A.1 List of articles in which the author has participated

A list of published articles related with the work presented in this thesis is attached. The two articles in which the author of this thesis is the first author are also attached.

Articles published in peer review journals

A. Camps, J. Font, J. Etcheto V. Caselles, A. Weill, I. Corbella, M. Vall-llossera, N. Duffo, F. Torres, R. Villarino, L. Enrique, A. Julià, **C. Gabarró**, J. Boutin, E. Rubio, S. C. Reising, P. Wursteisen, M. Berger, M. Martín-Neira. "Sea Surface Emissivity Observations at L-band: First Results of the Wind and Salinity Experiment WISE-2000". *IEEE Trans. Geosciences and Remote Sensing*, Vol. 40, N° 10, pp. 2117–2130, 2002.

A. Camps, I. Corbella, M. Vall-llossera, N. Duffo, F. Torres, R.Villarino, L. Enrique, F. Julbe, J. Font, A. Julià, **C. Gabarró**, J. Etcheto, J. Boutin, A. Weill, E. Rubio, V. Caselles, P. Wursteisen, M. Martín-Neira." L-band sea surface emissivity: Preliminary results of the WISE-2000 campaign and its application to salinity retrieval in the SMOS mission". *Radio Science*, Vol. 93, N° 4, pp. 8071, doi:10.1029/2002RS002629, 2003.

C. Gabarró, J. Font, A. Camps, M. Vall-llossera. " Determination of Sea Surface Salinity and Wind speed by L-band Radiometry from a fixed platform.". *Internation Journal of Remote Sensing*, Vol. 25, N° 1, pp. 111-128, 2004.

C. Gabarró, J. Font, A. Camps, M. Vall-llosera. "A New Empirical Model of Sea Surface Microwave Emissivity for Salinity Remote Sensing". *Geophysical Research Letters*, Vol. 31, N° L01309, pp. 1-5, 2004.

A. Camps, J. Font, M. Vall-llossera, **C. Gabarró**, I. Corbella, N. Duffo, F. Torres, S. Blanch, A. Aguasca, R. Villarino, L. Enrique, J. Miranda, J. Arenas, A. Julià, J. Etcheto, V. Caselles, A. Weill, J. Boutin, S. Contardo, R. Niclós, R. Rivas, S.C. Reising, P. Wursteisen, M. Berger, M. Martín-Neira. "The WISE 2000 and 2001 field experiments in support of the SMOS mission: sea surface L-Band brightness temperature observations and their application to Multi-Angular salinity retrieval". *IEEE Trans. Geosciences and Remote Sensing*, Vol. 42, N° 4, pp. 804-823, 2004.

Proceedings and communications to congresses

A. Camps, I. Corbella, M. Vall-llossera, R. Villarino, L. Enrique, J. Font, A. Julià, **C. Gabarró**, J. Etcheto, J. Boutin, A. Weil, F. Torres, N. Duffo, J. Barà, R. Niclòs, V.C aselles, P. Wursteisen, M.Martín-Neira. "Sea surface emissivity observations at L-band: First preliminary results of the Wind and Salinity Experiment WISE-2000", *Proceedings IEEE International Geosciences and Remote Sensing Symposium IGARSS 2001*, pp. 1371-1373, 2001.

J. Font, A. Camps, J. Etcheto, P.Wursteisen, M. Martin-Neira, J. Barà, I. Corbella, N. Duffo, L. Enrique, F. Torres, M. Vall-llossera, R.V illarino, M. Emilianov, **C. Gabarró**, A. Julià, J. Boutin, A. Weil, V. Caselles, L. Martínez, R. Niclòs, E.M. Rubio, M. Moll. "WISE 2000 : Can we measure salinity from satellite?".*Rapp. Int. Mer. Comm.* Int Mer Medit. Septiembre 2001.

C. Gabarró, J. Font, A. Camps, M. Vall-llossera. "Sea Surface Salinity and Wind speed retrieved from a Tower-based L-band Radiometer in the NW Mediterranean.". Congress: *Recent Advances in Quantitative Remote Sensing Symposium*, September 2002. Valencia, Spain 2002.

A. Camps, I. Corbella, M. Vall-llossera, F. Torres, N. Duffo, R. Villarino, L. Enrique, J. Miranda, J. Arenas, J. Font, A. Julià, **C. Gabarró**, J. Etcheto, J. Boutin, S. Contardo, A. Weill, R. Niclòs, V. Caselles, P. Wursteisen, M. Berger,

M. Martín-Neira. "Wind Effects on the Sea Surface Emissivity at L-band: Preliminary Results of WISE 2000 and 2001". *Proceedings URSI Commission-F Open Symposium*, 2002.

A. Camps, J. Font, J. Etchetto, A. Weill, V. Caselles, I. Corbella, M. Vall-llossera, F. Torres, N. Duffo, R. Villarino, L. Enrique, J. Miranda, A. Julià, **C. Gabarró**, J. Boutin, R. Niclòs, P. Wursteisen, M. Martín-Neira. "L-band Sea Surface Emissivity Radiometric Observations under High Winds: Preliminary Results of the Wind and Salinity Experiment WISE-2001". *Proceedings IEEE International Geosciences and Remote Sensing Symposium IGARSS 2002, Toronto*, 2002.

A. Camps, J. Font, J. Etcheto, V. Caselles, A. Weill, I. Corbella, M. Vall-llossera, F. Torres, N. Duffo, R. Villarino, L. Enrique, J. Miranda, J. Arenas, A. Julià, **C. Gabarró**, J. Boutin, S. Contardo, R. Niclòs, R. Rivas, S. C. Reising, P. Wursteisen, M. Berger, M. Martín-Neira. "Sea Surface Radiometric Observations At L-Band: Wind Speed Sensitivity Derived from WISE 2000 and 2001". *Proceedings International Union of Radio Science 27th General Assembly*, 2002

C. Gabarró, J. Font, A. Camps, M. Vall-llossera. "Errors on the Retrieved Sea Surface Salinity from Microwave Radiometry due to Inaccuracies in the Ancillary Data". Congress: *IEEE International Geoscience and Remote Sensing Symposium IGARSS 2003.* Toulouse, France 2003.

C. Gabarró, J. Font, A. Camps, M. Vall-llossera. "Retrieved sea surface salinity and wind speed from L-Band measurements for WISE and EuroSTARRS campaign.". *Proceedings of the WISE/LOSAC/EuroSTARRS Campaigns Workshop, ESA PUBLICATIONS*, Vol. SP-525, pp. 163-172, 2003.

J. Font, **C. Gabarró** , A. Julià, M. Emilianov, M. Lloret, M. Moll. " Oceanographic conditions during Wind and Salinity Experiment 2000 and 2001, NW Mediterranean Sea.". *Proceedings of the WISE/LOSAC/EuroSTARRS Campaigns Workshop, ESA PUBLICATIONS*, Vol. SP-525, pp. 163-172, 2003.

M. Emelianov, J. Font, A. Julià, **C. Gabarró** , M. Lloret, J. Solé, L. Enrique. "Sea Surface fields at Casablanca site during the EuroSTARRS Campaign". *Proceedings of the WISE/LOSAC/EuroSTARRS Campaigns Workshop, ESA PUBLICATIONS*, Vol. SP-525, pp. 163-172, 2003.

C. Gabarró, J. Font, A. Camps, M. Vall-llossera, M. Portabella. "A new empirical model of sea surface microwave emissivity for salinity remote sensing". Congress:*MICRORAD 04*. Rome, Italy, 2004

C. Gabarró, J. Font, J. L. Miller. "Sea surface measured by an airborne microwave radiometer in the NW Mediterranean". Congress: *CIESM*. Barcelona, Spain, 2004.

A.2 International Journal of Remote Sensing

This manuscript was submitted in September 2002 and published in January 2004.

INT. J. REMOTE SENSING, 10 JANUARY, 2004,
VOL. 25, NO. 1, 111–128

Taylor & Francis
Taylor & Francis Group

Determination of sea surface salinity and wind speed by L-band microwave radiometry from a fixed platform

C. GABARRÓ*†, M. VALL-LLOSSERA‡, J. FONT† and A. CAMPS‡

†Institut de Ciències del Mar CMIMA – CSIC, Passeig Maritim de la Barceloneta 37–49, 08003 Barcelona, Spain

‡Departament de Teoria del Senyal i Comunicacions, UPC, Campus Nord, D4 08034 Barcelona, Spain

Abstract. In May 1999, the European Space Agency (ESA) selected SMOS (Soil Moisture and Ocean Salinity) as an Earth Explorer Opportunity mission. One of its goals is the generation of global sea surface salinity (SSS) maps. The satellite sensor is an L-band interferometric radiometer with full-polarimetric capability called MIRAS. The retrieval of SSS from microwave measurements is based on the fact that the brightness temperature (T_B) of seawater is a function of the dielectric constant, temperature and sea surface state (roughness, foam…). The sensitivity of T_B to SSS is maximum at L-band, but it is necessary to quantify the other effects to have reliable SSS retrieval. In order to improve the present understanding of these effects on T_B, ESA sponsored the Wind and Salinity Experiment (WISE) 2000 and 2001 field campaigns. These experimental results are of great importance for the development of sea surface emissivity models that will be used in the future SMOS SSS retrieval algorithms. This paper presents the influence of the emissivity models on the derived SSS from the data obtained in both campaigns. It also presents the impact on the retrieved SSS of using *in situ* measured or satellite derived wind information, or even simultaneously estimating the wind speed from the measured multi-angular T_B.

1. Introduction

The distribution and variability of salinity in the world oceans is a key parameter both for the marine ecosystems and for the role of the oceans in the climate system (Reynolds *et al.* 1998, Hopkins 2001). Systematic global surface sampling by satellite is now a usual tool for monitoring many ocean variables such as temperature, colour, topography and even surface winds. However, until now remote sensing of the sea surface salinity (SSS) has not been possible due to major technical difficulties. Using the interferometric microwave radiometry concept, in early 2007 the European Space Agency (ESA) will launch the Soil Moisture and Ocean Salinity (SMOS) mission to fill this gap and provide global SSS maps for climatic and large-scale ocean circulation studies (Kerr *et al.* 2000).

The brightness temperature (T_B) of the sea at L-band is dependent on the SSS, in particular through the dielectric constant (Klein and Swift 1977), as well as on other factors like the sea roughness (mainly produced by wind stress), the sea

*Corresponding author; e-mail: cgabarro@icm.csic.es

International Journal of Remote Sensing
ISSN 0143-1161 print/ISSN 1366-5901 online © 2004 Taylor & Francis Ltd
http://www.tandf.co.uk/journals
DOI: 10.1080/0143116031000115175

surface temperature (SST), the presence of foam, the incidence angle, etc. Even though the sensitivity of the brightness temperature on the SSS is maximum at L-band, it is quite low: $\sim 0.5\,K\,psu^{-1}$ at SST = 20° C, decreasing to $\sim 0.25\,K\,psu^{-1}$ at SST = 0° C (Skou 1995, Lagerloef *et al.* 1995, Lagerloef 1998). The sensitivity of T_B to SST is about the same order, 0.2–0.4 K $°C^{-1}$ (Swift and McIntosh 1983) (see figure 1), and the sensitivity to wind speed (WS) is in the range 0–0.4 K/m s^{-1}, depending on the incidence angle (Hollinger 1971, Webster and Wilheit 1976, Lerner and Hollinger 1977). These numbers indicate that it is important to have a good knowledge of all the variables affecting T_B to retrieve the salinity from radiometric measurements with good accuracy.

To improve the present understanding of these effects on T_B, the ESA has sponsored the WISE (Wind and Salinity Experiment) 2000 and 2001 field campaigns. This paper describes the results of salinity retrieval from WISE data using wind and SST data measured *in situ*, and also from satellite measurements. Furthermore, it considers the possibility of retrieving both the wind speed and the SSS simultaneously from the multi-angular T_B measurements. Previous efforts on measuring surface salinity with an L-band radiometer airborne can be found in Swift (1993), Miller *et al.* (1998) and Wilson *et al.* (2001).

2. Campaign description

The WISE experiments were held at the Casablanca oil platform 40 km from the coast of Tarragona (Catalonia, Spain), in the north-west Mediterranean Sea (40.72° N, 1.36° E). Both experiments took place in autumn, when there are usually high winds in the region. The WISE 2000 campaign was held from 16 November to 18 December 2000 and continued from 9–15 January 2001, while the WISE 2001 campaign was held from 23 October to 22 November 2001.

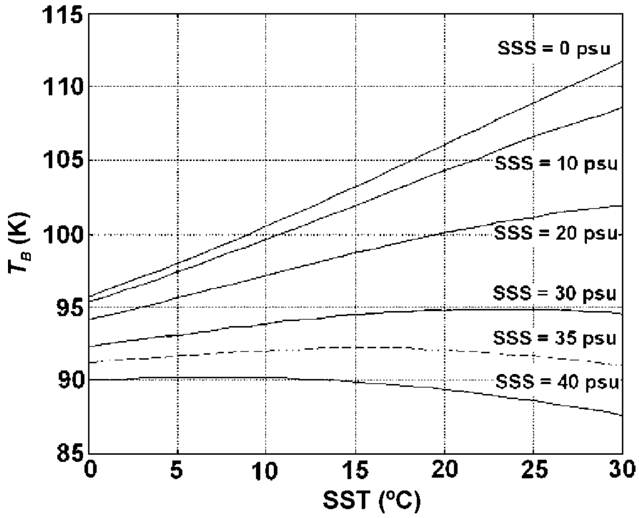

Figure 1. Brightness temperature (T_B) as a function of sea surface temperature (SST) and salinity.

The WISE participants were the Universitat Politècnica de Catalunya (UPC, Barcelona, Spain; the prime contractor with ESA), the Institut de Ciències del Mar (ICM–CSIC, Barcelona, Spain), the Laboratoire d'Océanographie Dynamique et Climatologie (LODYC, Paris, France), the Universitat of Valencia (UV, Valencia, Spain), the Centre d'Études Terrestres et Planétaires (CETP, Paris, France), and the University of Massachusetts (UMass, Amherst, USA) as a guest institution. The deployed instruments were:

- an L-band polarimetric radiometer—LAURA (L-band AUtomatic RAdiometer)
- a K_a-band polarimetric radiometer
- a stereo-camera to determine surface topography and rms slopes of the sea surface
- four oceanographic and meteorological moored buoys
- a sub-surface conductivity and temperature sensor
- a portable meteorological station
- a video camera to determine sea surface foam coverage
- an infrared radiometer to determine SST estimates

Additionally, ocean colour, wind vector and sea surface temperature were acquired simultaneously by several satellites.

A full description of the measurements performed can be found in Camps *et al.* (2002, 2003a). As can be appreciated in figure 2, during the WISE 2001 campaign the SST ranged between 16.0°C and 22.5°C, due to the seasonal variation. Measured sea surface salinity remained very stable around 38 psu, except on 18 November due to an intense rain event. The 10 m wind speed varied greatly, reaching up to 25.5 m s^{-1} during a strong storm on 15 November, when significant wave heights of almost 12 m were measured.

In the WISE campaigns the brightness temperatures in both (horizontal and vertical) polarizations were acquired by the radiometer LAURA. One of the modes of acquisition consisted of measuring in five or nine different elevation positions from θ_i=25–65°, in 5° or 10° steps respectively, at a fixed azimuth angle (Camps *et al.* 2002, 2003a). Data acquired in these conditions are used for the work presented below.

3. Applied methods

WISE campaign data are very useful for validating different empirical and theoretical sea surface emissivity models that exist in the literature for L-band. A new semi-empirical model based on these data has already been derived (Camps *et al.* 2003a). However, it should be noted that the data were obtained for west Mediterranean conditions (limited fetch), and the results may not be directly extrapolated to other ocean environments.

Different emissivity models and wave spectra were used in this study. The algorithm used to retrieve the salinity from T_B data is based on the minimization of a cost function (equation (1)) using a recurrent least-squares fit called Levenberg–Marquardt (Press *et al.* 1992).

$$\min \sum_{i=1}^{N} w_i \Big(T_{B,i} - T_{B,i}^{\mathrm{mod}}(a) \Big)^2 \qquad (1)$$

where i indicates the acquisitions, a is the vector for the parameters to estimate and w is the weight assigned to each acquisition. Here the vector of parameters to

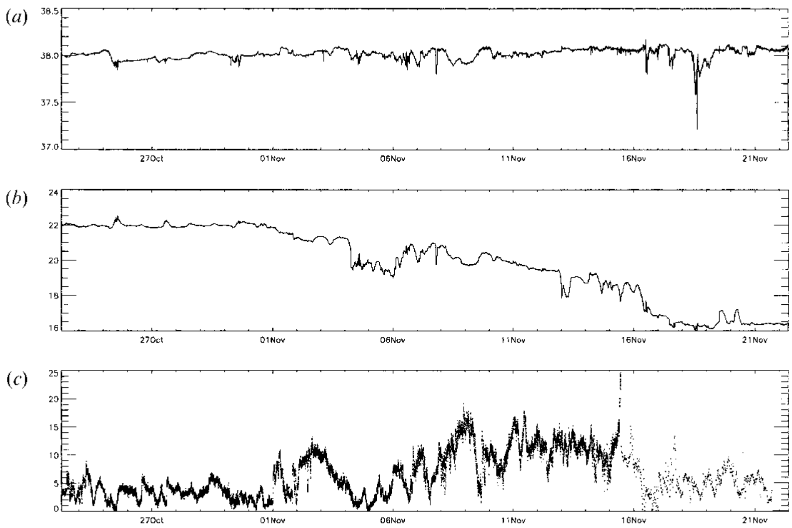

Figure 2. (*a*) Sea surface salinity (psu), (*b*) sea surface temperature (°C) and (*c*) wind speed (m s^{-1}) during WISE 2001.

estimate, *a*, is the salinity and in some cases also wind speed and the weights are set to 1.

This algorithm was chosen for its easy implementation and computational efficiency. T_B is computed setting an initial guess for SSS into the chosen direct emissivity model. This value is compared with the measured T_B by the radiometer and then an increment (ΔSSS) is added to the initial salinity. This recursive process is stopped when the difference between the measured and the computed T_B is smaller than a specified threshold (it might not be the smallest value).

Several aspects are studied in this work. We first consider the relationship between the retrieved salinity error and the number of incidence angles. The retrieval of SSS with different emissivity models is studied and compared with the *in situ* SSS measurements from the WISE campaigns, which were obtained by the oceanographic buoys close to the radiometer field of view. We also compare the results using a wave height dependent model versus a wind speed dependent model. Finally we study the impact of errors in the ancillary data (wind speed, wave height and SST) on the salinity retrievals.

3.1. *Emissivity models*

In the past few years, improved methods have been developed to model the polarimetric emission of the sea surface (Gasiewski and Kunkee 1994, Yueh *et al.* 1997, Camps and Reising 2001, Laursen and Skou 2001). However, these models have been developed or tuned at frequencies higher than L-band (1.4 GHz), typically 19 and 37 GHz. Additionally, sea foam effects at L-band are difficult to model since they have never been measured. According to recent modelling results

(Reuil and Chapron 2001), only sea foam thicker than 2 cm may produce an increase in the L-band brightness temperatures, but experimental validation has not yet been performed.

For the different emissivity models, the brightness temperature collected by the radiometer antenna follows equation (2) (Ulaby *et al.* 1981),

$$T_B = \left(T'_B + T_{SC}\right)/L_A + T_{UP} \tag{2}$$

where T'_B is the terrain emission, and T_{SC} is the radiometric temperature of energy scattered by the terrain. The primary source of T_{SC} is the downward-emitted atmospheric radiation (T_{DN}), although it may also have a component due to extraterrestrial radiation incident upon the terrain (T_{EBT}). The atmospheric attenuation L_A and the atmospheric upwelling self-emission T_{UP} can be neglected for the WISE conditions (radiometer located at 33 m above sea level). The term T_{SC} is estimated from numerical models and the knowledge of the antenna radiation pattern (Camps *et al.* 2003b).

Four different emissivity models have been studied in this work, two of them are semi-empirical and two analytical.

3.1.1. *Semi-empirical models*

The effect of wind on the T_B at L-band is quite small, even though it is great compared to the salinity effect. For this small effect an approximation considering a first order Taylor series can be applied. Thus, equation (2) can be reduced to equation (3),

$$T_B = e_p(\text{SSS, SST}, \theta_i)\ \text{SST} + \Delta T_{w,p}(\theta_i, U_{10}) \tag{3}$$

where the first term is the contribution of a flat surface and the second one is the brightness temperature variation produced by the surface roughness. The ocean emissivity at angle θ_i, $e(\text{SSS, SST}, \theta_i)$, can be calculated from the Fresnel power reflection coefficients at horizontal and vertical polarization, as shown in equation (4).

$$\begin{aligned} e_H &= 1 - \left| \frac{\cos(\theta_i) - \sqrt{\varepsilon - \sin^2(\theta_i)}}{\cos(\theta_i) + \sqrt{\varepsilon - \sin^2(\theta_i)}} \right|^2 \\ e_v &= 1 - \left| \frac{\varepsilon \cdot \cos(\theta_i) - \sqrt{\varepsilon - \sin^2(\theta_i)}}{\varepsilon \cdot \cos(\theta_i) + \sqrt{\varepsilon - \sin^2(\theta_i)}} \right|^2 \end{aligned} \tag{4}$$

The dielectric constant ($\varepsilon = \varepsilon' + i\ \varepsilon''$) is calculated following Klein and Swift (1977), and θ_i is the incidence angle. $\Delta T_{w,p}$ is the brightness temperature due to the roughness of the surface (mainly due to wind speed) and U_{10} is the wind speed at 10 m height.

Considering the above approximation, two different wind speed dependencies are studied in this work,

A. *Hollinger's linear regression model.* This is a derived wind speed sensitivity from measurements made at Argus Island Tower by Hollinger (1971), and it is shown in equation (5)

$$\begin{cases} \Delta T_h \approx 0.2\left(1+\theta_i/55^\circ\right) U_{10} \\ \Delta T_v \approx 0.2\left(1-\theta_i/55^\circ\right) U_{10} \end{cases} \quad (5)$$

for incidence angles, θ_i, smaller than 55°. This model was used by the National Oceanic and Atmospheric Administration (NOAA) for their experiments in 1997 with the SLFMR (Scanning Low-Frequency (L-Band) Microwave Radiometer) sensor (Goodberlet and Miller 1997).

B. *WISE-derived model*. The brightness temperature to wind dependence for each incidence angle is now derived from WISE 2001 data (Camps *et al*. 2003a), considering an unstable atmosphere. Figure 3 shows the points obtained after performing the regression of the measurements for each angle and the linear-fit to these points, which results in equation (6):

$$\begin{cases} \Delta T_h \approx 0.25\left(1+\theta_i/94^\circ\right) U_{10} \\ \Delta T_v \approx 0.24\left(1-\theta_i/48^\circ\right) U_{10} \end{cases} \quad (6)$$

3.1.2. *Analytical models*

Among the different analytical physically-based scattering models we have used, the Two-Scale Method and the Small Slope Approximation, as in a recent comparison (Vall-llossera *et al*. 2003), appear to best fit with the WISE data.

C. *Two-Scale Method—Durden and Vesecky* ×2. The Two-Scale Method (TSM) employed in this study is the one developed by Yueh *et al*. (1997). Two-scale sea surface models approximate the sea surface as a two-scale surface with small ripples

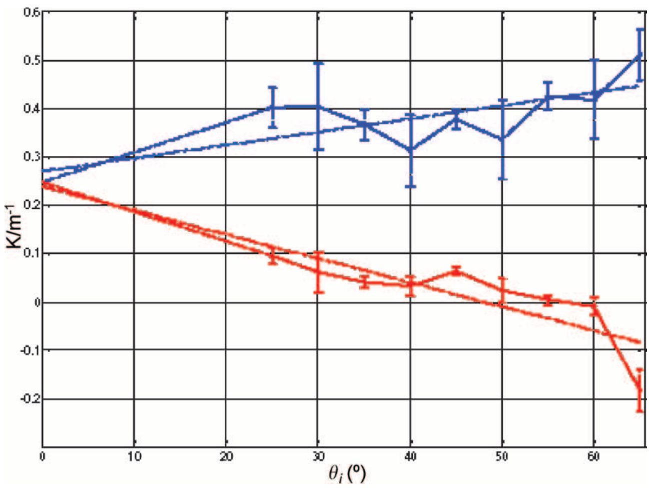

Figure 3. Brightness temperature dependence to wind speed with respect to incidence angle, derived from WISE 2001 measurements.

or capillary waves on the top of large-scale surfaces. With this approximation, the total thermal emission from the surface is the sum of emissions from individual, slightly perturbed surface patches tilted by the underlying large-scale surface. This model uses the Durden and Vesecky (1985) wave spectrum multiplied by a factor of two. It has been recently found to compare well with brightness temperature measurements made at higher frequencies (Lagerloef 2001). The input values to the model are SSS, SST, wind speed, azimuth and incidence angle.

D. *SPM/SSA model—Elfouhaily*. This model follows the Small Slope Approximation (SSA) theory for free-foam rough surfaces (Voronovich 1994) with the wave spectrum derived by Elfouhaily (Elfouhaily *et al.* 1997). We have used the theoretical development by Johnson and Zhang (1999) in which the physics of the emission process predicted by SPM/SSA was clarified. Use of the SPM/SSA up to the second order produces an expansion in surface slope, with zero order terms reproducing flat surface emission results, first order terms identically zero, and the second order terms providing the first prediction of changes from flat surface brightnesses. Second order terms take the form of an integral of a set of weighting functions over the surface directional spectrum. Properties of a directional spectrum result in no first harmonic variation being obtained; a third order SPM/SSA is required to obtain the first harmonics. Only the second order expansion is considered in this study. No artificial cut-off wavenumber is required to separate small- and large-scale waves in this method. The input values to the model are SSS, SST, wind speed, azimuth and incidence angle.

None of those models considers the foam effects. All of them have been implemented with the Klein and Swift dielectric constant model because, after some studies at the Jet Propulsion Laboratory (National Aeronautics and Space Administration (NASA)), it seems to be more accurate at L-band than the Ellison dielectric constant model (Ellison *et al.* 1996). This state is also confirmed when both dielectric models are tested with WISE data.

4. Results and discussion

The measurements performed in elevation scan are the best suited to study the retrieval problems. Figure 4 compares the results using different numbers of acquisition angles. It shows the error in the retrieved salinity (using the WISE-derived wind sensitivity model) as a function of the number of incidence angles. Only measurements acquired when the radiometer was pointing in a north direction (nine incidence angles) were considered. The number of incidence angles acquired (x axis) in the plot means nine different acquisition angles per two polarizations minus the discarded measurements. Measurements were discarded when the level of radio frequency interference (RFI), constant during the whole measurement or part of it, led to too large variance in T_B values. It is clear that the SSS retrieval quality increases with the number of acquisition angles used in the retrieval. For the following work only the datasets obtained with a number of incidence angles higher than 12 were considered, except when explicitly stated.

4.1. *Analysis of the results using different models*

The four models described above were run over 25 different datasets. They were acquired on different days and therefore under different wind and temperature conditions. In order to run the algorithm for retrieving the salinity, in addition to the measured T_B, it is necessary to introduce as input the wind speed and SST.

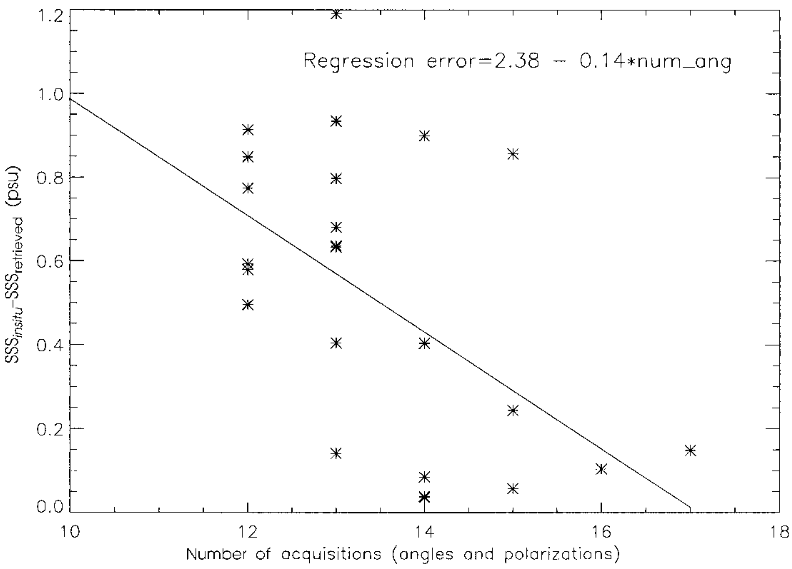

Figure 4. Retrieval errors as a function of the number of acquisition angles. The computations were performed with the UPC model.

Those variables were measured by the oceanographic buoys simultaneously to T_B measurements (Font *et al.* 2003).

Figure 5 shows the difference between the retrieved salinity and the salinity measured *in situ* (with an absolute accuracy of 0.02 psu) for all the studied models. It is clear that the one that best fits with the campaign measurements is the WISE-derived model, as was expected. The mean and the variance of the errors in the retrieved salinity for the 25 measurements were calculated and are presented in table 1.

The retrieved salinity was also obtained using the individual points of the WISE-derived model, and not the linear fit (figure 3). The results demonstrate that the approximation made with the linear fit produces errors in the retrieved salinity lower than 0.01 psu.

The TSM model always highly underestimates the salinity. This problem could be due to a bias on the modelled T_B of about 1–1.5 K that produces a negative bias of 2–3 psu in the salinity. It may also be due to a weak wind dependence that forces the algorithm to decrease the salinity in order to increase the T_B.

The SSA model overestimates the salinity, i.e. the wind dependence is too high. In figure 6 it can be observed that the retrieved salinity accuracy is poorer for events with low wind speed and small waves than in other conditions. This is in agreement with Voronovich and Zavorotny (2001), because they conclude that the Elfouhaily spectrum overestimates the probability of having short waves by 2–4 dB in the cross-wind direction. The results show that this model is not recommended for low-wind events.

From these results it can be concluded that the semi-empirical models seem to recover better than the analytical ones, and that the best model to use in order to

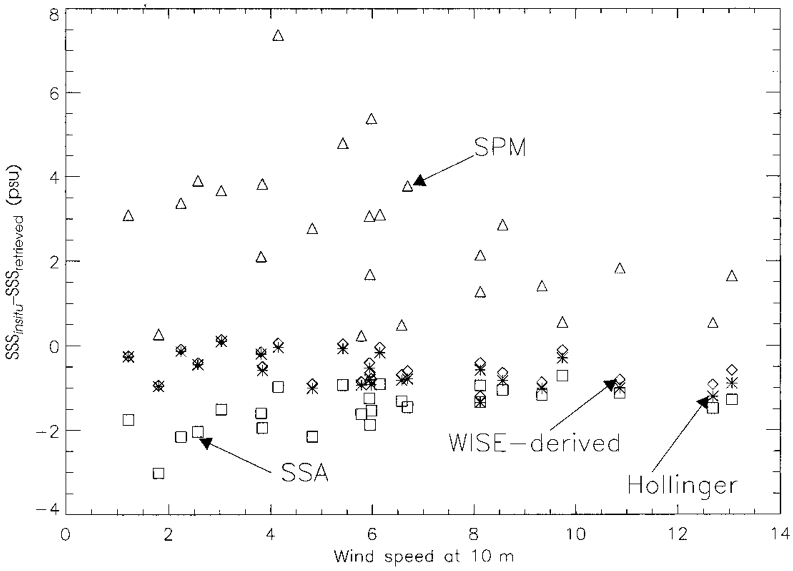

Figure 5. Error in the salinity retrieved using different emissivity models.

Table 1. Mean and variance of the retrieved salinity error for different models, considering $\Delta SSS = |SSS_{insitu} - SSS_{retrieved}|$.

	Mean (ΔSSS) (psu)	$\sigma_{\Delta SSS}$ (psu)
Hollinger's model	0.63	0.15
WISE-derived model	0.52	0.12
Two-scale + Durden and Vesecky ×2	4.28	3.18
SSA + Elfouhaily	1.48	0.27

retrieve salinities from WISE data is the WISE-derived model. Consequently, the work presented below was done using this model.

Figure 7 shows that the error in the retrieved salinity tends to increase linearly with increasing wind speed and wave height. This effect can be explained by the fact that the foam effect has not been taken into account in the models. Normally, the foam coverage increases with wind speed (or wave height) and its effect can be considered negligible only with wind speeds below $10\,m\,s^{-1}$. The foam increases the brightness temperature. If this ΔT_{Bfoam} is not expressed in the model equations, the inversion algorithm will decrease the salinity to compensate for this increase in T_B. This is exactly what can be seen in the results.

Another way to retrieve salinity is to use a model that considers the sea surface roughness term as a function of the significant wave height (SWH) instead of the wind speed. The advantage of this dependence should be that the wave height is not as variable as the wind. In addition, surface roughness may be due to the swell and not only to wind waves. The spectrum models usually consider fully developed sea dependent on the local wind (they usually neglect the swell effect). The retrieval

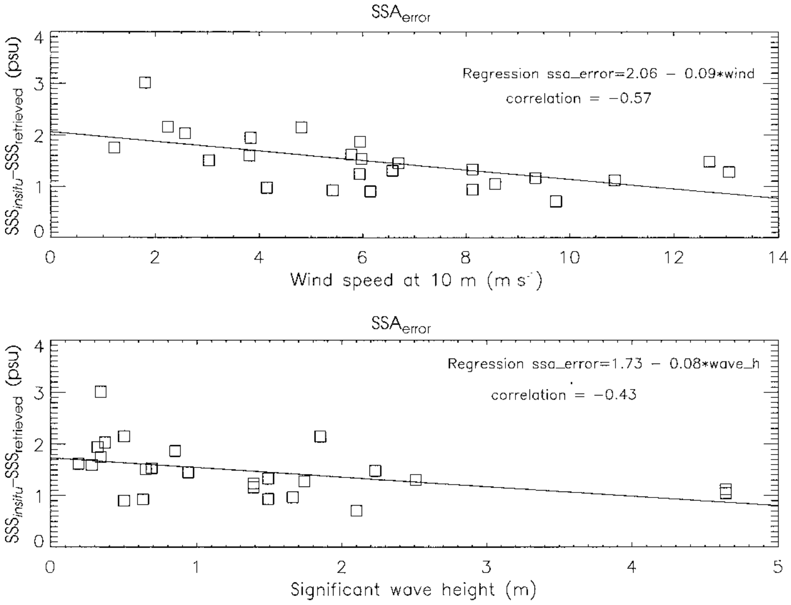

Figure 6. Error in the salinity retrieved for the SSA+Elfouhaily model as a function of wind speed and significant wave height (defined as the average of the highest third of the waves).

computation was performed using the wave height dependence derived from WISE 2000 and 2001 data (Camps *et al.* 2003a):

$$\begin{cases} \Delta T_h \approx 1.09 \left(1+\theta/_{142^\circ}\right) \mathrm{SWH}_{(m)} \\ \Delta T_v \approx 0.92 \left(1-\theta/_{51^\circ}\right) \mathrm{SWH}_{(m)} \end{cases} \quad (7)$$

SWH being the significant wave height, defined as the average of the highest third of the waves, measured by one of the moored buoys. Since the dominant wind during WISE 2001 was from the north, some reflection waves produced by the platform legs were observed. It is therefore recommended to use only data acquired when the radiometer was pointing west, so to compute the retrieved salinities here, only these data (with five incidence angles) were used. To obtain better results the T_B of different measurements made on the same day were averaged (minimum three measurements).

Figure 8 presents the comparison of the retrieved salinity errors using the wind speed dependence and the wave height dependence. The results considering the SWH appear to be slightly worse than those considering the wind dependence (see table 2).

4.2. *Impact on the retrieved SSS due to errors in ancillary data*

To retrieve salinity from SMOS, other variables (wind speed or wave height and SST) are needed as simultaneously as possible in time and space to the radiometer

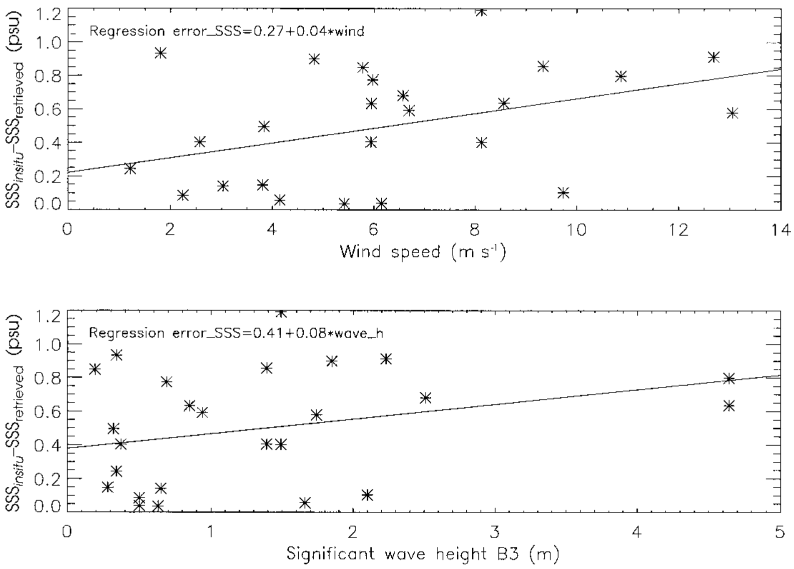

Figure 7. Relation between error in the retrieved salinity and wind speed and wave height with WISE-derived model.

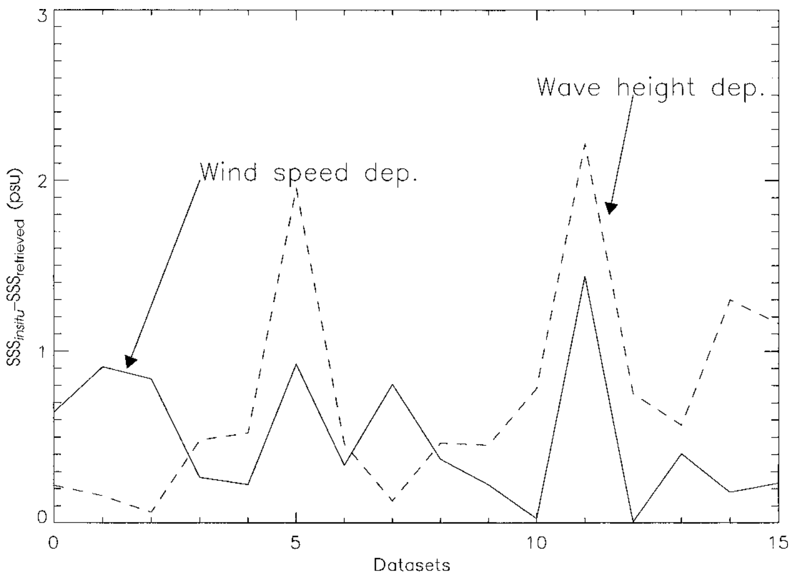

Figure 8. Comparison of the retrieval error using the wind and wave height dependence model for files acquired with five incidence angles (pointing to the west).

Table 2. Mean and variance of the retrieved salinity error using wind speed dependence and wave height dependence, considering $\Delta SSS = |SSS_{insitu} - SSS_{retrieved}|$ (five θ_i files + average). Only daily averages (with similar wind speed) of west pointing data are used.

	Mean (ΔSSS) (psu)	$\sigma_{\Delta SSS}$ (psu)
Wind speed dependence	0.30	0.07
Wave height dependence	0.34	0.07

measurement. In the first SMOS proposal, a second frequency radiometer to measure wind speed was foreseen. But this initial idea was cancelled due to budget constraints. There is the possibility of retrieving wind speed from the L-band measurements (third and fourth Stoke parameters), but this is under study at the moment. Another possibility is to obtain these data from other sensors embarked on a satellite with a similar orbit, but these measurements will have instrumental errors (accuracy) and non-simultaneously orbit errors. Data from meteorological models with satellite data assimilation could also be used.

In this section the errors in the retrieved salinity produced by errors in the wind speed (or SWH) and SST measurements from the satellite and from a model are quantified.

Wind speed measured by the QuikSCAT satellite during the WISE campaigns was collected. This scatterometer has an accuracy of $2\,\mathrm{m\,s^{-1}}$ and a spatial resolution of $25 \times 25\,\mathrm{km^2}$. Wind speed computed from the ARPEGE model (Météo France) in the Casablanca area was also obtained. This model gives data every 6 hours with a net of 0.250° in latitude and longitude, but does not assimilate satellite data. Figure 9 compares the wind speed measured by an *in situ* buoy, the QuikSCAT satellite and the ARPEGE model.

Figure 10 shows the errors in the retrieved salinity obtained using the three different sources of wind speed explained above plus leaving the wind speed as an unknown parameter, and allowing the inversion algorithm to converge simultaneously to a value for the wind speed and another for the salinity. Consequently, in this last situation the algorithm uses an initial guess for both wind speed and salinity values.

It is noticeable that when the wind measured by the satellite shows large errors (cases 10–14), the retrieved salinity increases excessively. The option of leaving the wind as a free parameter seems to retrieve with reasonably good accuracy both the salinity and the wind speed. The dependence of the initial wind and salinity guess values on the results was also studied. It was found that the results are almost independent of these initial values. The wind speed must be considered in a wide range of values, and the QuikSCAT wind speed measurement could be used as an initial guess.

Table 3 shows the mean and the variance of the errors of 25 retrieved salinities using the WISE-derived model with four different wind sources. It can be concluded that it is better to leave the wind variable as a free parameter to retrieve, than to use the satellite measurement of QuikSCAT. On the other hand, when the wind speed obtained from the ARPEGE model is used, quite good results are achieved (the time resolution of this model is 6 hours).

The use of the SWH from a satellite instead of the wind speed could be a good solution since SWH shows smoother changes in time and space. The SWH

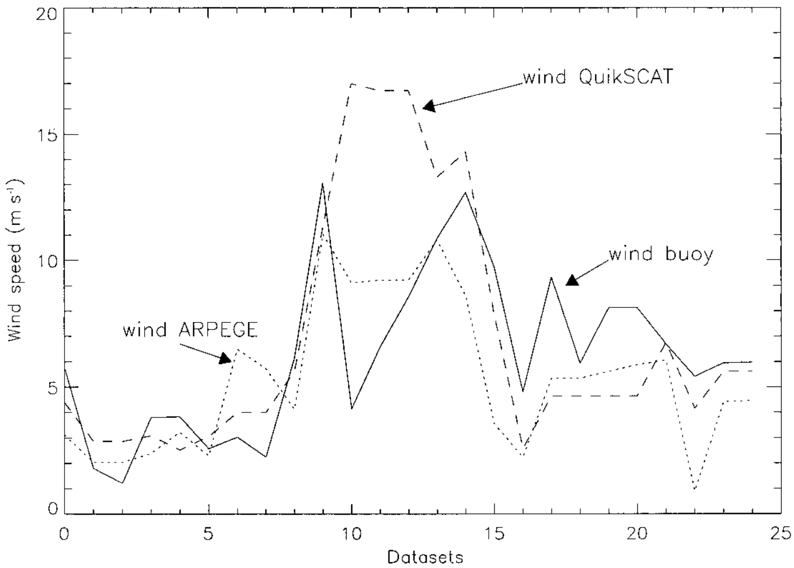

Figure 9. Comparison of wind speed measured by a buoy, QuikSCAT and the ARPEGE model.

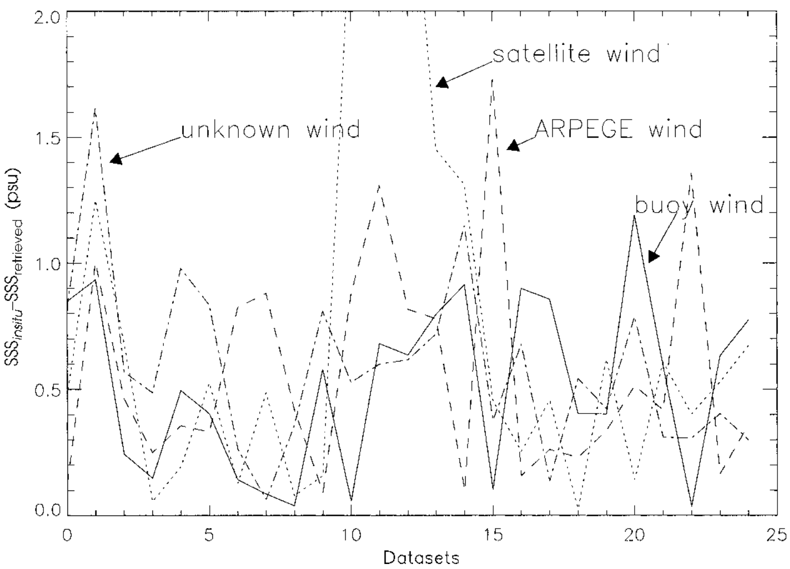

Figure 10. Retrieved salinity using four different methods for measuring wind speed.

Table 3. Mean and variance of the retrieved salinity error for different wind speed sources, considering $\Delta SSS = |SSS_{insitu} - SSS_{retrieved}|$ and $\Delta WS = |WS_{insitu} - WS_{retrieved}|$.

	Mean (ΔSSS) (psu)	$\sigma_{\Delta SSS}$ (psu)	Mean (ΔWS) m s^{-1}	$\sigma_{\Delta WS}$ m s^{-1}
In situ wind measurements	0.52	0.12	–	–
QuikSCAT wind measurements	0.77	0.72	2.63	10.12
Wind speed from ARPEGE model	0.57	0.19	2.23	2.78
Wind unknown parameter	0.59	0.12	1.15	0.54

measured by the radar altimeter (RA) onboard ERS-2 (ESA) for the Casablanca area during the WISE campaigns was obtained. This instrument has an accuracy of 0.5 m or 10%, whichever is smaller, and a spatial resolution of $20 \times 20\,km^2$. The measurement is defined as four times the standard deviation of the wave slope (as one of the WISE buoys, wave rider B3) which is a different definition from the one used above (average of the highest third of the waves, WISE buoy B2). To convert from one definition to the other, the first definition must be divided by $\sqrt{2}$. Figure 11 shows the comparison between the wave height obtained by buoy B2, that obtained by B3 and that obtained by the RA satellite (the latter two with the necessary correction).

Table 4 compares the errors in the retrieved salinities using wind speed or SWH both measured from satellite. The results show that it is better to use the wave height measurement from the European Remote Sensing Satellite (ERS)-2 RA than to use the QuikSCAT data to retrieve the salinity, even though the differences

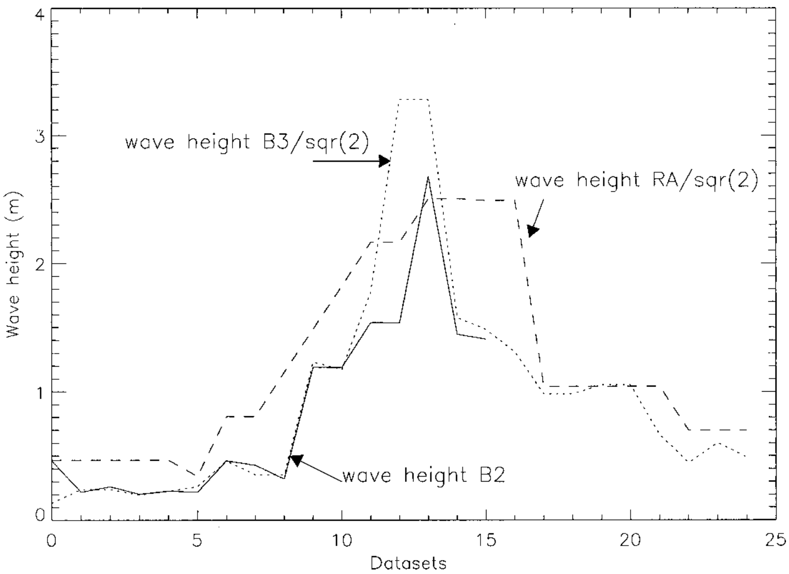

Figure 11. Comparison of wave height from two buoys and from the satellite.

Table 4. Error in the retrieved salinity using different dependence (dep.) and satellite data, considering $\Delta\mathrm{SSS} = |\mathrm{SSS}_{insitu} - \mathrm{SSS}_{\mathrm{retrieved}}|$.

	Mean (ΔSSS) (psu)	$\sigma_{\Delta\mathrm{SSS}}$ (psu)
Wind speed dep. QuikSCAT	0.69	0.17
Wave height dep. RA-ERS	0.60	0.27

are not significant. The problem of RA from ERS-2 is its low temporal resolution (35 days repetition), so to have data with the required time resolution we averaged all the measurements in a $170 \times 440\,\mathrm{km}^2$ area. This of course will introduce additional error due to the horizontal inhomogeneity of the wave field.

Figure 12 presents the errors in the retrieved salinity using SST measured by the *in situ* buoy plus a Gaussian noise with a standard deviation of 0.3 K (accuracy of the onflight satellites) (Au Li *et al.* 2001, Llewellyn-Jones *et al.* 2001). It can be observed that errors in SST do not produce high errors in the retrieved SSS: the maximum error is 0.1 psu. Then, SST measured by satellite is accurate enough for SSS retrieval.

5. Conclusions

The WISE campaigns provided new data to better understand the emissivity process of the sea at L-band. The results of this work confirm that it is feasible to retrieve salinity from these measurements with reasonably good accuracy. They show that the empirical emissivity models retrieve salinity with greater accuracy

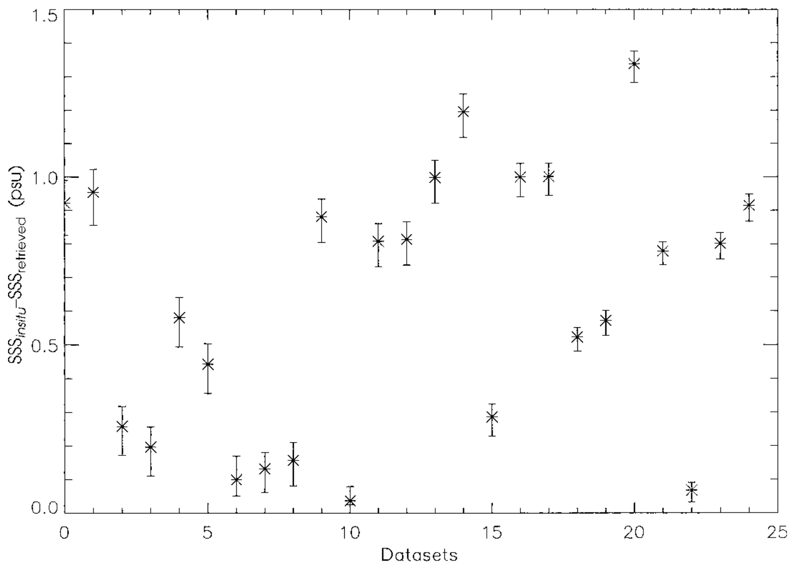

Figure 12. Uncertainty in the retrieved salinity errors due to adding random noise ($\sigma = 0.3°$ C) to SST.

than the theoretical models. They also show that errors on the wind speed measurement produce large errors on the salinity retrievals. The main conclusions of this study can be summarized as follows.

- As was expected, the retrieved salinity accuracy increases with the number of incidence angles used in T_B measurements.
- An inverse algorithm applied to the brightness temperature measured by the LAURA radiometer and by different emissivity models indicates that the most realistic model is the one with the wind dependence derived from WISE. This result, expected here, must be verified by applying this model to measurements in other sea conditions. It is also shown that the Yueh model (Two-Scale Method with Durden and Vesecky $\times 2$ wave spectrum) gives poor results. The SSA model with Elfouhaily spectrum seems to work quite well for high wind speed (high wave) conditions, but for low wind conditions the retrieved salinity errors are large.
- It is necessary to study the effect of the foam at L-band, because it may be important for wind speeds higher than $10\,\mathrm{m\,s^{-1}}$. In these conditions the data retrieved with the WISE-derived model were underestimated. This can be explained because the increase in the emissivity due to the foam was not taken into account and the inverse algorithm thus compensates for its effect.
- From the study of the errors in the retrieved salinity due to errors in the ancillary data, the main conclusion is that unacceptable errors appeared when the wind speed measured by the QuikSCAT scatterometer was used for salinity retrieval. It was also demonstrated that better accuracy is achieved using the ARPEGE data. To allow the inverse algorithm to find a value of wind speed as well as salinity is a potential solution when there are a large number of different views (incidence angles).
- Errors in the SST of the order of 0.3°C (accuracy of onflight satellites) produce a small impact on the retrieved salinity.
- The attempt to retrieve salinity using a wave height dependence model (instead of wind speed dependence) gives quite good results, although they are worse than using wind speed dependence when ancillary data are obtained from the buoys for WISE data. Nevertheless, it has been demonstrated that when one is using satellite data it is better to use data of wave height measured by a radar altimeter (RA–ERS) than to use wind speed data obtained by a scatterometer (QuikSCAT), since wave height has a lower variability than wind speed.

Further research should focus on studying the effect of the spatial and temporal lags between ancillary data and SMOS T_B measurements, using different data analysis and models. It should also study the possibility of considering wind speed obtained from meteorological models to retrieve the salinity for SMOS, and determine which model would be the most appropriate. We have also initiated the retrieval of salinity from L-band data acquired during the ESA sponsored EuroSTARRS airborne campaign (Gabarró *et al.* 2003).

Acknowledgments

This study was funded by ESA–ESTEC under WISE contract 14188/00/NL/DC and by the Spanish National Program on Space Research under grant ESP2001-4523-PE. The authors very much appreciate all the cooperation and help provided by the personnel of Repsol Investigaciones Petrolíferas in the Casablanca platform and the crew of the different boats that were used. The authors also thank the

LODYC team for providing them with the Yueh model output tables, and J. Miranda for providing the analytical models.

References

AU LI, X., PICHEL, W., CLEMENTE-COLON, P., KRASNOPOLSKY, V., and SAPPER, J., 2001, Validation of coastal sea and lake surface temperature measurements derived from NOAA/AVHRR data. *International Journal of Remote Sensing*, **22**, 1285–1303.

CAMPS, A., and REISING, S. C., 2001, Wind direction azimuthal signature in the Stokes emission vector from the ocean surface at microwave frequencies. *Microwave and Optical Technology Letters*, **29**, 426–432.

CAMPS, A., FONT, J., ETCHETO, J., CASELLES, V., WEILL, A., CORBELLA, I., VALL-LLOSSERA, M., DUFFO, N., TORRES, F., VILLARINO, R., ENRIQUE, L., JULIÀ, A., GABARRÓ, C., BOUTIN, J., RUBIO, E., REISING, S. C., WURSTEISEN, P., BERGER, M., and MARTÍN-NEIRA, M., 2002, Sea surface emissivity observations at L-band: first results of the Wind and Salinity Experiment WISE-2000. *IEEE Transactions on Geoscience and Remote Sensing*, **40**, 2117–2130.

CAMPS, A., FONT, J., VALL-LLOSSERA, M., GABARRÓ, C., VILLARINO, R., ENRIQUE, L., MIRANDA, J., CORBELLA, I., DUFFO, N., TORRES, F., BLANCH, S., ARENAS, J., JULIÀ, A., ETCHETO, J., CASELLES, V., WEILL, A., BOUTIN, J., CONTARDO, S., NICLÒS, R., RIVAS, R., REISING, S. C., WURSTEISEN, P., BERGER, M., and MARTÍN-NEIRA, M., 2003a, The WISE 2000 and 2001 campaigns in support of the SMOS mission: sea surface L-band brightness temperature observations and their application to multi-angular salinity retrieval. *IEEE Transactions on Geoscience and Remote Sensing*, in press.

CAMPS, A., VILLARINO, R., ENRIQUE, L., VALL-LLOSSERA, M., MIRANDA, J., and CORBELLA, I., 2003b, Sea surface emissivity at L-band: derived dependence with incidence and azimuth angles. *Proceedings of the WISE/LOSAC/EuroSTARRS Campaigns Workshop*, ESA SP-525 (Noordwijk: ESTEC).

DURDEN, S. L., and VESECKY, J. F., 1985, A physical radar cross-section model for a wind-driven sea with swell. *IEEE Journal of Oceanic Engineering*, **10**, 445–451.

ELFOUHAILY, T., CHAPRON, B., KATSAROS, K., and VANDERMARK, D., 1997, A unified directional spectrum for long and short wind-driven waves. *Journal of Geophysical Research*, **102**, 15 781–15 796.

ELLISON, W. J., BALANA, A., DELBOS, G., LAMKAOUCHI, K., EYMARD, L., GUILLOU, C., and PRIGENT, C., 1996, Study and measurement of the dielectric properties of the sea Water. European Space Agency contract No. 11197/94/NL/CL.

FONT, J., GABARRÓ, C., JULIÀ, A., EMELIANOV, M., LLORET, M., ETCHETO, J., CONTARDO, S., LOURENÇO, A., BOUTIN, J., and MOLL, M., 2003, Oceanographic conditions during WISE 2000 and 2001. *Proceedings of the WISE/LOSAC/EuroSTARRS Campaigns Workshop*, ESA SP-525 (Noordwijk: ESTEC), pp. 51–59.

GABARRÓ, C., CAMPS, A., FONT, J., and VALL-LLOSSERA, M., 2003, Retrieved sea surface salinity and wind speed from L-band measurements for WISE and EuroSTARRS campaigns. *Proceedings of the WISE/LOSAC/EuroSTARRS Campaigns Workshop*, ESA SP-525 (Noordwijk: ESTEC), pp. 163–171.

GASIEWSKI, A. J., and KUNKEE, D. B., 1994, Polarized microwave emission from water waves. *Radio Science*, **29**, 1449–1466.

GOODBERLET, M., and MILLER, J., 1997, NPOESS sea surface salinity. NOAA Contract No. 43AANE704017, Final Report.

HOLLINGER, J. P., 1971, Passive microwave measurements of sea surface roughness. *IEEE Transactions on Geoscience Electronics*, **9**, 165–169.

HOPKINS, T. S., 2001, Thermohaline feedback loops and natural capital. *Scientia Marina*, **65** (suppl. 2), 231–256.

JOHNSON, J. T., and ZHANG, M., 1999, Theoretical study of the small slope approximation for ocean polarimetric thermal emission. *IEEE Transactions on Geoscience and Remote Sensing*, **37**, 2305–2316.

KERR, Y., FONT, J., WALDTEUFEL, P., and BERGER, M., 2000, The second of ESA's Opportunity Missions: The Soil Moisture and Ocean Salinity Mission—SMOS. *Earth Observation Quarterly*, **66**, 18–26.

KLEIN, L., and SWIFT, C. T., 1977, An improved model for the dielectric constant of sea water at microwave frequencies. *IEEE Transactions on Antennas and Propagation*, **25**, 104–111.

LAGERLOEF, G., 2001, Oral communication at 3rd SMOS Workshop, Oberpfaffenhofen, Germany.

LAGERLOEF, G. S. E., 1998, Report of the First Workshop, Salinity Sea Ice Working Group, La Jolla, USA, 7–8 February.

LAGERLOEF, G. S. E., SWIFT, C. T., and LEVINE, D. M., 1995, Sea surface salinity: the next remote sensing challenge. *Oceanography*, **8**, 44–50.

LAURSEN, B., and SKOU, N., 2001, Wind direction over the ocean determined by an airborne, imaging, polarimetric radiometer system. *IEEE Transactions on Geoscience and Remote Sensing*, **39**, 1547–1555.

LERNER, R. M., and HOLLINGER, J. P., 1977, Analysis of 1.4 GHz radiometric measurements from Skylab. *Remote Sensing of Environment*, **6**, 251–269.

LLEWELLYN-JONES, D., EDWARDS, M. C., MUTLOW, C. T., BIRKS, A. R., BARTON, I. J., and TAIT, H., 2001, AATSR: global-change and surface-temperature measurements from Envisat. ESA Bulletin, European Space Agency.

MILLER, J. L., GOODBERLET, M. A., and ZAITZEFF, J. B., 1998, Airborne salinity mapper makes debut in coastal zone. *EOS Transactions of the American Geophysical Union*, **79**, 175–177.

PRESS, W., TEUKOLSKY, S., VETTERLING, W., and FLANNERY, B., 1992, *Numerical Recipes in C. The Art of Scientific Computing*, 2nd edn (New York: Cambridge University Press).

REUIL, N., and CHAPRON, B., 2001, Foam emissivity at L-band. ESA Salinity Requirement Study, WP1300 Report.

REYNOLDS, R., JI, M., and LEETMAA, A., 1998, Use of salinity to improve ocean modelling. *Physics and Chemistry of the Earth*, **23**, 545–555.

SKOU, N., 1955, An overview of requirements and passive microwave radiometer options. Consultative Meeting on Soil Moisture and Ocean Salinity measurement requirements and radiometer techniques (SMOS). Noordwijk, ESA, pp. 41–48.

SWIFT, C. T., 1993, ESTAR—The Electronically Scanned Thinned Array Radiometer for remote sensing measurement of soil moisture and ocean salinity. NASA Technical Memorandum 4523, 40 pp.

SWIFT, C. T., and MCINTOSH, R. E., 1983, Considerations for microwave remote sensing of ocean-surface salinity. *IEEE Transactions on Geoscience Electronics*, **21**, 480–491.

ULABY, F., MOORE, R., and FUNG, A., 1981, *Microwave Remote Sensing. Active and Passive*. vol. I, 1st edn (Reading, MA: Addison-Wesley).

VALL-LLOSSERA, M., CAMPS, A., and VILLARINO, R., 2003, Sea surface emissivity modeling at L-band: an intercomparison study. *Proceedings of the WISE/LOSAC/Euro-STARRS Campaigns Workshop*, ESA SP-525 (Noordwijk: ESTEC).

VORONOVICH, A. G., 1994, Small-slope approximation for electromagnetic wave scattering at rough interface of two dielectric half-spaces. *Waves in Random Media*, **4**, 337–367.

VORONOVICH, A. G., and ZAVOROTNY, V. U., 2001, Modelling of backscattering of radar signals from sea surface at Ka- and C-bands. Proceedings of the URSI General Assembly Maastricht, The Netherlands, (CD ROM).

WEBSTER, W. J., and WILHEIT, T. T., 1976, Spectral characteristics of the microwave emission from wind derived foam coverage sea. *Journal of Geophysical Research*, **81**, 3095–3099.

WILSON, W. J., YUEH, S. H., DINARDO, S. J., CHAZANOFF, S., LI, F. K., and RAHMAT-SAMII, Y., 2001, Passive Active L- and S-band (PALS) microwave sensor for ocean salinity and soil moisture measurements. *IEEE Transactions on Geoscience and Remote-Sensing*, **37**, pp. 1039–1048.

YUEH, S. H., WILSON, W. J., LI, F. K., NGHIEM, S. V., and RICKETTS, W. B., 1997, Polarimetric brightness temperatures of the sea surface measured with aircraft K- and Ka-band radiometers. *IEEE Transactions on Geoscience and Remote Sensing*, **35**, 1177–1187.

A.3 Geophysical Research Letters

This manuscript was submitted in October 2003 and published in January 2004.

GEOPHYSICAL RESEARCH LETTERS, VOL. 31, L01309, doi:10.1029/2003GL018964, 2004

A new empirical model of sea surface microwave emissivity for salinity remote sensing

C. Gabarró
Institut de Ciències del Mar, CMIMA-CSIC, Barcelona, Spain

J. Font
Institut de Ciències del Mar, CMIMA-CSIC, Barcelona, Spain

A. Camps
Departament de Teoria del Senyal i Comunicacions, UPC, Barcelona, Spain

M. Vall-llossera
Departament de Teoria del Senyal i Comunicacions, UPC, Barcelona, Spain

A. Julià
Institut de Ciències del Mar, CMIMA-CSIC, Barcelona, Spain

Received 31 October 2003; accepted 15 December 2003; published 14 January 2004.

[1] SMOS (Soil Moisture and Ocean Salinity) is a European Space Agency mission that aims at generating global ocean salinity maps with an accuracy of 0.1 psu, at spatial and temporal resolution suitable for climatic studies. The satellite sensor is an L-band (1400–1427 MHz) aperture synthesis interferometric radiometer. Sea surface salinity (SSS) can be retrieved since the brightness temperature of sea water is dependent on the frequency, angle of observation, dielectric constant of sea water, sea surface temperature and sea surface state. This paper presents a new empirical sea water emissivity model at L-band in which surface roughness effects are parameterized in terms of wind speed and significant wave height. For the SMOS mission these parameters can be obtained from external measurements and model diagnostics. An analysis has been done on the effect on SSS retrieval of different sources for this auxiliary information. *INDEX TERMS:* 4275 Oceanography: General: Remote sensing and electromagnetic processes (0689); 6969 Radio Science: Remote sensing; 0619 Electromagnetics: Electromagnetic theory; 6924 Radio Science: Interferometry. **Citation:** Gabarró, C., J. Font, A. Camps, M. Vall-llossera, and A. Julià (2004), A new empirical model of sea surface microwave emissivity for salinity remote sensing, *Geophys. Res. Lett.*, *31*, L01309, doi:10.1029/2003GL018964.

1. Introduction

[2] The distribution and variability of salinity in the world's oceans is a key parameter to understand the role of the oceans in the climate system. However, until now, remote sensing of the sea surface salinity (SSS) from space has not been attempted. Using the interferometric microwave radiometry concept (MIRAS instrument, Microwave Imaging Radiometer by Aperture Synthesis), SMOS will fill this gap and will provide global sea surface salinity maps for climate and large-scale ocean circulation studies [*Kerr et al.*, 2000]. The SSS maps are expected to have an accuracy of 0.1 psu at a spatial resolution of 100–200 km every 10–30 days.

[3] Salinity modifies the dielectric constant of sea water and it is one of the parameters that determine the sea surface emissivity [*Klein and Swift*, 1977]. At L-band (1400–1427 MHz), a restricted band for passive observations, the brightness temperature (T_B, measure of the sea surface emission) presents a maximum sensitivity to SSS. However, the sensitivity is quite low: 0.5 K/psu at sea surface temperature (SST) = 20°C, and decreases to 0.25 K/psu at SST = 0°C [*Lagerloef et al.*, 1995]. On the other hand, T_B at this frequency is also sensible to sea surface roughness, 0–0.4 K/(*m*/*s*), (when roughness is parameterised in terms of wind speed) depending on the incidence angle [*Hollinger*, 1971; *Webster and Wilheit*, 1976; *Lerner and Hollinger*, 1977], and to SST, 0.2–0.4 K/°C. This situation indicates that it is necessary to have an accurate knowledge of the surface roughness and SST to retrieve salinity with enough accuracy.

[4] To increase the present understanding of the L-band T_B sensitivity to wind speed and direction, the European Space Agency (ESA) sponsored the WInd and Salinity Experiments (WISE). These experiments aimed, among other activities, at improving and validating the actual sea surface emissivity models at L-band.

2. Campaigns Description

[5] WISE 2000 and 2001 [*Camps et al.*, 2004] took place at the Casablanca oil rig platform in the Mediterranean Catalan coast, at 40°43.02′N 1°21.50′E, 40 Km offshore. They were performed during one month in autumn, when maximum wind speed is expected in the region. An L-band full-polarimetric radiometer measured T_B from 33 m above sea level at different incidence and azimuth angles, while several oceanographic and meteorological buoys measured SSS, SST, wind speed and direction, significant wave height (SWH) and period, and wave spectrum.

[6] Radiometer measurements were performed at different elevation angles from 25° to 65° to emulate the

0094-8276/04/2003GL018964$05.00

Table 1. Number of Data Points for Each Incidence Angle and Polarization in WISE 2001

θ_i	25°	30°	35°	40°	45°	50°	55°	60°	65°
H-pol	143	36	232	35	478	33	348	36	125
V-pol	305	34	532	56	656	57	511	49	190

performance of SMOS, since the two-dimensional imaging capability of MIRAS will allow the observation of pixels in a wide range of incidence angles. This is a unique characteristic of this data set to study SSS retrievals and to test several theoretical electromagnetic L-band emissivity models. Table 1 shows the amount of data acquired during the campaign for each elevation angle. The radiometric sensitivity is 0.2 K for 1 s integration time and the absolute calibration accuracy is lower than 0.5 K.

[7] EuroSTARRS was an airborne campaign also organized by ESA in November 2001 as part of the SMOS preparatory studies [*Berger et al.*, 2002]. An L-band V-polarized multi-angular radiometer [*Miller and Goodberlet*, 2003] of different technology was flown over the same oil platform area in coincidence with WISE 2001.

3. Models

[8] The brightness temperature of the sea surface can be modeled by equation 1, composed of a term due to the emissivity of a flat surface plus the term that accounts for the effect of the sea roughness,

$$T_{B,p}(\theta, SST, SSS, U_{10}) = e_p(\theta, SST, SSS) \cdot SST + \Delta T_{B\ rough,p}(\theta, U_{10}) \quad (1)$$

where $e_p = 1 - \Gamma_p$ is the emissivity of the flat sea surface for each polarization (horizontal and vertical), Γ_p is the Fresnel power reflection coefficient and θ is the elevation angle. In this formulation, the information on sea surface roughness is parameterized through the wind speed measured at 10 m above sea level (U_{10}).

[9] *Camps et al.* [2004] have proposed an empirical model of $T_{B\ rough}$ derived from WISE data, by fitting the sensitivity of T_B to wind speed at different incidence angles, and the two polarizations.

[10] *Gabarró et al.* [2003] retrieved surface salinity from WISE measurements using in the computation different theoretical sea surface emissivity models and the above-mentioned empirical model, all depending on wind speed. Two models for electromagnetic surface scattering (Two-scale, and Small Slope Approximation) and two theoretical wave spectrum models [*Durden and Vesecky*, 1985; *Elfouhaily et al.*, 1997] were tested. The retrieval of SSS appeared to be more efficient when using the empirical model derived from WISE measurements than any other combination of theoretical models.

[11] All these models consider the surface wave spectrum only dependent on the local wind speed, and consequently fully developed sea conditions. So, they do not include either the possible situation of growing and decaying winds or the swell effect. *Miranda et al.* [2003] demonstrated that the measured spectra frequently are not well approximated using fully developed models.

[12] New formulations for the modelisation of the sea surface are being developed now based on the Local Curvature Approximation concept [*Elfouhaily et al.*, 2003]. The effects of sea roughness on L-band emissivity occur in the range of decimetric wavelengths, but the present situation indicates that we will probably have to rely only on the regularly available diagnosed parameters at global scale: wind speed and direction, if necessary, and SWH.

[13] From these considerations, a new empirical model of $\Delta T_{B\ rough,p}$ derived from WISE 2001 measurements is presented here (Equation 2). It explains the variability of T_B depending on local wind speed (U_{10}), and also on SWH, by fitting simultaneously the T_B data to both variables recorded in situ.

$$\begin{aligned} \Delta T_h &\approx 0.12 \cdot \left(1 + \frac{\theta}{24^\circ}\right) \cdot U_{10} + 0.59 \cdot \left(1 - \frac{\theta}{50^\circ}\right) \cdot SWH \\ \Delta T_v &\approx 0.12 \cdot \left(1 - \frac{\theta}{40^\circ}\right) \cdot U_{10} + 0.59 \cdot \left(1 - \frac{\theta}{50^\circ}\right) \cdot SWH \end{aligned} \quad (2)$$

Then, this model considers the effects on surface roughness of both the local wind and other processes that can contribute to SWH formation.

4. Sea Surface Salinity Retrieval

4.1. WISE Field Experiment

[14] Inverting this new forward model, SSS has been retrieved again from WISE T_B data. The algorithm used is a recurrent Levenberg-Marquardt least-square fit [*Press et al.*, 1992], applied to ensembles of data recorded in a series of multi-angular radiometric observations performed under constant sea and wind conditions. T_B is computed setting an initial guess for SSS into the direct emissivity model (Equations 1 and 2). The Klein and Swift model (*Klein and Swift* [1977]) has been applied in order to calculate the dielectric constant from SSS and SST, and then e_p. This T_B value is compared with the T_B measured by the radiometer, and then an increment δSSS is added to the previous SSS to initiate a new computation. This recursive system stops when the difference between the measured and the computed T_B is smaller than a threshold. The retrieved salinity is mostly insensitive to the initial guess for SSS.

[15] An assessment of the retrieval error is obtained by the difference between the retrieved SSS and the one measured in situ by a SeaBird 37 instrument (effective accuracy 0.02 psu) during the series of T_B observations. The average error when using the new model dependent on wind speed and wave height (ΔSSS = 0.33 psu and $\sigma_{\Delta SSS}$ = 0.05) is considerably smaller than using the empirical model that considers only local wind speed (ΔSSS = 0.52 psu and $\sigma_{\Delta SSS}$ = 0.12) [*Gabarró et al.*, 2003]. The standard deviation has also been reduced. A reduction in error budget is expected in any regression when the degree of freedom is increased. But in this case it has a physical meaning since SWH data contain information from processes that modify the sea surface spectrum other than contemporaneous local wind. The substantial reduction on the SSS error (about 35%) confirms that swell and varying winds have an important role in the final balance of emissivity of the sea.

4.2. EuroSTARRS Field Experiment

[16] This model has also been tested to retrieve salinity from the EuroSTARRS data set. Although the data resulted

Table 2. Comparison of Different Sources for Wind Speed and Significant Wave Height

SOURCE	Spatial resolution	Temporal resolution
HIRLAM	0.12°	3 hours
ARPÈGE	0.25°	6 hours
QuikSCAT	25 Km	3 days
WAM	0.12°	3 hours
RA-ERS	15 Km	35 days

to be very noisy and some beams were affected by calibration problems, a series of 800 data points along a straight line over relatively homogeneous fields were averaged to retrieve salinity. The results confirm that this new model retrieves salinity much better (ΔSSS = 0.13 psu) than the model only dependent on U_{10} (ΔSSS = 0.24 psu). These EuroSTARRS errors are highly improved with respect to WISE results due to the much larger number of radiometer snapshot measurements averaged before retrieval, and hence reducing the experimental noise. Nevertheless, the model should be tested with other data sets measured in different locations and sea conditions to validate this conclusion.

5. Sea Surface Salinity Using Auxiliary Data

[17] To retrieve salinity from SMOS, auxiliary variables (wind speed, wave height and SST) are needed with good quality, and as simultaneous in time and space as possible to the spaceborne radiometer measurements. One possibility is to use observations made by other sensors (scatterometers, altimeters, SAR) embarked on satellites with similar orbit, but these measurements will hardly be simultaneous. On the other hand meteorological and oceanographic marine models could also be used, with the advantage of having much higher temporal resolution, and having assimilated satellite and other sources of information. Both cases will present inaccuracies on the measurements due to instrumental errors and sampling limitations.

[18] The determination of sea roughness non-coincidental to SMOS overpasses is a major problem due to its high variability and accuracy limitations in satellite measurements and models. Sea surface temperature, nevertheless, is not as critical as roughness, since its variability is much lower, the sensitivity of T_B to SST is also lower, and satellite measurements are very accurate (0.3 K) and frequent. We have analyzed here the effect on SSS retrieval of using different sources for roughness information.

[19] The following numerical model outputs and satellite measurements of wind speed and SWH were obtained for the area and time of the WISE 2001 campaign,

[20] 1. Wind speed information:

[21] (i) HIRLAM: numerical model with assimilation of satellite data (Spanish Instituto Nacional de Meteorología)

[22] (ii) ARPÈGE: numerical model with assimilation (Météo-France)

[23] (iii) QuikSCAT: radar scatterometer on board SEAWINDS NASA polar orbit satellite

[24] 2. Significant wave height information:

[25] (i) WAM: numerical model with assimilation of satellite data, only for atmospheric parameters

[26] (ii) RA-ERS: radar altimeter on board ESA ERS-2 satellite

[27] Table 2 summarizes the spatial and temporal resolutions of each data source. Figures 1 and 2 show the temporal sequence of wind speed and wave height obtained from these sources. For wind speed, the models and satellite outputs are quite similar to in situ measurements except for some punctual occasions. The mean difference between wind speed in situ measurements and HIRLAM model output is 1.98 m/s, with respect to ARPÈGE model output is 1.93 m/s, while to satellite data is 1.59 m/s (although in this last case there are much less data points available). These differences are above the 1.5 m/s accuracy in wind speed initially required for SMOS SSS retrieval from preliminary simulations.

[28] The SWH given by the model is similar to the buoy measurement, except for high wave height events, where the model overestimates it. The satellite measurements are not very realistic, which is not surprising since their temporal resolution is very low and a lot of spatial averaging has to be done to cover the WISE area. The mean difference between in situ measurements and WAM model is 0.22 m,

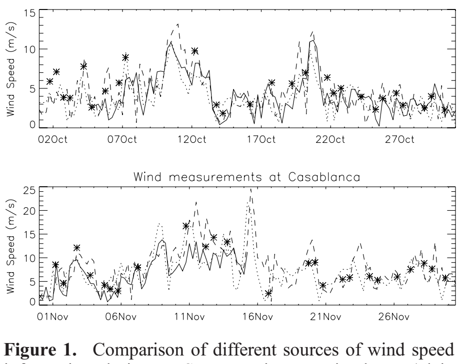

Figure 1. Comparison of different sources of wind speed information during WISE campaign. In situ buoy (plain line), HIRLAM model (dashed line), ARPÈGE model (dotted line) and QuikSCAT satellite (*).

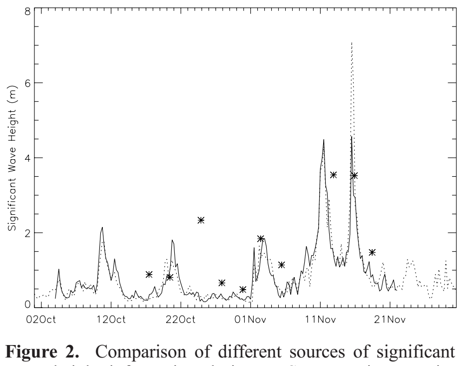

Figure 2. Comparison of different sources of significant wave height information during WISE campaign. In situ buoy (plain line), WAM model (dotted line) and Radar Altimeter-ERS (*).

while the mean difference grows to 1.16 m with respect to satellite measurements.

[29] The retrieval of SSS in the WISE case has been tested using different combinations of these sources of wind speed and wave height information. For SST in situ measurements have always been used.

[30] An alternative way to retrieve salinity, in case of missing or bad quality auxiliary data, is to consider the two variables as unknown parameters in the forward model, and then allow the inversion algorithm to converge simultaneously to a value for salinity, and also for U_{10} and SWH. In this case the cost function to minimize would have three parameters instead of only one. This option has also been tested for WISE and the selected first guess values for U_{10} and SWH have been the HIRLAM and WAM model outputs.

[31] Table 3 summarizes the error on the SSS retrieved for different sources of auxiliary data with the model presented in equation 2. It shows that better results are obtained when leaving the auxiliary data free as variables to optimize, than fixing them with excessively erroneous values. Furthermore, the error on the wind speed and wave height retrieved with the optimization process ($\Delta U_{10} = |U_{10\ in\ situ} - U_{10\ retrieved}|$) is smaller than the error of the model outputs and satellite measurements. Figure 3 plots the results of retrieved U_{10} respect to in situ measurements and HIRLAM output model for several data sets. It shows that the retrieved U_{10} is nearer to in situ measurements than HIRLAM output, even though the first guess parameter was that model. So it seems that by leaving U_{10} as free parameter for retrieval, the algorithm can improve its initial values.

[32] Table 3 shows also that the use of meteorological model data (with assimilation of space-borne observations) is better than to use satellite data directly, since the latter have much worse temporal resolution.

6. Conclusion

[33] This paper describes a new empirical model of L-band sea surface emissivity dependent on wind speed and significant wave height derived from radiometric and in situ data gathered in the NW Mediterranean. Salinity is retrieved with smaller errors when using this model than other models dependent on wind speed and then considering only the presence of fully-developed wind waves.

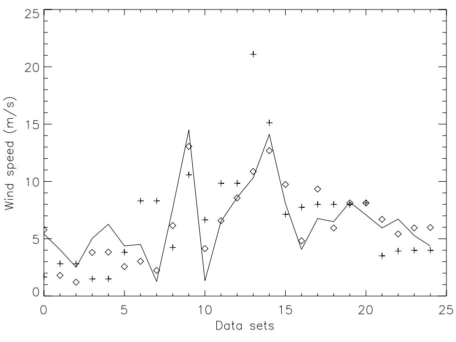

Figure 3. Comparison of wind speed measurement U_{10} determinations: measured in situ (diamonds), output from HIRLAM analysis (crosses), and retrieved by the algorithm when it is set to be free (line). It can be seen that retrieved wind speed is nearer to in situ measurements than model output.

Table 3. Errors on the Retrieved Salinity $\Delta SSS = |SSS_{in\ situ} - SSS_{retrieved}|$, Error on Wind Speed ΔU_{10} and on Wave Height ΔSWH for Different Ancillary Data

Source U_{10}	Source SWH	ΔSSS	ΔU_{10}	ΔSWH
In situ	in situ	0.33	–	–
HIRLAM	WAM	0.59	1.98	0.22
ARPÈGE	WAM	0.49	1.94	0.22
QuikSCAT	ERS	0.61	1.59	0.46
Free	free	0.40	1.22	0.22

[34] Since T_B is sensitive to surface roughness, it is necessary to have accurate auxiliary data to obtain accurate estimates of SSS. In this paper different sources for acquiring auxiliary data during the SMOS mission have been presented. The error with respect to in situ measurements and the influence of this error on the accuracy of the SSS retrieval have been analyzed.

[35] An important conclusion is that using data from meteorological models to retrieve salinity is better than using direct satellite data, since the former have smaller temporal resolution. From the analysis of WISE dataset, it appears that in absence of accurate in situ observations, the best method to retrieve salinity is to leave U_{10} and SWH as free parameters, and let the retrieval algorithm to take advantage of the multi-angular view capability of SMOS imaging configuration.

[36] These conclusions are only applicable to the WISE field site, in the north Mediterranean, and can not be automatically extrapolated to other ocean areas. This empirical model may need to be adapted to different oceanographic characteristics. The accuracy and resolution of meteorological models can also vary in other regions, as well as the accuracy of satellite data. This work is a regional study, but could be a first step for a global scheme applicable to SMOS observations.

[37] **Acknowledgments.** This study was funded by ESA-ESTEC under WISE (14188/00/NL/DC) and EuroSTARRS (15950/02/NL/SF) contracts, and by the Spanish National Program on Space Research under grant ESP2001-4523-PE.

References

Berger, M., A. Camps, J. Font, Y. Kerr, J. Miller, J. Johannessen, J. Boutin, M. Drinkwater, N. Skou, N. Floury, M. Rast, and H. Rebhan (2002), Measuring Ocean Salinity with ESA's SMOS mission — Advancing the Science, *ESA Bulletin — European Space Agency, 111*, 113–121.

Camps, A., J. Font, M. Vall-llossera, C. Gabarró, R. Villarino, L. Enrique, J. Miranda, I. Corbella, N. Duffo, F. Torres, S. Blanch, J. Arenas, A. Julià, J. Etcheto, V. Caselles, A. Weill, J. Boutin, S. Contardo, R. Niclòs, R. Rivas, S. Reising, P. Wursteisen, M. Berger, and M. Martín-Neira (2004), The WISE 2000 and 2001 Campaigns in Support of the SMOS Mission: Sea Surface L-band Brightness Temperature Observations and their Application to Multi-Angular Salinity Retrieval, *IEEE Trans. Geosci. Remote Sens*, in press.

Durden, S., and J. Vesecky (1985), A Physical Radar Cross-Section Model for a Wind-Driven Sea with Swell, *IEEE J. Oceanic Eng.*, OE-*10*, 445–451.

Elfouhaily, T., B. Chapron, K. Katsaros, and D. Vandermark (1997), A Unified Directional Spectrum for Long and Short Wind-driven Waves, *J. Geophys. Res.*, *102*(C7), 15,781–15,796.

Elfouhaily, T., S. Guignard, R. Awadallah, and D. Thompson (2003), Local and Non-local Curvature Approximation: A New Asymptotic Theory for Wave Scattering, *Waves Random Media*, *13*(4), October.

Gabarró, C., M. Vall-llossera, J. Font, and A. Camps (2003), Determination of Sea Surface Salinity and Wind Speed by L-band Microwave Radiometry from a fixed Platform, *Internat. J. Remote Sens.*, *25*(1), 111–128.
Hollinger, J. (1971), Passive Microwave Measurements of Sea Surface Roughness, *IEEE Trans. Geosci. Electron.*, GE-*9*(3), 165–169.
Kerr, Y., J. Font, P. Waldteufel, and M. Berger (2000), The Second of ESA's Opportunity Missions: The Soil Moisture and Ocean Salinity Mission-SMOS, *Earth Observation Quarterly*, *66*, 18–26.
Klein, L., and C. Swift (1977), An Improved Model for the Dielectric Constant of Sea Water at Microwave Frequencies, *IEEE Trans. Antennas Propag.*, *AP-25*(1), 104–111.
Lagerloef, G., C. Swift, and D. M. Levine (1995), Sea Surface Salinity: The Next Remote Sensing Challenge, *Oceanogr.*, *8*(2), 44–50.
Lerner, R., and J. Hollinger (1977), Analysis of 1.4 GHz Radiometric Measurements from Skylab, *Remote Sensing Environment*, *6*, 251–269.
Miller, J., and M. Goodberlet (2003), Development and Application of STARRS — a Next Generation Airborne Salinity Imager, *Internat. J. Remote Sens.*
Miranda, J., M. Vall-llossera, R. Villarino, and A. Camps (2003), Sea State and Rain Effects in the Sea Surface Emissivity at L-Band, *Proceedings of the WISE/LOSAC/EuroSTARRS campaigns Workshop. ESA*, SP-*525*, 155–162.
Press, W., S. Teukolsky, W. Vetterling, and B. Flannery (1992), *Numerical Recipes in C. The Art of Scientific computing*, 2nd edition, Cambridge Univ. Press.
Webster, W., and T. Wilheit (1976), Spectral Characteristics of the Microwave Emission from wind Derived foam Coverage Sea, *J. Geophys. Res.*, *81*, 3095–3099.

C. Gabarró, J. Font, and A. Julià, Institut de Ciències del Mar, CMIMA-CSIC, Passeig Marítim de la Barceloneta 39–47, Barcelona 08003, Spain. (cgabarro@icm.csic.es)
A. Camps and M. Vall-llossera, Departament de Teoria del Senyal i Comunicacions, UPC, Campus Nord, D4 08034 Barcelona, Spain.

Appendix B

Instrumentation technical documentation

This appendix summarise the performance characteristics for several instruments used during WISE 2000 and WISE 2001 campaigns. A diagram of data acquisition and transmission in buoy 1 has also been included. Finally, the specifications of the microprocessor that was used and programed are attached.

SeaBird MicroCAT system (model SBE37-SM)

The SeaBird SBE37-SM is a conductivity and temperature recorder, with internal power supply and memory for data recording. It has a RS232C serial interface and it can be programmed to give sampling rates between 10 seconds and 9.1 hours. The system uses a 24-bit A/D converter to digitise the temperature sensor voltage.

The RMS deviation on the salinity calculation from conductivity and temperature is 0.002 psu. The memory capacity, expressed as number of samples, of the SBE 37-SM MicroCAT, is 410.000 samples (C and T only). For C, T and time, the capacity is 225.000 samples. The battery power pack is made of six 9 V lithium batteries, having a total of 6 Ah charge.

Salinometer Guildline Autosal

	Temperature	Conductivity
Measurement range	-5 to 35°C	0 to 7 S/m
Initial accuracy	0.002°C	0.0003 S/m
Typical stability (per month)	0.0002 °C	0.0003 S/m
Resolution	0.0001 °C	0.0001 S/m

Table B.1: Temperature and conductivity characteristics of SeaBird Microcat instrument

The salinometer that was used is the Model 8400B. This instrument measures the conductivity and the temperature of a sample comparing from a reference water. This reference water, called "Copenhagen water", has a salinity of 35.0000 psu. The technical characteristics of the instrument are the following:

	salinity
Accuracy	0.002 psu
Resolution	0.0002 psu
Stability on temperature	0.001 °C/day

Table B.2: Salinity characteristics of Salinometer Guildline Autosal

USONIC anemometer

The Usonic is a competent ultrasonic anemometer for universal usage. It is constructed for high precision, inertia free measurements of wind speed, directions and temperature.

It has the big advantage of no wear of mechanical parts. The whole system with all electronic parts is completely integrated in a robust stainless steel housing.

The data output is pre configurable by remote PC. It can transmit digital (RS-232/RS485) or analogue data from the interface.

Coastal Monitoring Buoy (CMB3280) from Aanderaa Instruments

	Wind speed	Wind direction	Temperature
Meas. range	0 to 60 m/s	0°-360°	-30° C .. 60°
Meas. accuracy	0.1 m/s (below 5 m/s) or	$< \pm 3°$	$< \pm 1°$ C
	$<$ 1.5% (above 5 m/s)		
Resolution	0.05 m/s	1°	0.1° C

Table B.3: Performance characteristics of the Doppler ultrasonic anemometer model 5010-0005 from USONIC.

Parameter	Accuracy	Resolution
Wind speed	2%	0.075 m/s
Wind direction	5° mag.	0.4 °
Air temperature	0.1 °C	0.05 °C
Solar radiation	20 W/m2	0.4 W/m2
Relative humidity	2%	0.1 %
Wave height	0.2 m, 10%	0.01 m
Wave period	10%	0.03 s

Table B.4: Performance characteristics of the standard Coastal Monitoring Buoy (CMB3280) from Aanderaa Instruments.

The method of measurement for this instrument is the average over the past measured interval. The wind speed measurements have been done with a three-cup rotor. Significant wave height is measured as the mean of the highest third of all the waves during the sampling interval.

AANDERAA RCM9 current meter

The instrument is a Doppler sensor, and the acoustic frequency is 2MHz .

	Current speed	Current direction	Water temp.
Meas. range	0 to 500 cm/s	0°-360°	-8 to 41° C
Meas. accuracy	0.2 cm/s or ±2% of actual speed	±5° to 0-15° tilt of the buoy and ±7.5° for 15 - 35° tilt of the buoy	±0.1°C

Table B.5: Performance characteristics of the AANDERAA RCM9 current meter

Meteorological Station on the platform

This meteorological station was manufactured by MCV,S.A. This station was located in a tower, 69 m above sea level. Just before starting the WISE experiments the wind instruments were calibrated.

	Wind speed	Wind direction
Meas. range	0 to 56 m/s	0°-360°
Meas. accuracy	< ±1 m/s (<10 m/s) or < ±10% elsewhere	< ±10°
Resolution	0.2 m/s	1°

Table B.6: Performance characteristics of the meteorological station manufactured by MCV.

Microprocessor FM-200 Embedded controller

This microprocessor if manufactured at the Cambridge MICROPROCESSOR system limited company.

Features of the microprocessor are:

- 68000 Compatible CPU
- 512 k-bytes of on board programmable Flash EEPROM
- 512 k-bytes of battery backed Static RAM

- Three independent serial ports
- I2C high speed serial
- Real Time Calendar Clock
- Two timer/counters
- Software Watchdog
- 5 Volt only operation
- Ten TTL/CMOS digital I/O channels
- Small Size 90 x 100 mm

The code of the micro was programed in 'C' language. More information on this microprocessor can be found in http://www.cms.uk.com/.

Figure B.1 shows a diagram of the data acquisitions, the storage and the transmission all controlled by the microprocessor located in buoy 1.

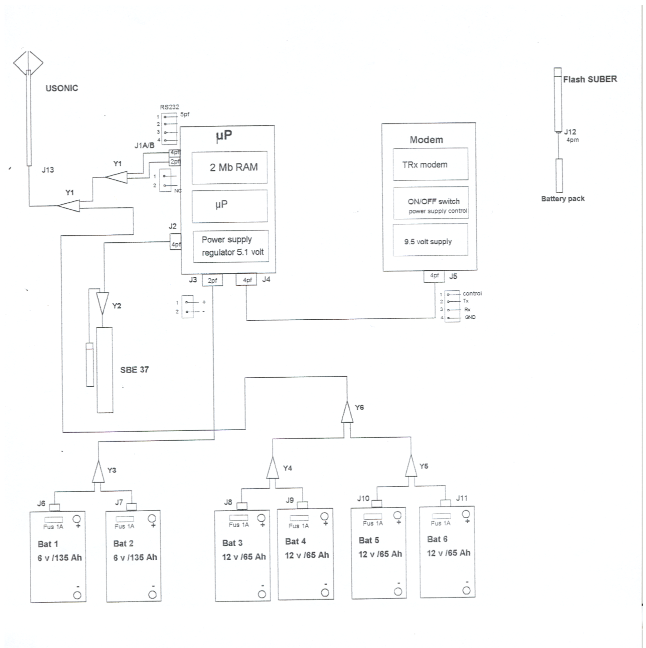

Figure B.1: Diagram of data acquisition and transmission.

Bibliography

Blanch, S. and Aguasca, A. (2004). Seawater dielectric permittivity model from measurements at l-band. *Proceedings of IGARSS 2004, Alaska.*

Blume, H., Kendall, B., and Fedors, J. (1978). Measurements of Ocean Temperature and Salinity vis Microwave Radiometry. *Boundary-Layer Meteorology*, 13:295–308.

Blume, H., Love, A., Van Melle, M., and Ho, W. (1977). Radiometric observations of sea temperature at 2.65 GHz over the Chesapeake Bay. *IEEE Transactions on Antennas and Propagation*, AP-25:121–128.

Camps, A. (1996). *Application of Interferometric Radiometry to Earth Observation. Ph.D.* PhD thesis, Universitat Politècnia de Catalunya.

Camps, A., Corbella, I., Vall-llossera, M.and Duffo, N., Marcos, F., Martínez-Fadrique, and Greiner, M. (2003a). The SMOS End-to-end Performance Simulator: Description and Scientific Applications. *Proceedings International Geoscience and Remote Sensing Symposium, Toulouse, France.*

Camps, A., Corbella, I., Vall-llossera, M.and Duffo, N., Torres, F., Villarino, R., Enrique, L., Miranda, J., Julbe, J., Font, J., Julià, A., Gabarró, C., Etcheto, J., Boutin, J., Weill, A., Caselles, V., Rubio, E., Wursteisen, P., Berger, M., and Martín-Neira, M. (2003b). L-band Sea Surface emissivity: Premilinary results of the WISE-2000 campaign and its application to salinity restrieval in the SMOS mission. *Radio Science*, 93(4):8071,doi:10.1029/2002RS002629.

Camps, A., Duffo, N.and Vall-llossera, M., and Vallespin, B. (2002a). Sea Surface Salinity Retrieval using multi-angular L-band Radiometry: Numerical Study Using the SMOS End-to-end Performance Simulator. *Proceedings IGARSS, Toronto, Canada.*

Camps, A. et al. (2001). Wind and Salinity Experiment 2000 (WISE 2000): Scientific Analysis Report. Technical report, ESTEC, ESA. Contract No. 14188/00/NL/DC.

Camps, A., Font, J., Vall-llossera, M., Gabarró, C., Villarino, R., Enrique, L., Miranda, J., Corbella, I., Duffo, N., Torres, F., Blanch, S., Arenas, J., Julià, A., Etcheto, J., Caselles, V., Weill, A., Boutin, J., Contardo, S., Niclòs, R., Rivas, R., Reising, S., Wursteisen, P., Berger, M., and Martín-Neira, M. (2004a). The WISE 2000 and 2001 Campaigns in Support of the SMOS Mission: Sea Surface L-band Brightness Temperature Observations and their Application to Multi-Angular Salinity Retrieval. *IEEE Transactions on Geoscience and Remote Sensing*, 42(4):804–823.

Camps, A., Font, J.and Etcheto, J., Caselles, V., Weill, A., Corbella, I., Vall-llossera, M., Duffo, N., Torres, F., Villarino, R., Enrique, L., Julià, A., Gabarró, C., Boutin, J., Rubio, E., Reising, S., Wursteisen, P., Berger, M., and Martín-Neira, M. (2002b). Sea Surface Emissivity Observations at L-band: First Results of the Wind and Salinity Experiment WISE-2000. *IEEE Transactions on Geoscience and Remote Sensing*, 40(10):2117–2130.

Camps, A., Vall-llossera, M., Bartes, F., Torres, F., Duffo, N., and Corbella, I. (2004b). External Calibration In L-Band 2D Synthetic Aperture Radiometers: Application To Sea Surface Salinity Retrieval. *Proceedings International Geoscience and Remote Sensing Symposium (IGARSS) , Anchorage, Alaska (EEUU)*, pages 0–7803–8743–0/04.

Camps, A., Vall-llossera, M., Bartes, F., Torres, F., Duffo, N., and Corbella, I. (2004c). Retrieving Sea Surface Salinity with Multi-Angular L-band Brightness Temperature Improvements by Spatio-Temporal Averaging. *IEEE Transactions on Geoscience and Remote Sensing, in press.*

Corbella, I., Camps, A., Zapata, M., Marcos, F., Martínez, F., and Vall-llossera (2003). End-to-end simulator of 2D interferometric radiometry. *Radio Science*, 38(8058):doi:10.1029/2002RS002665.

Debye, P. (1929). *Polar Molecules.* New York: Reinhold.

Dinnat, E. (2003). *De la Détermination de la Salinité de la Surface des Océans à Partir de Mesures Radiométriques Hyperfréquences en bande L.* PhD thesis, Laboratoire d'Océanographie DYnamique et de Climatologie. France.

Drange, H., Johannessen, J., NERSC, CLS, LODYC, IFREMER, LEGI, SOC, UCL, UPC, DLR, and CSIC (2001). Scientific requirements and impact of space observations of ocean salinity for modelling and climate studies. Technical report, NOAA, USA. Agencia Espacial Europea (ESTEC Contract No. 14273/00/NL/DC).

Durden, S. and Vesecky, J. (1985). A Physical Radar Cross-Section Model for a Wind-Driven Sea with Swell. *IEEE Journal of Oceanic Engineering*, OE-10:445–451.

Elfouhaily, T., Chapron, B., Katsaros, K., and Vandermark, D. (1997). A Unified Directional Spectrum for Long and Short Wind-driven Waves. *Journal of Geophysical Research*, 102:15781–15796.

Ellison, W., Balana, A., Delbos, G., Lamkaouchi, K., Eymard, L., Guillou, C., and Prigent, C. (1998). New Permittivity Measurements of Sea Water. *Radio Science*, 33(3):639–648.

Emelianov, M., Font, J., J., A., Gabarró, C., LLoret, M., and Solé, J. (2003). Sea Surface Fiels at Casablanca Site (NW Mediterranean) during the EuroSTARRS Campaign. *Proceedings of the WISE/LOSAC/EuroSTARRS Campaigns Workshop. ESA PUBLICATIONS*, SP-525:73–80.

Emery, W. J. and Thomson, R. E. (1997). *Data analysis methods in physical oceanography*. Great Britain: Pergamon.

Etcheto, J., Dinnat, E., Boutin, J., Camps, A., Miller, J., Contardo, S., Wesson, J., Font, J., and Long, D. (2004). Wind speed effect on L-band brightness temperature inferred from EuroSTARRS and WISE 2001 field experiments. *IEEE Transactions on Geoscience and Remote Sensing (in press)*.

Flattau, T., Becker, S., and Leber, A. (1976). Passive l-band radiometer for remote sensing of earth resources. *Microwave Symposium Digest, MTT-S International*, 76(1):328–330.

Font, J., Gabarró, C., Julià, A., Emelianov, M., Lloret, M., Etcheto, J., Contardo, S., Lourenço, A., Boutin, J., and Moll, M. (2003a). Oceanographic Conditions during WISE 2000 and 2001. *Proceedings of the WISE/LOSAC/EuroSTARRS Campaigns Workshop. ESA PUBLICATIONS*, SP-525:51–60.

Font, J., Kerr, Y., and Berger, M. (2000). Measuring Ocean Salinity from Space: the European Space Agency's SMOS Mission. *Backscatter*, 11(3):17–19.

Font, J., Lagerloef, G., Kerr, Y., Skou, N., and Berger, M. (2003b). Sea surface salinity mapping with SMOS space mission. *Building the European capacity in operational oceanography. Proceedings of the 3rd EuroGOOS Conference: H.*

Dahlin, N.C. Flemming, K. Nittis, S.E. Petterson Eds., Elsevier Oceanography Series, 69:186–189.

Font, J., Lagerloef, G., LeVine, D., Camps, A., and Zanife, O. (2004). The Determination of Surface Salinity with the European SMOS Space Mission . *IEEE Transactions on Geoscience and Remote Sensing (in press).*

Gabarró, C., Camps, A., Font, J., and Vall-llossera, M. (2003). Retrieved Sea Surface Salinity and Wind Speed from L-band Measurements for WISE and EuroSTARRS Campaigns. *Proceedings of the WISE/LOSAC/EuroSTARRS Campaigns Workshop. ESA PUBLICATIONS*, SP-525:163–172.

Gabarró, C., Font, J., Camps, A., Vall-llossera, M., and Julià, A. (2004a). A New Emprical Model of Sea Surface Microwave Emissivity for Salinity Remote Sensing. *Geophysical Research Letters*, 31(L01309):1–5.

Gabarró, C., Vall-llossera, M., Font, J., and Camps, A. (2004b). Determination of Sea Surface Salinity and Wind Speed by L-band Microwave Radiometry from a fixed Platform. *Internation Journal of Remote Sensing*, 25(1):111–128.

Goodberlet, M. and Miller, J. (1997). NPOESS Sea surface Salinity. Technical report, NOAA, USA. contract 43AANE704017.FINAL REPORT.

Guerrero, R. and Piola, A. (1977). Masas de agua en la plataforma continental. *El mar Argentino y sus recursos pesqueros*, 1:107–118.

Hertz, J. A., Krogh, A., and Palmer, R. G. (1991). *Introduction to the theory of neural computation.* Addison-Wesley, Wokingham, U.K.

Ho, W. and Hall, W. (1973). Measurements of the Dielectric Properties of Seawater and NaCl Solutions at 2.65 GHz. *Journal of Geophysical Research*, 78(27):6301–6315.

Ho, W., Love, A., and MELLE, M. (1974). Measurements of the Dielectric Properties of Seawater at 1.43 GHz. Technical report, NASA. Technical Report CR-2458.

Hollinger, J. (1971). Passive Microwave Measurements of Sea Surface Roughness. *IEEE Transactions on Geoscience Electronics*, GE-9(3):165–169.

Klein, L. and Swift, C. (1977). An Improved Model for the Dielectric Constant of Sea Water at Microwave Frequencies. *IEEE Transactions on Antennas and Propagation*, AP-25(1):104–111.

Kudryatsev, N., Makin, V., and Chapron, B. (1999). Coupled Sea Surface - Atmosphere Model. Spectrum of Short Wind Waves. *Journal of Geophysical Research*, 104(C4):7625–7639.

Lagerloef, G. (1998). Report of the First Workshop, Salinity Sea Ice Working Group. Technical report, NASA, USA. La Jolla, USA, 7-8 Feb.

Lagerloef, G., Swift, C., and D. M., L. (1995). Sea Surface Salinity: the Next Remote Sensing Challenge. *Oceanography*, 8(2):44–50.

Le Vine, D. and Abraham, S. (2004). Galactic Noise and Passive Microwave Remote Sensing from Space at L-Band. *IEEE Transactions of Geoscience and Remote Sensing*, 42:119–129.

Le Vine, D., Griffis, a., Swift, C., and Jackson, T. (1994). ESTAR: A Synthetic Aperture Microwave Radiometer for Remote Sensing Applications. *Proceedings of the IEEE*, 82(12):1787–1801.

Levitus, S., Burgett, R., and Boyer, T. (1994). World Ocean Atlas 1994 Volume 3: Salinity. *NOAA NESDIS 3*.

Marquardt, D. (1963). An algorithm for least-squares estimation of non-linear parameters. *Journal on Applied mathematics*, 11(2):431–441.

Martín-Neira, M. and Goutoule, J. (1997). A Two-Dimensional Aperture-Synthesis Radiometer for Soil Moisture and Ocean Salinity Observations. *ESA Bulletin*, 92:95–104.

Miller, J., Goodberlet, M., and Zaitzeff, J. (1998). Airborne Salinity Mapper makes Debut in Coastal Zone. *EOS Trans. American Geophysical Union*, 79(14):175–177.

Miranda, J., Vall-llossera, M., Camps, A., Duffo, N., Corbella, I., and Etcheto, J. (2003). Sea State on the Sea Surface Emissivity at L-Band. *IEEE Transactions of Geoscience and Remote Sensing*, 41(10):2307–2315.

Nelder and Mead (1965). Sea State on the Sea Surface Emissivity at L-Band. *Computer Journal*, 7:308–313.

Piola, A., Campos, E., Möller, O., Charo, M., and Martinez, C. (2000). Subtropical shelf front off eastern South America. *Journal of Geophysical Research*, 105:6566–6578.

Ribó, S. (2003). Research on Image Validation and Signal Processing of Aperture Synthesis Radiometry. Technical report, ESTEC. Internal ESTEC Working Paper No. 2182, pp. 81-92.

Ruf, C. (1988). Synthetic Aperture Interferometric Radiometer (SAIR). *Proceedings of the Earth Science Geostationary Platform Technology Workshop, NASA Langley Research Center, Hampton, VA, NASA*, 3040:179–190.

Sivestrin, P., Berger, M., Kerr, Y., and Font, J. (2001). ESA's Second Earth Explorer Opportunity Mission: The Soil Moisture and Ocean Salinity Observations. *IEEE Transactions of Geoscience and Remote Sensing Newsletter*, 118:11–14.

Skou, N. (1989). *Microwave Radiometer System: Design and Analysis.* Artech House.

Skou, N. (1995). An Overview of Requirements and Passive Microwave Radiometer options. Consultative Meeting on Soil Moisture and Ocean Salinity Measurement Requirements an Radiometer Techniques (SMOS). Technical report, Noordwijk ESA. pp. 41–48.

Skou, N. (2003). Faraday Rotation and L-band Oceanographic Measurements. *Radio Science*, 38(4):MAR24–1–8.

Smith, N. and Lefebvre, M. (1997). The Global Ocean Data Assimilation Experiment (GODAE), Monitoring the Oceans in the 2000s: An integrated Approach. *International Symposiun, Biarritz, October 15-17, 1997.*

Stoffelen, A. and Anderson, D. (1993). Wind retrieval and ERS-1 Scatterometer Backscatter Measurements. *Advance Space Research*, 13:553–560.

Swift, C. (1974). Microwave Radiometer Measurements of the Cape Cod Canal. *Radio Science*, 9(7):641–653.

Swift, C. (1980). Passive Microwave Remote Sensing. *Boundary-layer Meteorology*, 18:25–54.

Ulaby, F., Moore, R., and Fung, A. (1981). *Microwave Remote Sensing.Active and Passive.* Addison-Wesley Publishing Company.

UNESCO (1978). Background papers and supporting data on the Practical Salinity Scale. Technical Report 37, UNESCO Technical Papers in Marine Science.

Vall-llossera, M., Miranda, J., Camps, A., and Villarino, R. (2003). Sea Surface Emissivity Modeling At L-Band: An InterComparison Study. *Proceedings of the WISE/LOSAC/EuroSTARRS campaigns Workshop. ESA*, SP-525:143–154.

Villarino, R., Camps, A., Vall-llossera, M., Miranda, J., and Arenas, J. (2003). Sea Foam Effects on the Brightness temperature at L-Band. *IGARSS 2003, Toulouse, France.*

Villarino, R., Enrique, L., Camps, A., Corbella, I., and Blanch, S. (2002). Design, implementation and test of the UPC L-band Automatic Radiometer. *URSI Commission-F 2002 Open Symposium,Garmisch-Partenkirchen, Germany.*

Voronovich, A. and Zavorotny, V. (2001). Modelling of Backscattering of Radar Signals from Sea Surface at Ka- and C-bands. *Proceedings of the URSI General Assembly Maastricht.CD-ROM.*

Wilson, W., Yueh, S., Dinardo, S., Chazanoff, S., Li, F., and Rahmat-Samii, Y. (2001). Passive Active L- and S-band (PALS) Microwave Sensor for Ocean Salinity and Soil Moisture Measurements. *IEEE Transactions on Geoscience and Remote Sensing*, 39(5):1039–1047.

Wilson, W., Yueh, S., Dinardo, S., and Li, F. (2004). High stability l-band radiometer measurements of saltwater. *IEEE Transactions on Geoscience and Remote Sensing*, 42(9):1829–1835.

Wursteisen, P. and Fletcher, P. (2003). EuroSTARRS, WISE, LOSAC. First Results Workshop. *Proceedings of the WISE/LOSAC/EuroSTARRS Campaigns Workshop. ESA PUBLICATIONS*, SP-525:1–249.

Yueh, S., West, R., Wilson, W., Li, F., Nghiem, S., and Rahmat-Samii, Y. (2001). Error Sources and Feasibility for Microwave Remote Sensing of Ocean Surface Salinity. *IEEE Transactions on Geoscience and Remote Sensing*, 39(5):1049–1059.

Yueh, S., Wilson, W., Li, F., Nghiem, S., and Ricketts, W. (1997). Polarimetric Brightness Temperatures of the Sea Surface Measured with Aircraft K- and Ka-Band Radiometers. *IEEE Transactions of Geoscience and Remote Sensing*, 35(5):1177–1187.